Laboratori Nazionali di Frascati

LNF-92/047 (P)
5 Giugno 1992

CERN-TH.6504/92
BUTP-92/20

J. Bijnens, G. Ecker, J. Gasser:

SEMILEPTONIC KAON DECAYS IN CHIRAL PERTURBATION THEORY

Contribution to the DAΦNE Physics Handbook

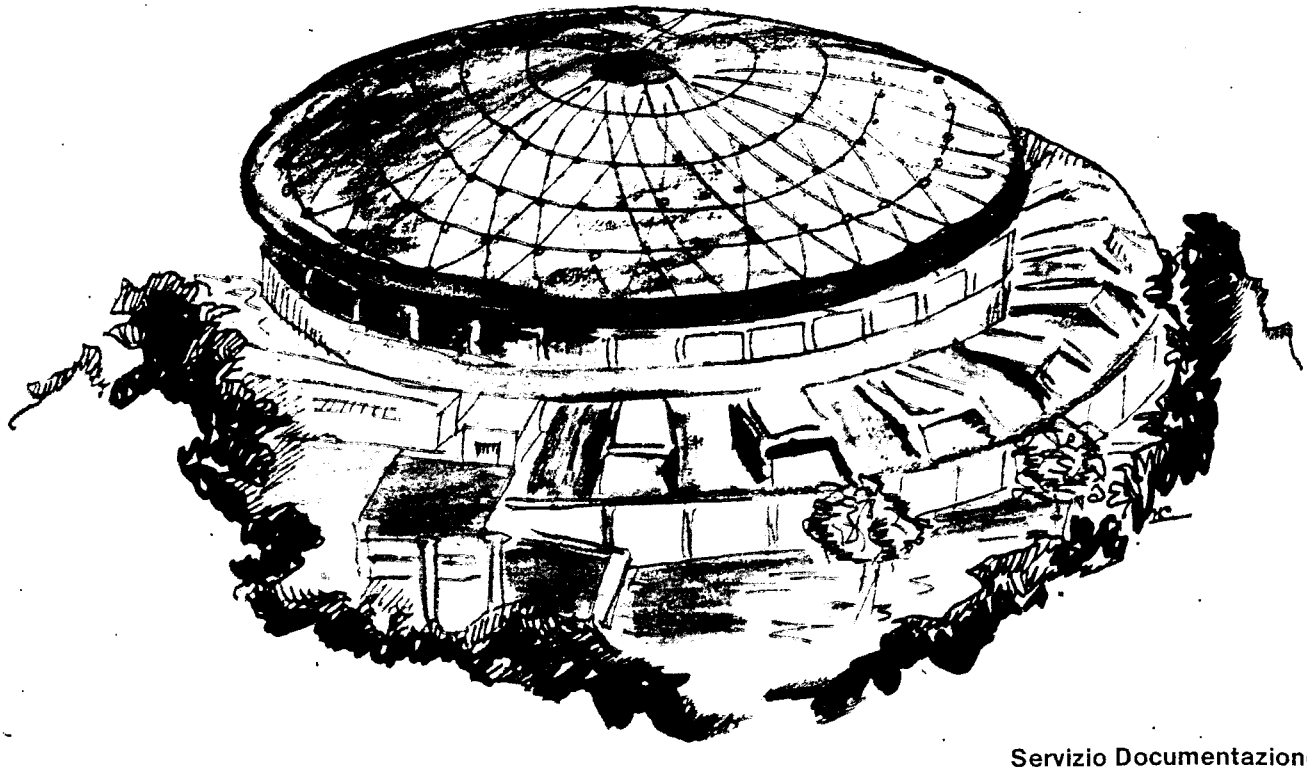

Servizio Documentazione
dei Laboratori Nazionali di Frascati
P.O. Box, 13 - 00044 Frascati (Italy)

INFN - Laboratori Nazionali di Frascati
Servizio Documentazione

LNF-92/047 (P)
5 Giugno 1992

CERN-TH.6504/92
BUTP-92/20

SEMILEPTONIC KAON DECAYS IN CHIRAL PERTURBATION THEORY

J. Bijnens and G. Ecker[♯]

CERN
CH–1211 Geneva 23

and

J. Gasser*

Institut für theoretische Physik
Universität Bern, Sidlerstrasse 5
CH–3012 Bern

Abstract

We present the matrix elements for the semileptonic kaon decays $K_{l2\gamma}$, $K_{l2l^+l^-}$, $K_{l2l'^+l'^-}$, K_{l3}, $K_{l3\gamma}$ and K_{l4} at next-to-leading order in chiral perturbation theory and compare the predictions with experimental data. Monte Carlo event generators are used to calculate the corresponding rates at DAFNE. We discuss the possibilities to improve our knowledge of the low-energy structure of the Standard Model at this and similar machines.

♯ Permanent address: Institut für theoretische Physik, Universität Wien, Boltzmanngasse 5, A–1090 Wien, Austria

* Research supported in part by Schweizerischer Nationalfonds

Contents

1 INTRODUCTION TO CHIRAL SYMMETRY 5

Bibliography 13

2 SEMILEPTONIC KAON DECAYS 15

1 Radiative K_{l2} decays 17

1.1 Matrix elements and kinematics 17

1.2 Decay rates 18

1.3 Determination of $A(W^2)$ and $V(W^2)$ 20

1.4 Previous experiments 23

1.5 Theory 24

1.6 Improvements at DAFNE 27

2 The decays $K^{\pm} \to l^{\pm}\nu l'^{+}l'^{-}$ 28

2.1 Matrix elements 28

2.2 Decay distributions 29

2.3 Theory 30

2.4 Numerical results 31

2.5 Present experimental status 32

2.6 Improvements at DAFNE 33

3 K_{l3} decays 34

3.1 Matrix elements and kinematics 34

3.2 Decay rates 35

3.3 Determination of the K_{l3} form factors 36

3.4 Previous measurements 37

3.5 Theory 38

3.6 Improvements at DAFNE 42

4 Radiative K_{l3} decays 44

4.1 Matrix elements 44
4.2 Decay rates 46
4.3 Previous experiments 48
4.4 Theory 48
4.5 Improvements at DAFNE 53
5 K_{l4} decays 54
5.1 Kinematics 54
5.2 Matrix elements 56
5.3 Decay rates 56
5.4 Isospin decomposition 58
5.5 Partial wave expansion 59
5.6 Previous experiments 60
5.7 Theory 62
5.8 Improvements at DAFNE 67
A Notation 71
B Loop integrals 73
C Decomposition of the hadronic tensors $I^{\mu\nu}$ 75
D Formulas for the traces in terms of x, y and z for the decays $K^+ \to l^+\nu l'^+ l'^-$ 77
E FORTRAN routine for the calculation of the reduced square of the $K_{l3\gamma}$ matrix element SM 79
List of Tables 83
List of Figures 85
Bibliography 86

Note:

- The number of events quoted for DAFNE are based on a luminosity of $5 \cdot 10^{32}\ cm^{-2}s^{-1}$, which is equivalent [1] to an annual rate of $9 \cdot 10^9$ $(1.1 \cdot 10^9)$ tagged $K^\pm$ (K_L) (1 year $= 10^7\ s$ assumed).
- Whenever we quote a branching ratio for a semileptonic K^0 decay, it stands for the branching ratio of the corresponding K_L decay, e.g.,

$$BR(K^0 \to \pi^- l^+ \nu) \equiv BR(K_L \to \pi^\pm l^\mp \nu)\ .$$

- More notation is provided in appendix A.

[1] P. Franzini, private communication.

Chapter 1

INTRODUCTION TO CHIRAL SYMMETRY

Chiral perturbation theory (CHPT) is a systematic approach to formulate the standard model as a quantum field theory at the hadronic level. In its general form, it uses only the symmetries of the standard model, in particular its spontaneously broken chiral symmetry. It is characterized by an effective chiral Lagrangian in terms of pseudoscalar meson fields (and possibly other low-lying hadronic states) giving rise to a systematic low-energy expansion of amplitudes [1, 2].

In the formulation of Ref.[2], one considers the generating functional $Z[v,a,s,p]$ of connected Green functions of quark currents associated with the fundamental Lagrangian

$$\mathcal{L} = \mathcal{L}^0_{QCD} + \bar{q}\gamma^\mu(v_\mu + \gamma_5 a_\mu)q - \bar{q}(s - i\gamma_5 p)q. \tag{1}$$

$\mathcal{L}^0_{QCD}$ is the QCD Lagrangian with the masses of the three light quarks set to zero. The external fields v_μ, a_μ, s and p are hermitian 3×3 matrices in flavour space. To describe electromagnetic and semileptonic interactions, the relevant external gauge fields of the standard model are [1]

$$\begin{aligned} r_\mu = v_\mu + a_\mu &= -eQA_\mu \\ l_\mu = v_\mu - a_\mu &= -eQA_\mu - \frac{e}{\sqrt{2}\sin\theta_W}(W^+_\mu T_+ + h.c.) \end{aligned} \tag{2}$$

$$Q = \frac{1}{3}\mathrm{diag}(2,-1,-1), \qquad \mathrm{T}_+ = \begin{pmatrix} 0 & V_{ud} & V_{us} \\ 0 & 0 & 0 \\ 0 & 0 & 0 \end{pmatrix}$$

where the V_{ij} are Kobayashi–Maskawa matrix elements. The quark mass matrix

$$\mathcal{M} = \mathrm{diag}(m_u, m_d, m_s) \tag{3}$$

is contained in the scalar field $s(x)$. The Lagrangian (1) exhibits a local $SU(3)_L \times SU(3)_R$ symmetry

$$\begin{aligned} q &\to g_R\frac{1}{2}(1+\gamma_5)q + g_L\frac{1}{2}(1-\gamma_5)q \\ r_\mu &\to g_R r_\mu g_R^\dagger + i g_R \partial_\mu g_R^\dagger \\ l_\mu &\to g_L l_\mu g_L^\dagger + i g_L \partial_\mu g_L^\dagger \\ s+ip &\to g_R(s+ip)g_L^\dagger \\ g_{R,L} &\in SU(3)_{R,L}. \end{aligned} \tag{4}$$

The generating functional Z admits an expansion in powers of external momenta and quark masses (CHPT). In the meson sector at leading order in CHPT, it is given by the classical action

$$Z = \int d^4x \mathcal{L}_2(U,v,a,s,p). \tag{5}$$

[1] We adopt the present conventions of the Particle Data Group [3].

$\mathcal{L}_2$ is the non-linear σ model Lagrangian coupled to the external fields v, a, s, p

$$\mathcal{L}_2 = \frac{F^2}{4}\langle D_\mu U D^\mu U^\dagger + \chi U^\dagger + \chi^\dagger U\rangle \tag{6}$$

where

$$D_\mu U = \partial_\mu U - i r_\mu U + i U l_\mu, \qquad \chi = 2B_0(s + ip), \tag{7}$$

and $\langle A\rangle$ stands for the trace of the matrix A. U is a unitary 3×3 matrix

$$U^\dagger U = 1, \qquad \det U = 1,$$

which transforms as

$$U \to g_R U g_L^\dagger \tag{8}$$

under $SU(3)_L \times SU(3)_R$. U incorporates the fields of the eight pseudoscalar Goldstone bosons. A convenient parametrization is [2]

$$U = \exp(i\sqrt{2}\Phi/F), \qquad \Phi = \begin{pmatrix} \frac{\pi^0}{\sqrt{2}} + \frac{\eta_8}{\sqrt{6}} & -\pi^+ & -K^+ \\ \pi^- & -\frac{\pi^0}{\sqrt{2}} + \frac{\eta_8}{\sqrt{6}} & -K^0 \\ K^- & -\overline{K^0} & -\frac{2\eta_8}{\sqrt{6}} \end{pmatrix}. \tag{9}$$

The parameters F and B_0 are the only free constants at $O(p^2)$: F is the pion decay constant in the chiral limit,

$$F_\pi = F(1 + O(m_{quark})) = 93.2 MeV, \tag{10}$$

whereas B_0 is related to the quark condensate,

$$\langle 0|\bar{u}u|0\rangle = -F^2 B_0(1 + O(m_{quark})). \tag{11}$$

B_0 always appears multiplied by quark masses. At $O(p^2)$, the product $B_0 m_q$ can be expressed in terms of meson masses, e.g.

$$M_{\pi^+}^2 = B_0(m_u + m_d). \tag{12}$$

The Lagrangian (6) is referred to as the effective chiral Lagrangian of $O(p^2)$. The chiral counting rules are the following: the field U is of $O(p^0)$, the derivative ∂_μ and the external gauge fields v_μ, a_μ are terms of $O(p)$, and the fields s, p count as $O(p^2)$.

At order p^4 the generating functional consists of three terms [2] :

i) The one-loop graphs generated by the lowest order Lagrangian (6).

[2] We follow the Condon-Shortley-de Swart phase conventions.

ii) An explicit local action of order p^4.

iii) A contribution to account for the chiral anomaly.

We briefly discuss the contributions ii) and iii) and start with the local action of $O(p^4)$. It is generated by the Lagrangian $\mathcal{L}_4$ [2]:

$$\begin{aligned}\mathcal{L}_4 &= L_1\langle D_\mu U^\dagger D^\mu U\rangle^2 + L_2\langle D_\mu U^\dagger D_\nu U\rangle\langle D^\mu U^\dagger D^\nu U\rangle \\ &+L_3\langle D_\mu U^\dagger D^\mu U D_\nu U^\dagger D^\nu U\rangle + L_4\langle D_\mu U^\dagger D^\mu U\rangle\langle \chi^\dagger U + \chi U^\dagger\rangle \\ &+L_5\langle D_\mu U^\dagger D^\mu U(\chi^\dagger U + U^\dagger\chi)\rangle + L_6\langle \chi^\dagger U + \chi U^\dagger\rangle^2 + L_7\langle \chi^\dagger U - \chi U^\dagger\rangle^2 \\ &+L_8\langle \chi^\dagger U\chi^\dagger U + \chi U^\dagger\chi U^\dagger\rangle - iL_9\langle F_R^{\mu\nu} D_\mu U D_\nu U^\dagger + F_L^{\mu\nu} D_\mu U^\dagger D_\nu U\rangle \\ &+L_{10}\langle U^\dagger F_R^{\mu\nu} U F_{L\mu\nu}\rangle + L_{11}\langle F_{R\mu\nu}F_R^{\mu\nu} + F_{L\mu\nu}F_L^{\mu\nu}\rangle + L_{12}\langle \chi^\dagger\chi\rangle, \qquad (13)\end{aligned}$$

where

$$\begin{aligned}F_R^{\mu\nu} &= \partial^\mu r^\nu - \partial^\nu r^\mu - i[r^\mu, r^\nu] \qquad (14)\\ F_L^{\mu\nu} &= \partial^\mu l^\nu - \partial^\nu l^\mu - i[l^\mu, l^\nu].\end{aligned}$$

The twelve new low-energy couplings $L_1, \ldots, L_{12}$ arising here are in general divergent (except L_3, L_7). They absorb the divergences of the one-loop graphs via the renormalization

$$\begin{aligned}L_i &= L_i^r + \Gamma_i\lambda \\ \lambda &= (4\pi)^{-2}\mu^{d-4}\left\{\frac{1}{d-4} - \frac{1}{2}\left(\ln(4\pi) + \Gamma'(1) + 1\right)\right\} \qquad (15)\end{aligned}$$

in the dimensional regularization scheme. The coefficients Γ_i are displayed in table 1. They govern the scale dependence of the renormalized, finite couplings $L_i^r(\mu)$,

$$L_i^r(\mu_2) = L_i^r(\mu_1) + \frac{\Gamma_i}{16\pi^2}\ln\frac{\mu_1}{\mu_2}\ . \qquad (16)$$

Observable quantities are independent of the scale μ, once the loop contributions are included.

The constants F, B_0, together with $L_1^r, \ldots, L_{10}^r$, completely determine the low-energy behaviour of pseudoscalar meson interactions to $O(p^4)$. L_{11}^r and L_{12}^r are contact terms which are not directly accessible to experiment. Similarly to F and B_0 discussed above, the constants L_i^r are not determined by chiral symmetry – they are fixed by the dynamics of the underlying theory through the renormalization group invariant scale Λ and by the heavy quark masses $m_c, m_b, \ldots$. With present techniques, it is, however, not possible to evaluate them directly from the QCD Lagrangian. In the absence of such a calculational scheme, they have been determined by comparison with experimental low-energy information and by using large–N_C arguments. The result is shown in column 2 of table 1, where $L_1^r, \ldots, L_{10}^r$ are displayed at the scale $\mu = M_\rho$. The experimental information underlying these values

Table 1: Phenomenological values and source for the renormalized coupling constants $L_i^r(M_\rho)$. The quantities Γ_i in the fourth column determine the scale dependence of the $L_i^r(\mu)$ according to Eq. (16). L_{11}^r and L_{12}^r are not directly accessible to experiment.

i	$L_i^r(M_\rho) \times 10^3$	source	Γ_i
1	0.7 ± 0.5	$K_{e4}, \pi\pi \to \pi\pi$	3/32
2	1.2 ± 0.4	$K_{e4}, \pi\pi \to \pi\pi$	3/16
3	-3.6 ± 1.3	$K_{e4}, \pi\pi \to \pi\pi$	0
4	-0.3 ± 0.5	Zweig rule	1/8
5	1.4 ± 0.5	$F_K : F_\pi$	3/8
6	-0.2 ± 0.3	Zweig rule	11/144
7	-0.4 ± 0.2	Gell-Mann-Okubo, L_5, L_8	0
8	0.9 ± 0.3	$M_{K^0} - M_{K^+}, L_5,$ $(2m_s - m_u - m_d) : (m_d - m_u)$	5/48
9	6.9 ± 0.7	$< r^2 >_{em}^{\pi}$	1/4
10	-5.5 ± 0.7	$\pi \to e\nu\gamma$	$-$ 1/4
11			$-1/8$
12			5/24

is shown in column 3. [L_1, L_2 and L_3 are taken from a recent overall fit to K_{e4} and $\pi\pi$ data [4], see also the subsection on K_{l4} decays in section 2 and Ref. [5]. $L_4, \ldots, L_{10}$ are from [2]. For L_9 see also [6]. In Refs. [2, 7] it was shown that the values for the $L_i^r(M_\rho)$ can be understood in terms of meson resonance exchange. For recent attempts to evaluate L_i directly from the QCD Lagrangian see [8].]

Here, it is of interest to know which of the low-energy couplings occur in the matrix elements for the semileptonic kaon decays discussed in section 2. This information is given in table 2. (There is an ambiguity concerning the bookkeeping of L_4 and L_5: some of these contributions may be absorbed into the physical decay constants F_π, F_K. Here we have chosen the convention which corresponds to the amplitudes displayed in section 2. Furthermore, in $K_{\mu 4}$ decays, additional constants may occur via the form factor R which has not yet been worked out at one-loop level [9]. This channel is therefore omitted in the table.)

We now turn to point iii) above. A functional $Z[U, l, r]$ which reproduces the chiral anomaly was first constructed by Wess and Zumino [10]. For practical purposes, it is useful to write it in the explicit form given by Witten [11]:

$$\begin{aligned} Z[U,l,r]_{WZW} &= -\frac{iN_C}{240\pi^2}\int_{M^5} d^5x\epsilon^{ijklm}\langle\Sigma_i^L\Sigma_j^L\Sigma_k^L\Sigma_l^L\Sigma_m^L\rangle \\ &\quad -\frac{iN_C}{48\pi^2}\int d^4x\varepsilon_{\mu\nu\alpha\beta}\left(W(U,l,r)^{\mu\nu\alpha\beta} - W(1,l,r)^{\mu\nu\alpha\beta}\right) \end{aligned} \tag{17}$$

Table 2: Occurrence of the low-energy coupling constants $L_1, \ldots, L_{10}$ and of the anomaly in the semileptonic decays discussed in section 2.

	$K_{l2\gamma}$	K_{l2ll}	K_{l3}	$K_{l3\gamma}$	$K^+ \to \pi^+\pi^-e^+\nu_e$	$K^+ \to \pi^0\pi^0e^+\nu_e$	$K^0 \to \pi^0\pi^-e^+\nu_e$
L_1					×	×	
L_2					×	×	
L_3					×	×	×
L_4					×	×	
L_5					×	×	×
L_9		×	×	×	×	×	×
$L_9 + L_{10}$	×	×		×			
Anomaly	×	×		×	×		×

$$
\begin{aligned}
W(U,l,r)_{\mu\nu\alpha\beta} \;=\; & \langle U l_\mu l_\nu l_\alpha U^\dagger r_\beta + \frac{1}{4} U l_\mu U^\dagger r_\nu U l_\alpha U^\dagger r_\beta + iU\partial_\mu l_\nu l_\alpha U^\dagger r_\beta \\
& + i\partial_\mu r_\nu U l_\alpha U^\dagger r_\beta - i\Sigma^L_\mu l_\nu U^\dagger r_\alpha U l_\beta + \Sigma^L_\mu U^\dagger \partial_\nu r_\alpha U l_\beta \\
& - \Sigma^L_\mu \Sigma^L_\nu U^\dagger r_\alpha U l_\beta + \Sigma^L_\mu l_\nu \partial_\alpha l_\beta + \Sigma^L_\mu \partial_\nu l_\alpha l_\beta \\
& - i\Sigma^L_\mu l_\nu l_\alpha l_\beta + \frac{1}{2}\Sigma^L_\mu l_\nu \Sigma^L_\alpha l_\beta - i\Sigma^L_\mu \Sigma^L_\nu \Sigma^L_\alpha l_\beta \rangle \\
& - (L \leftrightarrow R) \\
& \Sigma^L_\mu = U^\dagger \partial_\mu U \qquad \Sigma^R_\mu = U \partial_\mu U^\dagger \\
& N_C = 3 \qquad \epsilon_{0123} = 1
\end{aligned}
\tag{18}
$$

where $(L \leftrightarrow R)$ stands for the interchange

$$U \leftrightarrow U^\dagger, \qquad l_\mu \leftrightarrow r_\mu, \qquad \Sigma^L_\mu \leftrightarrow \Sigma^R_\mu.$$

The integration in the first term in Eq. (17) is over a five-dimensional manifold whose boundary is four-dimensional Minkowski space, such that

$$\int_{M^5} d^5x \epsilon^{ijklm} \partial_m T_{ijkl} = \int d^4x \epsilon^{\mu\nu\rho\sigma} T_{\mu\nu\rho\sigma} \tag{19}$$

according to Stoke's theorem. [This term involves at least five pseudoscalar fields and will not be needed in the following section.] The convention used in Eq. (17) ensures that $Z[U,l,r]_{WZW}$ conserves parity and reproduces the anomaly under $SU(3)_L \times SU(3)_R$ transformations in Bardeen's form [12] (in particular, it is invariant under transformations generated by the vector currents).

The Wess-Zumino-Witten functional contains all the anomalies which contribute to the semileptonic meson decays considered in the following section. The relevant piece for e.g. K_{l4} decays is

$$Z[U,l,r]_{WZW} = \frac{i\sqrt{2}}{4\pi^2 F^3} \int d^4x \epsilon_{\mu\nu\rho\sigma} < \partial^\mu \Phi \partial^\nu \Phi \partial^\rho \Phi v^\sigma > + \cdots \; . \tag{20}$$

This short introduction to CHPT (see Refs.[13, 14] for more extensive treatments with references to the original literature) contains all the ingredients necessary for the calculation of semileptonic K decay amplitudes to $O(p^4)$ presented in the next section. For the low energies involved in these decays, the momentum dependence of the W propagator connecting to the lepton-neutrino pair in the final state can be neglected. The chiral realization of the non-leptonic weak interactions is discussed in the corresponding sections on non-leptonic K decays.

Bibliography

[1] S. Weinberg, Physica 96A (1979) 327.

[2] J. Gasser and H. Leutwyler, Ann. Phys. 158 (1984) 142; Nucl. Phys. B250 (1985) 465.

[3] Review of Particle Properties, Phys. Lett. B239 (1990).

[4] C. Riggenbach, J. Gasser, J.F. Donoghue and B.R. Holstein, Phys. Rev. D43 (1991) 127.

[5] J. Bijnens, Nucl. Phys. B337 (1990) 635.

[6] J. Bijnens and F. Cornet, Nucl. Phys. B296 (1988) 557.

[7] G. Ecker, J. Gasser, A. Pich and E. de Rafael, Nucl. Phys. B321 (1989) 311;
G. Ecker, J. Gasser, H. Leutwyler, A. Pich and E. de Rafael, Phys. Lett. B223 (1989) 425;
J.F. Donoghue, C. Ramirez and G. Valencia, Phys. Rev. D39 (1989) 1947;
M. Praszalowicz and G. Valencia, Nucl. Phys. B341 (1990) 27.

[8] D. Espriu, E. de Rafael and J. Taron, Nucl. Phys. B345 (1990) 22; Erratum ibid. B355 (1991) 278 and references therein.

[9] G. Colangelo and J. Gasser, in preparation.

[10] J. Wess and B. Zumino, Phys. Lett. B37 (1971) 95.

[11] E. Witten, Nucl. Phys. B223 (1983) 422; for further discussions see also
C.G. Callan and E. Witten, Nucl. Phys. B239 (1984) 161;
Ö. Kaymakcalan, S. Rajeev and J. Schechter, Phys. Rev. D30 (1984) 594;
K. Chou et al., Phys. Lett. B134 (1984) 67;
H. Kawai and S. Tye, Phys. Lett. B140 (1984) 403.

[12] W.A. Bardeen, Phys. Rev. 184 (1969) 1848.

[13] H. Georgi, Weak Interactions and Modern Particle Theory, Benjamin/Cummings, Menlo Park, 1984;

J.F. Donoghue, E. Golowich and B.R. Holstein, Dynamics of the Standard Model, Cambridge Univ. Press, Cambridge, 1992.

[14] J. Gasser, The QCD Vacuum and Chiral Symmetry, in: Hadrons and Hadronic Matter, eds. D. Vautherin et al. (Plenum, New York, 1990) p.87; Chiral dynamics, in: Proceedings of the Workshop on Physics and Detectors for DAFNE, Frascati, April 9-12, 1991, ed. G. Pancheri (Servizio Documentazione dei Laboratori Nazionali di Frascati, P.O. Box, 13-I-00044 Frascati (Italy)) p. 291;
H. Leutwyler, Chiral Effective Lagrangians, Lectures given at the 30. Int. Universitätswochen für Kernphysik, Schladming and at the Advanced Theoretical Study Institute in Elementary Particle Physics, Boulder, 1991.

Chapter 2

SEMILEPTONIC KAON DECAYS

1 Radiative K_{l2} decays

We consider the $K_{l2\gamma}$ decay

$$K^+(p) \to l^+(p_l)\nu_l(p_\nu)\gamma(q) \qquad [K_{l2\gamma}] \tag{1.1}$$

where l stands for e or μ, and γ is a real photon with $q^2 = 0$. Processes where the (virtual) photon converts into a e^+e^- or $\mu^+\mu^-$ pair are considered in the next subsection. The K^- mode is obtained from (1.1) by charge conjugation.

1.1 Matrix elements and kinematics

The matrix element for $K^+ \to l^+\nu_l\gamma$ has the structure

$$T = -iG_F e V_{us}^\star \epsilon_\mu^\star \{F_K L^\mu - H^{\mu\nu} l_\nu\} \tag{1.2}$$

with

$$\begin{aligned} L^\mu &= m_l \bar{u}(p_\nu)(1+\gamma_5)\left(\frac{2p^\mu}{2pq} - \frac{2p_l^\mu + \not{q}\gamma^\mu}{2p_l q}\right) v(p_l) \\ l^\mu &= \bar{u}(p_\nu)\gamma^\mu(1-\gamma_5)v(p_l) \\ H^{\mu\nu} &= iV(W^2)\epsilon^{\mu\nu\alpha\beta}q_\alpha p_\beta - A(W^2)(qW g^{\mu\nu} - W^\mu q^\nu) \\ W^\mu &= (p-q)^\mu = (p_l + p_\nu)^\mu . \end{aligned} \tag{1.3}$$

Here, ϵ_μ denotes the polarization vector of the photon with $q^\mu\epsilon_\mu = 0$, whereas A, V stand for two Lorentz invariant amplitudes which occur in the general decomposition of the tensors

$$I^{\mu\nu} = \int dx e^{iqx+iWy} < 0 \mid TV_{em}^\mu(x) I_{4-i5}^\nu(y) \mid K^+(p) > \ , \ I = V, A \ . \tag{1.4}$$

The form factor A (V) is related to the matrix element of the axial (vector) current in (1.4). In appendix C we display the general decomposition of $A^{\mu\nu}$, $V^{\mu\nu}$ for $q^2 \neq 0$ and provide also the link with the notation used by the PDG [1] and in [2, 3].

The term proportional to L^μ in (1.2) does not contain unknown quantities – it is determined by the amplitude of the nonradiative decay $K^+ \to l^+\nu_l$. This part of the amplitude is usually referred to as "inner Bremsstrahlung (IB) contribution", whereas the term proportional to $H^{\mu\nu}$ is called "structure dependent (SD) part" .

The form factors are analytic functions in the complex W^2-plane cut along the positive real axis. The cut starts at $W^2 = (M_K + 2M_\pi)^2$ for A (at $W^2 = (M_K + M_\pi)^2$ for V). In our phase convention, A and V are real in the physical region of $K_{l2\gamma}$ decays,

$$m_l^2 \leq W^2 \leq M_K^2. \tag{1.5}$$

The kinematics of (spin averaged) $K_{l2\gamma}$ decays needs two variables, for which we choose the conventional quantities

$$x = 2pq/M_K^2 \ , \ y = 2pp_l/M_K^2 \ . \tag{1.6}$$

In the K rest frame, the variable x (y) is proportional to the photon (charged lepton) energy,

$$x = 2E_\gamma/M_K \ , \ y = 2E_l/M_K \ , \tag{1.7}$$

and the angle $\theta_{l\gamma}$ between the photon and the charged lepton is related to x and y by

$$x = \frac{(1-y/2+A/2)(1-y/2-A/2)}{1-y/2+A/2\cos\theta_{l\gamma}} \ ; A = \sqrt{y^2-4r_l} \ . \tag{1.8}$$

In terms of these quantities, one has

$$W^2 = M_K^2(1-x) \ ; \ (q^2=0) \ . \tag{1.9}$$

We write the physical region for x and y as

$$2\sqrt{r_l} \le y \le 1+r_l$$

$$1-\frac{1}{2}(y+A) \le x \le 1-\frac{1}{2}(y-A) \tag{1.10}$$

or, equivalently, as

$$\begin{aligned} 0 \le \ & x \ \le 1-r_l \\ 1-x+\frac{r_l}{(1-x)} \le \ & y \ \le 1+r_l \end{aligned} \tag{1.11}$$

where

$$r_l = m_l^2/M_K^2 = \begin{cases} 1.1\cdot 10^{-6} (l=e) \\ 4.6\cdot 10^{-2} (l=\mu) \end{cases} \ . \tag{1.12}$$

1.2 Decay rates

The partial decay rate is

$$d\Gamma = \frac{1}{2M_K(2\pi)^5} \sum_{spins} |T|^2 d_{LIPS}(p;p_l,p_\nu,q). \tag{1.13}$$

The Dalitz plot density

$$\rho(x,y) = \frac{d^2\Gamma}{dxdy} = \frac{M_K}{256\pi^3} \sum_{spins} |T|^2 \tag{1.14}$$

is a Lorentz invariant function which contains V and A in the following form [4],

$$\begin{aligned}
\rho(x,y) &= \rho_{\rm IB}(x,y) + \rho_{\rm SD}(x,y) + \rho_{\rm INT}(x,y) \\
\rho_{\rm IB}(x,y) &= A_{\rm IB} f_{\rm IB}(x,y) \\
\rho_{\rm SD}(x,y) &= A_{\rm SD} M_K^2 \left[(V+A)^2 f_{\rm SD+}(x,y) + (V-A)^2 f_{\rm SD-}(x,y)\right] \\
\rho_{\rm INT}(x,y) &= A_{\rm INT} M_K \left[(V+A) f_{\rm INT+}(x,y) + (V-A) f_{\rm INT-}(x,y)\right] \qquad (1.15)
\end{aligned}$$

where

$$\begin{aligned}
f_{\rm IB}(x,y) &= \left[\frac{1-y+r_l}{x^2(x+y-1-r_l)}\right]\left[x^2 + 2(1-x)(1-r_l) - \frac{2xr_l(1-r_l)}{x+y-1-r_l}\right] \\
f_{\rm SD+}(x,y) &= [x+y-1-r_l]\,[(x+y-1)(1-x) - r_l] \\
f_{\rm SD-}(x,y) &= [1-y+r_l]\,[(1-x)(1-y) + r_l] \\
f_{\rm INT+}(x,y) &= \left[\frac{1-y+r_l}{x(x+y-1-r_l)}\right][(1-x)(1-x-y) + r_l] \\
f_{\rm INT-}(x,y) &= \left[\frac{1-y+r_l}{x(x+y-1-r_l)}\right]\left[x^2 - (1-x)(1-x-y) - r_l\right] \qquad (1.16)
\end{aligned}$$

and

$$\begin{aligned}
A_{\rm IB} &= 4r_l \left(\frac{F_K}{M_K}\right)^2 A_{\rm SD} \\
A_{\rm SD} &= \frac{G_F^2 |V_{us}|^2 \alpha}{32\pi^2} M_K^5 \\
A_{\rm INT} &= 4r_l \left(\frac{F_K}{M_K}\right) A_{\rm SD} \ . \qquad (1.17)
\end{aligned}$$

For later convenience, we note that

$$A_{\rm SD} = \frac{\alpha}{8\pi} \frac{1}{r_l(1-r_l)^2} \left(\frac{M_K}{F_K}\right)^2 \Gamma(K \to l\nu_l) \ . \qquad (1.18)$$

The indices IB, SD and INT stand respectively for the contribution from inner Bremsstrahlung, from the structure dependent part and from the interference term between the IB and the SD part in the amplitude.

To get a feeling for the magnitude of the various contributions IB,SD$^{\pm}$ and INT$^{\pm}$ to the decay rate, we consider the integrated rates

$$\Gamma_I = \int_{R_I} dxdy \rho_I(x,y) \ ; \ \ I = {\rm SD}^{\pm}, {\rm INT}^{\pm}, {\rm IB} \ , \qquad (1.19)$$

where $\rho_{SD} = \rho_{SD+} + \rho_{SD-}$ etc. For the region R_I we take the full phase space for $I \neq$ IB, and

$$R_{\rm IB} = 214.5 {\rm MeV/c} \leq p_l \leq 231.5 {\rm MeV/c} \ . \qquad (1.20)$$

Table 1.1: The quantities X_I, N_I. $SD^{\pm}$ and $INT^{\pm}$ are evaluated with full phase space, IB with restricted kinematics (1.20).

	SD^+	SD^-	INT^+	INT^-	IB	
X_I	$1.67 \cdot 10^{-2}$	$1.67 \cdot 10^{-2}$	$-8.22 \cdot 10^{-8}$	$3.67 \cdot 10^{-6}$	$3.58 \cdot 10^{-6}$	$K_{e2\gamma}$
X_I	$1.18 \cdot 10^{-2}$	$1.18 \cdot 10^{-2}$	$-1.78 \cdot 10^{-3}$	$1.23 \cdot 10^{-2}$	$3.68 \cdot 10^{-2}$	$K_{\mu 2\gamma}$
N_I	2	2	1	1	0	

for the Bremsstrahlung contribution. Here p_l stands for the modulus of the lepton three momentum in the kaon rest system [2]. We consider constant form factors V, A and write for the rates and for the corresponding branching ratios

$$\begin{aligned} \Gamma_I &= A_{\rm SD} \{M_K(V \pm A)\}^{N_I} X_I \\ {\rm BR}_I &\doteq \Gamma_I/\Gamma_{\rm tot} = N \{M_K(V \pm A)\}^{N_I} X_I \end{aligned} \tag{1.21}$$

with

$$N = A_{\rm SD}/\Gamma_{\rm tot} = 8.348 \cdot 10^{-2}. \tag{1.22}$$

The values for N_I and X_I are listed in table 1.1.

To estimate Γ_I and ${\rm BR}_I$, we note that the form factors V, A are of order

$$M_K(V+A) \simeq -10^{-1} \ , \ M_K(V-A) \simeq -4 \cdot 10^{-2} \ . \tag{1.23}$$

From this and from the entries in the table one concludes that for the above regions R_I, the interference terms $INT^{\pm}$ are negligible in $K_{e2\gamma}$, whereas they are important in $K_{\mu 2\gamma}$. Furthermore, IB is negligible for $K_{e2\gamma}$, because it is helicity suppressed as can be seen from the factor m_l^2 in $A_{\rm IB}$. This term dominates however in $K_{\mu 2\gamma}$.

1.3 Determination of $A(W^2)$ and $V(W^2)$

The decay rate contains two real functions

$$F^{\pm}(W^2) = V(W^2) \pm A(W^2) \tag{1.24}$$

as the only unknowns. In Figs. (1.1,1.2) we display contour plots for the density distributions $f_{\rm IB}, \ldots, f_{\rm INT^{\pm}}$ for $l = \mu, e$. These five terms have obviously very different Dalitz plots. Therefore, in principle, one can determine the strength of each term by choosing a suitable kinematical region of observation. To pin down $F^{\pm}$, it would be sufficient to measure at each photon energy the interference term $INT^{\pm}$. This has not yet been achieved so far, either because the contribution of $INT^{\pm}$ is too

[2] This cut has been used in [3] for $K_{\mu 2\gamma}$, because this kinematical region is free from $K_{\mu 3}$ background. We apply it here for illustration also to the electron mode $K_{e2\gamma}$.

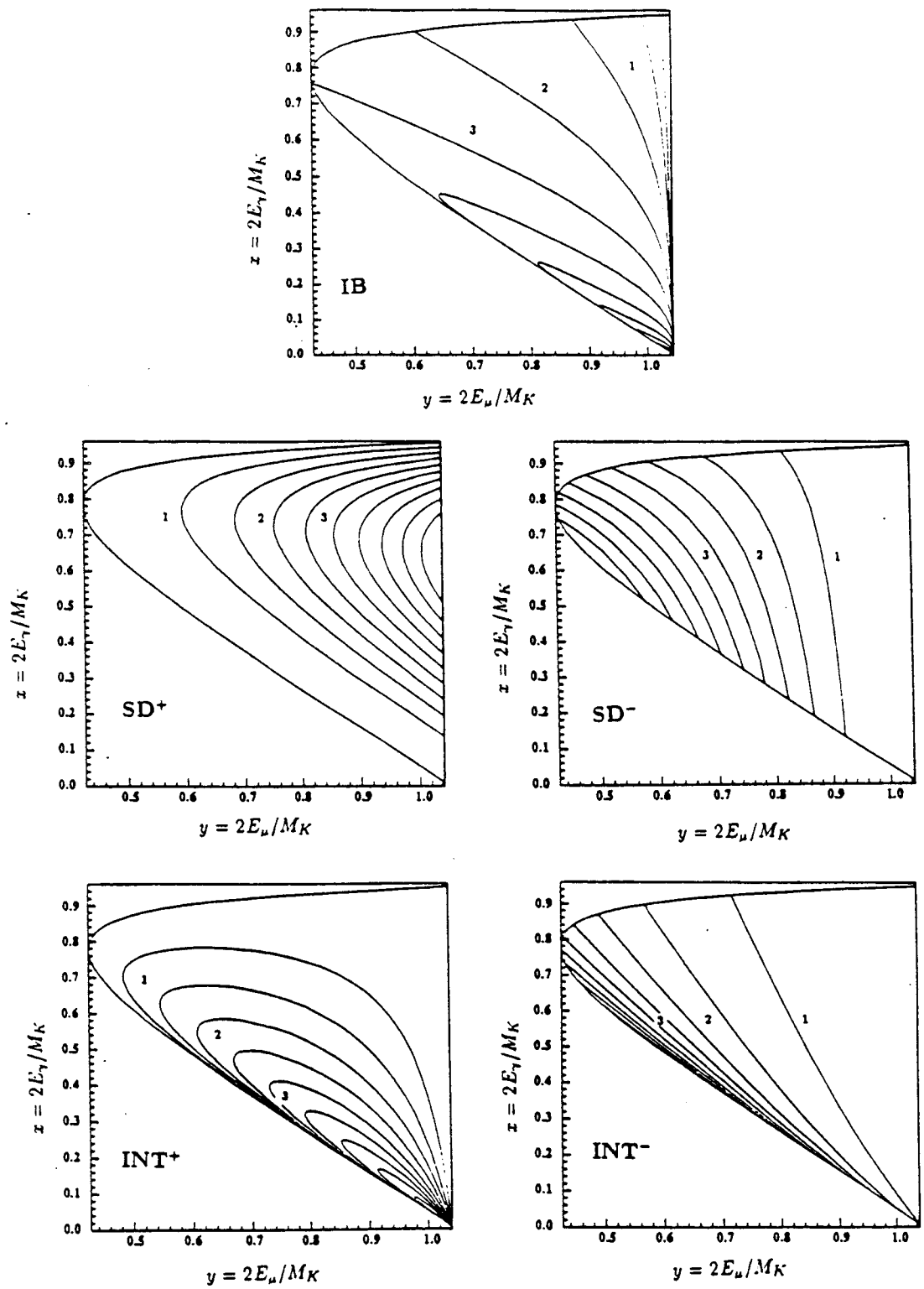

Figure 1.1: Contour plots for $f_{\rm IB}, \ldots, f_{\rm INT\pm}$ $[K_{\mu 2\gamma}]$. The numbering on the lines points towards increasing modulus. The normalization is arbitrary.

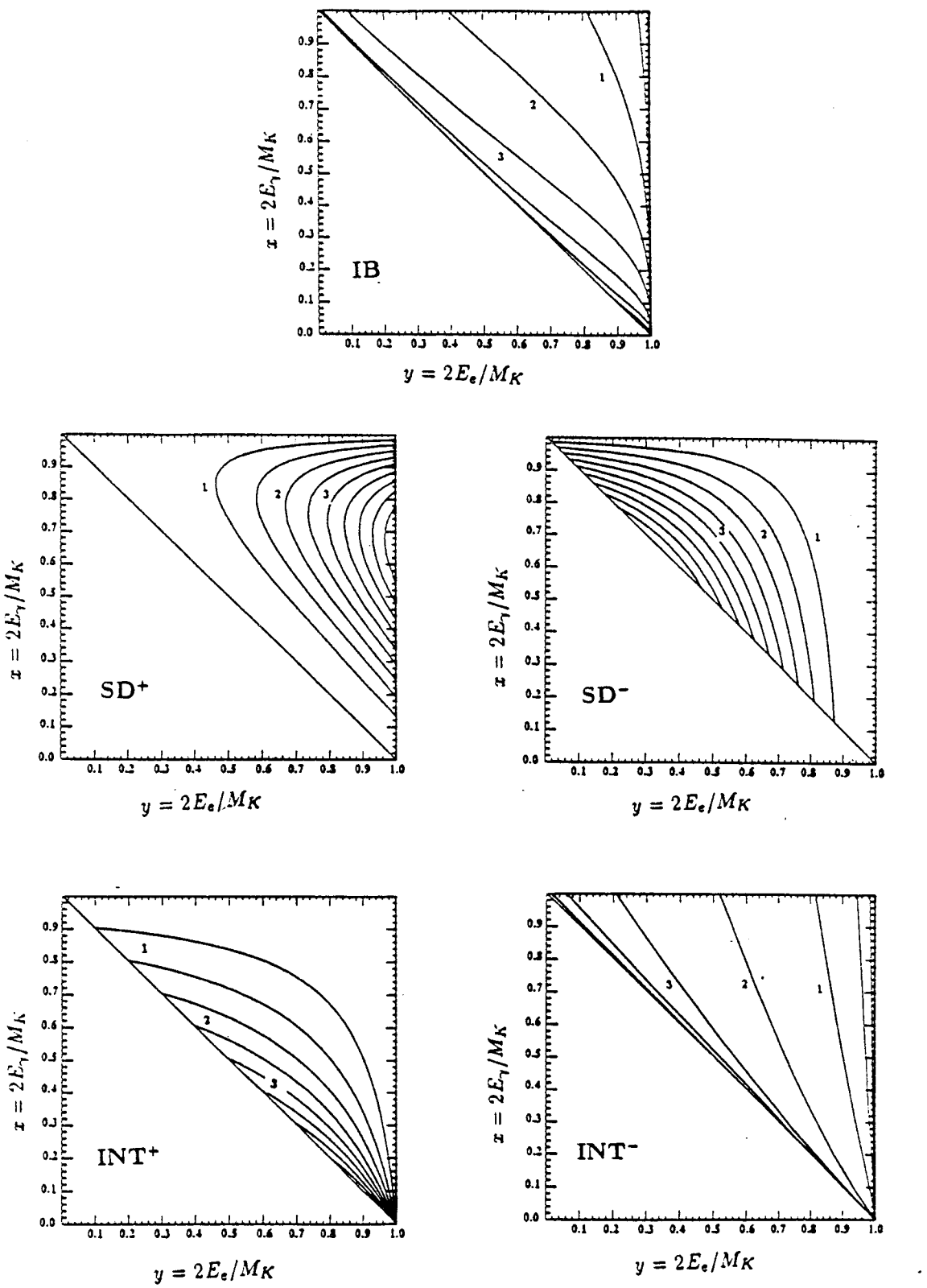

Figure 1.2: Contour plots for $f_{\rm IB}, \ldots, f_{\rm INT\pm}$ $[K_{e2\gamma}]$. The numbering on the lines points towards increasing modulus. The normalization is arbitrary.

small (in $K_{e2\gamma}$) , or because too few events have been collected (in $K_{\mu 2\gamma}$). On the other hand, from a measurement of $SD^{\pm}$ alone one can determine A, V only up to a fourfold ambiguity:

$$SD^{\pm} \rightarrow \{(V,A); -(V,A); (A,V); -(A,V)\}\,. \tag{1.25}$$

In terms of the ratio

$$\gamma_K = A/V \tag{1.26}$$

this ambiguity amounts to

$$SD^{\pm} \rightarrow \{\gamma_K; 1/\gamma_K\}\,. \tag{1.27}$$

Therefore, in order to pin down the amplitudes A and V uniquely, one must measure the interference terms $INT^{\pm}$ as well.

1.4 Previous experiments

$\underline{K^+ \rightarrow e^+\nu_e\gamma}$

The PDG uses data from two experiments [2, 5], both of which have been sensitive mainly to the SD^+ term in (1.15). In [5], 56 events with $E_\gamma > 100$ MeV, $E_{e^+} > 236$ MeV and $\theta_{e^+\gamma} > 120^0$ have been identified, whereas the later experiment [2] has collected 51 events with $E_\gamma > 48$ MeV, $E_{e^+} > 235$ MeV and $\theta_{e^+\gamma} > 140^0$. In these kinematical regions, background from $K^+ \rightarrow e^+\nu_e\pi^0$ is absent because $E_e^{max}(K_{e3}) = 228$ MeV. The combined result of both experiments is [3] [2]

$$\Gamma(SD^+)/\Gamma(K_{\mu 2}) = (2.4 \pm 0.36) \cdot 10^{-5}. \tag{1.28}$$

For SD^-, the bound

$$\Gamma(SD^-)/\Gamma_{total} < 1.6 \cdot 10^{-4} \tag{1.29}$$

has been obtained from a sample of electrons with energies 220 MeV $\leq E_e \leq$ 230 MeV [2]. Using (1.21,1.22), the result (1.28) leads to

$$M_K \mid V + A \mid = 0.105 \pm 0.008\ . \tag{1.30}$$

The bound (1.29) on the other hand implies [2]

$$\mid V - A \mid / \mid V + A \mid < \sqrt{11}, \tag{1.31}$$

from where one concludes [2] that γ_K is outside the range -1.86 to -0.54,

$$\gamma_K \notin [-1.86, -0.54]\ . \tag{1.32}$$

[3] In all four experiments [5, 2, 3, 6] discussed here and below , the form factors A and V have been treated as constants.

Table 1.2: Measured branching ratios $\Gamma(K \to l\nu_l\gamma)/\Gamma_{\text{total}}$. The $K_{e2\gamma}$ data are from [5, 2], the $K_{\mu 2\gamma}$ data from [3, 6]. The last column corresponds [3] to the cut (1.20).

	SD^+	SD^-	INT^+	$SD^- + INT^-$	total
$K_{e2\gamma}$	$(1.52 \pm 0.23) \cdot 10^{-5}$	$< 1.6 \cdot 10^{-4}$			
$K_{\mu 2\gamma}$	$< 3 \cdot 10^{-5}$		$< 2.7 \cdot 10^{-5}$ (modulus)	$< 2.6 \cdot 10^{-4}$ (modulus)	$(3.02 \pm 0.10) \cdot 10^{-3}$

As we already mentioned, the interference terms $INT^{\pm}$ in $K \to e\nu_e\gamma$ are small and can hardly ever be measured. As a result of this, the amplitudes A, V and the ratio γ_K determined from $K_{e2\gamma}$ are subject to the ambiguities (1.25), (1.27).

$\underline{K^+ \to \mu^+\nu_\mu\gamma}$

Here, the interference terms $INT^{\pm}$ are nonnegligible in appropriate regions of phase space (see Figs. (1.1,1.2)). Therefore, this decay allows one in principle to pin down V and A. The PDG uses data from two experiments [3, 6]. In [3], the momentum spectrum of the muon was measured in the region (1.20). In total 2 ± 3.44 SD^+ events have been found with 216 MeV/c $< p_\mu <$ 230 MeV/c and $E_\gamma >$ 100 MeV, which leads to

$$M_K \mid V + A \mid < 0.16 \ . \tag{1.33}$$

In order to identify the effect of the SD^- terms, the region 120 MeV/c $< p_\mu <$150 MeV/c was searched. Here, the background from $K_{\mu 3}$ decays was very serious. The authors found 142 $K_{\mu\nu\gamma}$ candidates and conclude that

$$-1.77 < M_K(V - A) < 0.21. \tag{1.34}$$

The result (1.33) is consistent with (1.30), and the bound (1.34) is worse than the result (1.31) obtained from $K_{e2\gamma}$. The branching ratios which follow [3] from (1.33,1.34) are displayed in table 1.2, where we also show the $K_{e2\gamma}$ results [5, 2]. The entry $SD^- + INT^-$ for $K_{\mu 2\gamma}$ is based on additional constraints from $K_{e2\gamma}$ [3].

1.5 Theory

The amplitudes $A(W^2)$ and $V(W^2)$ have been worked out in the framework of various approaches, viz., current algebra, PCAC, resonance exchange, dispersion relations, ... For a rather detailed review together with an extensive list of references up to 1976 see [7]. Here, we concentrate on the predictions of V, A in the framework of CHPT.

A) Chiral expansion to one loop

The amplitudes A and V have been evaluated [8, 9] in the framework of CHPT to one loop. At leading order in the low-energy expansion, one has

$$A = V = 0. \tag{1.35}$$

As a consequence of this, the rate is entirely given by the IB contribution at leading order. At the one-loop level, one finds

$$\begin{aligned} A &= -\frac{4}{F}(L_9^r + L_{10}^r) \\ V &= -\frac{1}{8\pi^2}\frac{1}{F} \\ \gamma_K &= 32\pi^2(L_9^r + L_{10}^r)\,, \end{aligned} \tag{1.36}$$

where L_9^r and L_{10}^r are the renormalized low-energy couplings evaluated at the scale μ (the combination $L_9^r + L_{10}^r$ is scale independent). The vector form factor stems from the Wess-Zumino term [10] which enters the low-energy expansion at order p^4, see section 1.

Remarks:

(i) At this order in the low-energy expansion, the form factors A, V do not exhibit any W^2-dependence. A nontrivial W^2-dependence only occurs at the next order in the energy expansion (two-loop effect, see the discussion below). Note that the available analyses of experimental data of $K \to l\nu_l\gamma$ decays [5, 2, 3, 6] use constant form factors throughout.

(ii) Once the combination $L_9 + L_{10}$ has been pinned down from other processes, Eq. (1.36) allows one to evaluate A, V unambiguously at this order in the low-energy expansion. Using $L_9 + L_{10} = 1.4 \cdot 10^{-3}$ and $F = F_\pi$, one has

$$\begin{aligned} M_K(A+V) &= -0.097 \\ M_K(V-A) &= -0.037 \\ \gamma_K &= 0.45\ . \end{aligned} \tag{1.37}$$

The result for the combination $(A + V)$ agrees with (1.30) within the errors, while γ_K is consistent with (1.32).

We display in table 1.3 the branching ratios BR_I (1.21) which follow from the prediction (1.37). These predictions satisfy of course the inequalities found from experimental data (see table 1.2).

Table 1.3: Chiral prediction at order p^4 for the branching ratios $\Gamma(K \to l\nu_l\gamma)/\Gamma_{\text{total}}$. The cut used in the last column is given in Eq. (1.20).

	SD^+	SD^-	INT^+	INT^-	total
$K_{e2\gamma}$	$1.30 \cdot 10^{-5}$	$1.95 \cdot 10^{-6}$	$6.64 \cdot 10^{-10}$	$-1.15 \cdot 10^{-8}$	$2.34 \cdot 10^{-6}$
$K_{\mu 2\gamma}$	$9.24 \cdot 10^{-6}$	$1.38 \cdot 10^{-6}$	$1.44 \cdot 10^{-5}$	$-3.83 \cdot 10^{-5}$	$3.08 \cdot 10^{-3}$

B) W^2-dependence of the form factors

The chiral prediction gives constant form factors at order p^4. Terms of order p^6 have not yet been calculated. They would, however, generate a nontrivial W^2 - dependence both in V and A. In order to estimate the magnitude of these corrections, we consider one class of p^6 - contributions: terms which are generated by vector and axial vector resonance exchange with strangeness [7, 11],

$$V(W^2) = \frac{V}{1 - W^2/M_{K^*}{}^2} \quad , \quad A(W^2) = \frac{A}{1 - W^2/M_{K_1}{}^2} \tag{1.38}$$

where V, A are given in (1.36). We now examine the effect of the denominators in (1.38) in the region $y \geq 0.95, x \geq 0.2$ which has been explored in $K^+ \to e^+\nu_e\gamma$ [2]. We put $m_e = 0$ and evaluate the rate

$$\frac{dP(x)}{dx} = \frac{N_{\text{tot}}}{\Gamma_{\text{tot}}} \int_{y=0.95}^{1} \rho_{SD^+}(x,y)dy \tag{1.39}$$

where N_{tot} denotes the total number of K^+ decays considered, and $\Gamma_{\text{tot}}^{-1} = 1.24 \cdot 10^{-8}$ sec.

The function $\frac{dP(x)}{dx}$ is displayed in Fig. (1.3) for three different values of M_{K^*} and M_{K_1}, with $N_{\text{tot}} = 9 \cdot 10^9$. The total number of events

$$N_P = \int_{x=0.2}^{1} dP(x) \tag{1.40}$$

is also indicated in each case. The difference between the dashed and the dotted line shows that the nearby singularity in the anomaly form factor influences the decay rate substantially at low photon energies. The effect disappears at $x \to 1$, where $W^2 = M_K^2(1-x) \to 0$. To minimize the effect of resonance exchange, the large x-region should thus be considered. The low x-region, on the other hand, may be used to explore the W^2-dependence of V and of A. For a rather exhaustive discussion of the relevance of this W^2 - dependence for the analysis of $K_{l2\gamma}$ decays we refer the reader to Ref. [7].

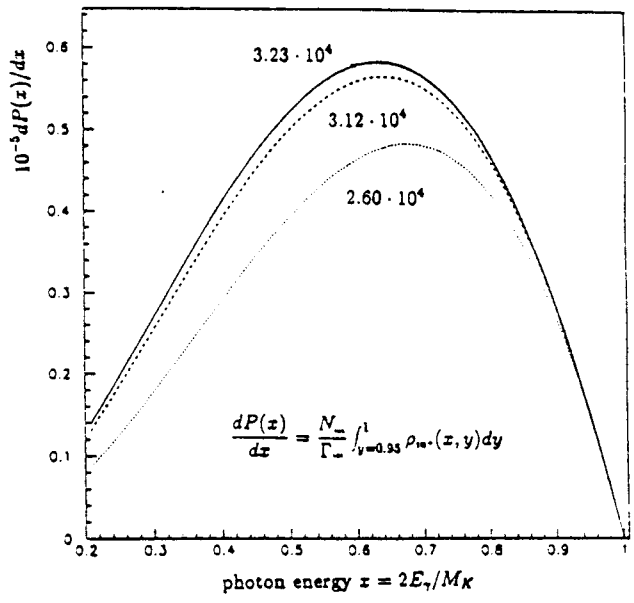

Figure 1.3: The rate $dP(x)/dx$ in (1.39), evaluated with the form factors (1.38) and $N_{tot} = 9 \cdot 10^9$. The solid line corresponds to $M_{K^*} = 890$ MeV, $M_{K_1} = 1.3$ GeV. The dashed line is evaluated with $M_{K^*} = 890$ MeV, $M_{K_1} = \infty$ and the dotted line corresponds to $M_{K^*} = M_{K_1} = \infty$. The total number of events is also indicated in each case.

1.6 Improvements at DAFNE

Previous experiments have used various cuts in phase space in order (i) to identify the individual contributions IB, $SD^{\pm}$, $INT^{\pm}$ as far as possible, and (ii) to reduce the background from K_{l3} decays. This background has in fact forced so severe cuts that only the upper end of the lepton spectrum remained.

The experimental possibilities to reduce background from K_{l3} decays are presumably more favourable with today's techniques. Furthermore, the annual yield of $9 \cdot 10^9 K^+$ decays at DAFNE is more than two orders of magnitude higher than the samples which were available in [2, 3, 5, 6]. This allows for a big improvement in the determination of the amplitudes A and V, in particular in $K_{\mu 2\gamma}$ decays. It would be very interesting to pin down the combination $L_9 + L_{10}$ of the low-energy constants which occur in the chiral representation of the amplitude A and to investigate the W^2-dependence of the form factors.

2 The decays $K^{\pm} \to l^{\pm}\nu l'^{+}l'^{-}$

Here we consider decays where the photon turns into a lepton-anti-lepton pair,

$$\begin{aligned} K^+ &\to e^+\nu\mu^+\mu^- && (2.1)\\ K^+ &\to \mu^+\nu e^+e^- && (2.2)\\ K^+ &\to e^+\nu e^+e^- && (2.3)\\ K^+ &\to \mu^+\nu\mu^+\mu^- \ . && (2.4) \end{aligned}$$

2.1 Matrix elements

We start with the processes (2.1) and (2.2),

$$\begin{aligned} K^+(p) &\to l^+(p_l)\nu(p_\nu)l'^+(p_1)l'^-(p_2) \\ (l,l') &= (e,\mu) \text{ or } (\mu,e). \end{aligned} \qquad (2.5)$$

The matrix element is

$$T = -iG_F e V_{us}^* \bar{\epsilon}_\rho \left\{ F_K \overline{L}^\rho - \overline{H}^{\rho\mu} l_\mu \right\} \qquad (2.6)$$

where

$$\begin{aligned} \overline{L}^\mu &= m_l \overline{u}(p_\nu)(1+\gamma_5)\left\{ \frac{2p^\mu - q^\mu}{2pq - q^2} - \frac{2p_l^\mu + \not{q}\gamma^\mu}{2p_l q + q^2} \right\} v(p_l) \\ l^\mu &= \overline{u}(p_\nu)\gamma^\mu(1-\gamma_5)v(p_l) \\ \overline{H}^{\rho\mu} &= iV_1\epsilon^{\rho\mu\alpha\beta}q_\alpha p_\beta - A_1(qWg^{\rho\mu} - W^\rho q^\mu) \\ &\quad -A_2(q^2 g^{\rho\mu} - q^\rho q^\mu) - A_4(qWq^\rho - q^2 W^\rho)W^\mu \end{aligned} \qquad (2.7)$$

with

$$A_4 = \frac{2F_K}{M_K^2 - W^2}\frac{F_V^K(q^2) - 1}{q^2} + A_3 \ . \qquad (2.8)$$

The form factors $A_i(q^2, W^2)$, $V_1(q^2, W^2)$ are the ones defined in appendix C. $F_V^K(q^2)$ is the electromagnetic form factor of the K^+. Finally the quantity $\bar{\epsilon}^\mu$ stands for

$$\bar{\epsilon}^\mu = \frac{e}{q^2}\overline{u}(p_2)\gamma^\mu v(p_1) \ , \qquad (2.9)$$

and the four-momenta are

$$q = p_1 + p_2, \ W = p_l + p_\nu = p - q \qquad (2.10)$$

such that $q_\mu \bar{\epsilon}^\mu = 0$.

In order to obtain the matrix element for (2.3) and (2.4),

$$K^+(p) \to l^+(p_l)\nu(p_\nu)l^+(p_1)l^-(p_2) \ , \qquad (2.11)$$

one identifies m_l and m_l' in (2.6) and subtracts the contribution obtained from interchanging $p_1 \leftrightarrow p_l$:

$$\begin{aligned} (p_1, p_l) &\rightarrow (p_l, p_1) \\ q &\rightarrow p_l + p_2 \\ W &\rightarrow p - q = p_\nu + p_1 \ . \end{aligned} \tag{2.12}$$

2.2 Decay distributions

The decay width is given by

$$d\Gamma = \frac{1}{2M_K(2\pi)^8} \sum_{spins} |T^2| d_{LIPS}(p; p_l, p_\nu, p_1, p_2) \tag{2.13}$$

and the total rate is the integral over this for the case $l \neq l'$. For the case $l = l'$ the integral has to be divided by the factor 2 for two identical particles in the final state.

We first consider the case where $l \neq l'$ and introduce the dimensionless variables

$$\begin{aligned} x &= \frac{2pq}{M_K^2} \\ y &= \frac{2p_l p}{M_K^2} \\ z &= \frac{q^2}{M_K^2} \\ r_l &= \frac{m_l^2}{M_K^2} \\ r_l' &= \frac{m_{l'}^2}{M_K^2} \ . \end{aligned} \tag{2.14}$$

Then one obtains, after integrating over p_1 and p_2 at fixed q^2 [12],

$$\begin{aligned} d\Gamma_{K^+ \rightarrow l^+ \nu l'^+ l'^-} &= \alpha^2 G_F^2 |V_{us}|^2 M_K^5 F(z, r_l') \left\{ - \sum_{spins} \overline{T}_\mu^* \overline{T}^\mu \right\} dx dy dz \\ F(z, r_l') &= \frac{1}{192\pi^3 z} \left\{ 1 + \frac{2r_l'}{z} \right\} \sqrt{1 - \frac{4r_l'}{z}} \\ \overline{T}^\mu &= M_K^{-2} \left\{ F_K \overline{L}^\mu - \overline{H}^{\mu\nu} l_\nu \right\} . \end{aligned} \tag{2.15}$$

The quantity $\left\{ - \sum_{spins} \overline{T}_\mu^* \overline{T}^\mu \right\}$ is displayed in appendix D. This result allows one to evaluate, e.g., the distribution $d\Gamma/dz$ of produced $l'^+ l'^-$ pairs rather easily. The

kinematically allowed region is

$$\begin{aligned} 4r_l' \leq\ & z & \leq 1 + r_l - 2\sqrt{r_l} \\ 2\sqrt{z} \leq\ & x & \leq 1 + z - r_l \\ A - B \leq\ & y & \leq A + B \end{aligned} \tag{2.16}$$

with

$$\begin{aligned} A &= \frac{(2-x)(1+z+r_l-x)}{2(1+z-x)} \\ B &= \frac{(1+z-x-r_l)\sqrt{x^2-4z}}{2(1+z-x)} \ . \end{aligned} \tag{2.17}$$

The case $l = l'$ is slightly more elaborate. We feel that it does not make sense to display the term $\sum_{spins} |T|^2$ because it is of considerable complexity in the general case when all the form factors A_i, V_1 and F_V^K are q^2 and W^2 dependent. The expression together with the Monte Carlo program to do the phase space integrals is available on request from the authors.

2.3 Theory

The form factors A_i, V_1 and F_V^K have been discussed in all kinds of models, Vector Meson Dominance, hard meson, etc.. For a discussion see Ref. [7]. We will restrict ourselves to the predictions in the framework of CHPT.

To leading order we have

$$\begin{aligned} V_1 &= 0 \\ A_1 = A_2 &= A_3 = 0 \ . \end{aligned} \tag{2.18}$$

We also have $F_V^K = 1$. The rate here is entirely given by the inner Bremsstrahlung contribution. At the one-loop level several form factors get non-zero values [9]

$$\begin{aligned} V_1 &= -\frac{1}{8\pi^2 F} \\ A_1 &= -\frac{4}{F}(L_9^r + L_{10}^r) \\ A_2 &= -\frac{2F_K(F_V^K(q^2)-1)}{q^2} \\ A_3 &= 0 \\ F_V^K(q^2) &= 1 + H_{\pi\pi}(q^2) + 2H_{KK}(q^2) \ . \end{aligned} \tag{2.19}$$

These results obey the current algebra relation of Ref. [7]. The function $F_V^K(q^2)$ does, however, deviate somewhat from the linear parametrization often used. The function $H(t)$ is defined in appendix B.

Table 2.1: Theoretical values for the branching ratios for the decay $K^+ \to \mu^+\nu e^+e^-$ for various cuts.

	tree level	form factors as given by CHPT
full phase space	$2.49 \cdot 10^{-5}$	$2.49 \cdot 10^{-5}$
$z \leq 10^{-3}$	$2.07 \cdot 10^{-5}$	$2.07 \cdot 10^{-5}$
$z \geq 10^{-3}$	$4.12 \cdot 10^{-6}$	$4.20 \cdot 10^{-6}$
$z \geq (20\ MeV/M_K)^2$	$3.15 \cdot 10^{-6}$	$3.23 \cdot 10^{-6}$
$z \geq (140\ MeV/M_K)^2$	$4.98 \cdot 10^{-8}$	$8.51 \cdot 10^{-8}$
$x \geq 40\ MeV/M_K$	$1.58 \cdot 10^{-5}$	$1.58 \cdot 10^{-5}$

The fact that the form factors at next-to-leading order could be written in terms of the kaon electromagnetic form factor in a simple way is not true anymore at the p^6 level. The Lagrangian at order p^6 contains a term of the form

$$\mathrm{tr}\left\{D_\alpha F_L^{\alpha\mu} U^\dagger D^\beta F_{R\beta\mu} U\right\} \tag{2.20}$$

that contributes to A_2 and A_3 but not to the kaon electromagnetic form factor, $F_V^K(q^2)$.

2.4 Numerical results

Using the formulas of the previous subsections and appendix D we have calculated the rates for a few cuts, including those given in the literature. For the case of unequal leptons, the results are given in table 2.1 for the decay $K^+ \to \mu^+\nu e^+e^-$. These include the cuts used in Refs. [12] and [13], $x \geq 40\ MeV/M_K$ and $z \geq (140\ MeV/M_K)^2$, respectively. It can be seen that for this decay most of the branching ratio is generated at very low electron-positron invariant masses. As can be seen from the result for the cuts used in Ref. [13], the effect of the structure dependent terms is most visible at high invariant electron-positron invariant mass. Our calculation, including the effect of the form factors agrees well with their data. We disagree, however, with the numerical result obtained by Ref. [12] by about an order of magnitude.

For the decay $K^+ \to e^+\nu\mu^+\mu^-$, we obtain for the tree level or IB contribution a branching ratio

$$BR_{IB}(K^+ \to e^+\nu\mu^+\mu^-) = 3.06 \cdot 10^{-12} \tag{2.21}$$

and, including the form factors,

$$BR_{total}(K^+ \to e^+\nu\mu^+\mu^-) = 1.12 \cdot 10^{-8}. \tag{2.22}$$

Here the structure dependent terms are the leading contribution since the inner Bremsstrahlung contribution is helicity suppressed as can be seen from the factor m_l in $\overline{L_\mu}$.

Table 2.2: Theoretical values for the branching ratios for the decay $K^+ \to e^+\nu e^+e^-$ for various cuts.

	tree level	form factors as given by CHPT
full phase space	$\approx 4 \cdot 10^{-9}$	$1.8 \cdot 10^{-7}$
$z,\ z_1 \geq 10^{-3}$	$3.0 \cdot 10^{-10}$	$1.22 \cdot 10^{-7}$
$z,\ z_1 \geq (50\ MeV/M_K)^2$	$5.2 \cdot 10^{-11}$	$8.88 \cdot 10^{-8}$
$z,\ z_1 \geq (140\ MeV/M_K)^2$	$2.1 \cdot 10^{-12}$	$3.39 \cdot 10^{-8}$

For the decays with identical leptons we obtain for the muon case a branching ratio of

$$BR_{total}(K^+ \to \mu^+\nu\mu^+\mu^-) = 1.35 \cdot 10^{-8} \tag{2.23}$$

for the full phase space including the effects of the form factors. The inner Bremsstrahlung or the tree level branching ratio for this decay is

$$BR_{IB}(K^+ \to \mu^+\nu\mu^+\mu^-) = 3.79 \cdot 10^{-9}. \tag{2.24}$$

For the decay with two positrons and one electron the integration over full phase space for the tree level results is very sensitive to the behaviour for small pair masses. We have given the tree level and the full prediction, including form factor effects in table 2.2. The cuts are always on both invariant masses :

$$\begin{aligned} z &= (p_1 + p_2)^2/M_K^2 \\ z_1 &= (p_l + p_2)^2/M_K^2\ . \end{aligned} \tag{2.25}$$

The values for the masses used are those of K^+ and π^+. For L_9 and L_{10} we used the values given in section 1,

$$\begin{aligned} L_9^r(M_\rho) &= 6.9 \cdot 10^{-3} \\ L_{10}^r(M_\rho) &= -5.5 \cdot 10^{-3}\ . \end{aligned} \tag{2.26}$$

2.5 Present experimental status

Only decays with an electron positron pair in the final state, decays (2.2) and (2.3), have been observed.

Both have been measured in the same experiment [13]. The decay $K^+ \to \mu^+\nu e^+e^-$ was measured with a branching ratio of $(1.23 \pm 0.32) \cdot 10^{-7}$ with a lower cut on the electron positron invariant mass of 140 MeV. The measurement is compatible with our calculation including the form factor effects for the relevant region of phase space. This measurement was then extrapolated [13] using the result of [12] to the full phase space. Since we disagree with that calculation, we also disagree with the extrapolation.

In the same experiment, 4 events of the type $K^+ \to e^+\nu e^+e^-$ were observed where both electron positron pair invariant masses were above 140 MeV. This corresponds to a branching ratio for this region of phase space of $(2.8^{+2.8}_{-1.4}) \cdot 10^{-8}$. This result is compatible within errors with our calculation, see table 2.2. The matrix element of Ref. [12] was again used for the extrapolation to full phase space[13]. Apart from our numerical disagreement, the calculation of Ref. [12] was for the case of non-identical leptons and cannot be applied here.

For the decay $K^+ \to \mu^+\nu\mu^+\mu^-$ an upper limit of $4.1 \cdot 10^{-7}$ exists [14]. This upper limit is compatible with our theoretical result, Eq. (2.23).

The decay $K^+ \to e^+\nu\mu^+\mu^-$ has not been looked for so far and should be within the capabilities of DAFNE given the branching ratio predicted in the previous subsection. This decay proceeds almost entirely through the structure dependent terms and is as such a good test of our calculation.

2.6 Improvements at DAFNE

The decays discussed in this subsection, $K^+ \to l^+\nu l^+l^-$, are complementary to the decays $K^+ \to l^+\nu\gamma$. As was the case for the analogous decay, $\pi^+ \to e^+\nu e^+e^-$ [15], it may be possible to explore phase space more easily with this process than with $K^+ \to l^+\nu\gamma$ to resolve ambiguities in the form factors.

As can be seen from our predictions, tables 2.1 and 2.2, all the decays considered in this subsection should be observable at DAFNE. Large improvements in statistics are possible since less severe cuts than those used in the past experiments should be possible. In the decays with a $\mu^+\mu^-$ pair and the decay $K^+ \to e^+\nu e^+e^-$ the effects of the form factors are already large in the total rates and should be easily visible at DAFNE. In the decay $K^+ \to \mu^+\nu e^+e^-$ most of the total rate is for small invariant mass of the pair and is given by the inner Bremsstrahlung contribution. There are, however, regions of phase space where the form factor effects are large and DAFNE should have enough statistics to be able to study these regions.

3 K_{l3} decays

The decay channels considered in this subsection are

$$K^+(p) \rightarrow \pi^0(p')l^+(p_l)\nu_l(p_\nu) \qquad [K^+_{l3}] \tag{3.1}$$
$$K^0(p) \rightarrow \pi^-(p')l^+(p_l)\nu_l(p_\nu) \qquad [K^0_{l3}] \tag{3.2}$$

and their charge conjugate modes. The symbol l stands for μ or e. We do not consider electromagnetic corrections and correspondingly set $\alpha = 0$ throughout this subsection.

3.1 Matrix elements and kinematics

The matrix element for K^+_{l3} has the general structure

$$T = \frac{G_F}{\sqrt{2}} V^*_{us} l^\mu F_\mu{}^+(p',p) \tag{3.3}$$

with

$$\begin{aligned} l^\mu &= \bar{u}(p_\nu)\gamma^\mu(1-\gamma_5)v(p_l) \\ F_\mu{}^+(p',p) &= < \pi^0(p') \mid V_\mu^{4-i5}(0) \mid K^+(p) > \\ &= \frac{1}{\sqrt{2}}[(p'+p)_\mu f_+^{K^+\pi^0}(t) + (p-p')_\mu f_-^{K^+\pi^0}(t)]. \end{aligned} \tag{3.4}$$

To obtain the matrix element for K^0_{l3} , one replaces F^+_μ by

$$\begin{aligned} F_\mu{}^0(p',p) &= < \pi^-(p') \mid V_\mu^{4-i5}(0) \mid K^0(p) > \\ &= (p'+p)_\mu f_+^{K^0\pi^-}(t) + (p-p')_\mu f_-^{K^0\pi^-}(t). \end{aligned} \tag{3.5}$$

The processes (3.1) and (3.2) thus involve the four K_{l3} form factors $f_\pm^{K^+\pi^0}(t)$, $f_\pm^{K^0\pi^-}(t)$ which depend on

$$t = (p'-p)^2 = (p_l+p_\nu)^2, \tag{3.6}$$

the square of the four momentum transfer to the leptons.

Let $f_\pm^{K\pi} = f_\pm^{K^+\pi^0}$ or $f_\pm^{K^0\pi^-}$. $f_+^{K\pi}$ is referred to as the vector form factor, because it specifies the P-wave projection of the crossed channel matrix elements $< 0 \mid V_\mu^{4-i5}(0) \mid K^+, \pi^0$ in $>$. The S-wave projection is described by the scalar form factor

$$f_0^{K\pi}(t) = f_+^{K\pi}(t) + \frac{t}{M_K^2 - M_\pi^2} f_-^{K\pi}(t) \ . \tag{3.7}$$

Analyses of K_{l3} data frequently assume a linear dependence

$$f_{+,0}^{K\pi}(t) = f_+^{K\pi}(0)\left[1 + \lambda_{+,0}\frac{t}{M^2_{\pi^+}}\right] \ . \tag{3.8}$$

For a discussion of the validity of this approximation see [16, 1] and references cited therein. Eq. (3.8) leads to a constant $f_-^{K\pi}(t)$,

$$f_-^{K\pi}(t) = f_-^{K\pi}(0) = f_+^{K\pi}(0)(\lambda_0 - \lambda_+)\frac{M_K^2 - M_\pi^2}{M_{\pi+}^2}. \tag{3.9}$$

The form factors $f_{+,0}^{K\pi}(t)$ are analytic functions in the complex t-plane cut along the positive real axis. The cut starts at $t = (M_K + M_\pi)^2$. In our phase convention, the form factors are real in the physical region

$$m_l^2 \leq t \leq (M_K - M_\pi)^2. \tag{3.10}$$

The kinematics of (spin averaged) K_{l3} decays needs two variables, for which we choose

$$y = 2pp_l/M_K^2 \ , \ \ z = 2pp'/M_K^2 = (-t + M_\pi^2 + M_K^2)/M_K^2 \ . \tag{3.11}$$

In the K rest frame, y (z) is proportional to the charged lepton (pion) energy,

$$y = 2E_l/M_K \ , \ \ z = 2E_\pi/M_K \ . \tag{3.12}$$

The physical region for y and z is

$$\begin{aligned} 2\sqrt{r_l} \leq \ & y \ \leq 1 + r_l - r_\pi \\ A(y) - B(y) \leq \ & z \ \leq A(y) + B(y) \\ A(y) \ = \ & (2-y)(1 + r_l + r_\pi - y)/[2(1 + r_l - y)] \\ B(y) \ = \ & \sqrt{y^2 - 4r_l}(1 + r_l - r_\pi - y)/[2(1 + r_l - y)] \\ r_l \ = \ & m_l^2/M_K^2, r_\pi = M_\pi^2/M_K^2. \end{aligned} \tag{3.13}$$

or, equivalently,

$$\begin{aligned} 2\sqrt{r_\pi} \leq \ & z \ \leq 1 + r_\pi - r_l \\ C(z) - D(z) \leq \ & y \ \leq C(z) + D(z) \\ C(z) \ = \ & (2-z)(1 + r_\pi + r_l - z)/[2(1 + r_\pi - z)] \\ D(z) \ = \ & \sqrt{z^2 - 4r_\pi}(1 + r_\pi - r_l - z)/[2(1 + r_\pi - z)] \ . \end{aligned} \tag{3.14}$$

3.2 Decay rates

The differential decay rate for K_{l3}^+ is given by

$$d\Gamma \ = \ \frac{1}{2M_K(2\pi)^5} \sum_{spins} |T|^2 d_{LIPS}(p; p_l, p_\nu, p') \ . \tag{3.15}$$

The Dalitz plot density

$$\rho(y,z) = \frac{d^2\Gamma}{dydz} = \frac{M_K}{256\pi^3} \sum_{spins} |T|^2 \tag{3.16}$$

is a Lorentz invariant function which contains $f_{\pm}^{K^+\pi^0}$ in the following form,

$$\rho(y,z) = \frac{M_K^5 G_F^2 \mid V_{us} \mid^2}{256\pi^3} \left[A(f_+^{K^+\pi^0})^2 + B f_+^{K^+\pi^0} f_-^{K^+\pi^0} + C(f_-^{K^+\pi^0})^2\right] \tag{3.17}$$

with

$$\begin{aligned} A(y,z) &= 4(z+y-1)(1-y) + r_l[4y+3z-3] - 4r_\pi + r_l(r_\pi - r_l) \\ B(y,z) &= 2r_l(3-2y-z+r_l-r_\pi) \\ C(y,z) &= r_l(1+r_\pi - z - r_l). \end{aligned} \tag{3.18}$$

The quantities (A,B,C) are related to the ones quoted by the PDG [1] by

$$(A,B,C) = \frac{8}{M_K^3}(A,B,C)_{\rm PDG} \ . \tag{3.19}$$

To obtain the rate for K_{l3}^0, one replaces in (3.17) $f_{\pm}^{K^+\pi^0}$ by $\sqrt{2} f_{\pm}^{K^0\pi^-}$.

For convenience we also display the $K_{\mu 3}/K_{e3}$ rates evaluated in the approximation (3.8) for the form factors,

$$\begin{aligned} \Gamma(K_{\mu 3}^+)/\Gamma(K_{e3}^+) &= \frac{0.645 + 2.087\lambda_+ + 1.464\lambda_0 + 3.375\lambda_+^2 + 2.573\lambda_0^2}{1 + 3.457\lambda_+ + 4.783\lambda_+^2} \\ \Gamma(K_{\mu 3}^0)/\Gamma(K_{e3}^0) &= \frac{0.645 + 2.086\lambda_+ + 1.459\lambda_0 + 3.369\lambda_+^2 + 2.560\lambda_0^2}{1 + 3.456\lambda_+ + 4.776\lambda_+^2} \ . \end{aligned} \tag{3.20}$$

We have used the physical masses [1] in evaluating these ratios and M_{π^+} to scale the slope in both cases. The terms linear and quadratic in λ_0 are proportional to m_l^2 and therefore strongly suppressed in the electron case. We do not include them in the denominators, because these coefficients are smaller than 10^{-4}. The interference term $\lambda_0\lambda_+$ is absent by angular momentum conservation. Furthermore, one has

$$\int dy\, dz A(y,z) = \begin{cases} 0.0623 & [K_{\mu 3}^+] \\ 0.0606 & [K_{\mu 3}^0] \end{cases} \ . \tag{3.21}$$

3.3 Determination of the K_{l3} form factors

Measurements of the Dalitz plot distribution (3.17) of $K_{\mu 3}$ data allow one in principle to pin down the form factors (up to a sign) in the range $m_\mu^2 \leq t \leq (M_K - M_\pi)^2$. Measuring the $K_{\mu 3}/K_{e3}$ branching ratio and then using (3.20) gives a relationship

between λ_+ and λ_0 which is valid in the approximation (3.8). Furthermore, muon polarization experiments measure the weighted average of the ratio $f_-^{K\pi}(t)/f_+^{K\pi}(t)$ over the t range of the experiment [1, 17]. On the other hand, the electron modes K_{e3} are sensitive to $f_+^{K\pi}$ only, because the other contributions are suppressed by the factor $(m_e/M_K)^2 \simeq 10^{-6}$, see eqs. (3.17), (3.18).

Isospin breaking effects in $f_+^{K^+\pi^0}(0)$ and $f_+^{K^0\pi^-}(0)$ play a central role in the determination of the Kobayashi-Maskawa matrix element V_{us} from K_{e3} data, see [18] for a detailed discussion of this point. In the following we concentrate on the measurement of the slopes $\lambda_{+,0}$.

3.4 Previous measurements

We refer the reader to the 1982 version of the PDG [19] [4] for a critical discussion of the wealth of experimental information on $\lambda_{+,0}^{K\pi}$. Here we content ourselves with a short summary.

K_{e3}-experiments

The λ_+ values obtained are fairly consistent. The average values are

$$\begin{aligned} K_{e3}^+ &: \lambda_+ = 0.028 \pm 0.004 \quad \text{Ref.[1]} \\ K_{e3}^0 &: \lambda_+ = 0.030 \pm 0.0016 \quad \text{Ref.[1]} \ . \end{aligned} \tag{3.22}$$

$K_{\mu 3}$-experiments

The result by Donaldson et al. [20]

$$\begin{aligned} \lambda_+ &= 0.030 \pm 0.003 \\ \lambda_0 &= 0.019 \pm 0.004 \end{aligned} \tag{3.23}$$

dominates the statistics in the $K_{\mu 3}^0$ case. The λ_+ value (3.23) is consistent with the K_{e3} value (3.22). However, the situation concerning the slope λ_0 is rather unsatisfactory, as the following (chronological) list illustrates.

$$\lambda_0 = \left\{ \begin{array}{lll} 0.0341 \pm 0.0067 & [21] \\ 0.050 \pm 0.008 & [22] \\ 0.039 \pm 0.010 & [23] \\ 0.047 \pm 0.009 & [24] \\ 0.025 \pm 0.019 & [25] \\ 0.019 \pm 0.004 & [20] \ . \end{array} \right. \tag{3.24}$$

The χ^2 fit to the $K_{\mu 3}^0$ data yields $\lambda_+ = 0.034 \pm 0.005$, $\lambda_0 = 0.025 \pm 0.006$ with a $\chi^2/DF = 88/16$ [19, p.76]! The situation in the charged mode $K_{\mu 3}^+$ is slightly better [19].

[4] Please note that the most recent measurements of $\lambda_{+,0}$ go back to 1981 [1]!

3.5 Theory

The theoretical prediction of K_{l3} form factors has a long history, starting in the sixties with the current algebra evaluation of $f_{\pm}^{K^+\pi^0}$. For an early review of the subject and for references to work prior to CHPT evaluations of $f_{\pm}$ we refer the reader to [26] (see also Ref.[27]). Here we concentrate on the evaluation of the form factors in the framework of CHPT. We restrict our consideration to the isospin symmetry limit $m_u = m_d$, as a result of which one has

$$f_{\pm,0}^{K^0\pi^-}(t) = f_{\pm,0}^{K^+\pi^0}(t) \equiv f_{\pm,0}(t)\,;\; m_u = m_d \;. \tag{3.25}$$

A) Chiral prediction at one-loop order

In Ref. [16], the vector current matrix elements $< M' \mid q\gamma^\mu \frac{\lambda^a}{2} q \mid M >$ have been calculated up to and including terms of order $t = (p' - p)^2$ and of order m_u, m_d and m_s in the invariant form factors. For reasons which will become evident below, we consider here, in addition to the K_{l3} form factors, also the electromagnetic form factor of the pion

$$< \pi^+(p') \mid V_{em}^\mu(0) \mid \pi^+(p) >= (p' + p)^\mu F_V^\pi(t). \tag{3.26}$$

The low-energy representation for $F_V^\pi(t)$ [16, 28] and $f_+(t)$ [16] reads

$$\begin{aligned} F_V^\pi(t) &= 1 + 2H_{\pi\pi}(t) + H_{KK}(t) \\ f_+(t) &= 1 + \frac{3}{2}H_{K\pi}(t) + \frac{3}{2}H_{K\eta}(t). \end{aligned} \tag{3.27}$$

The quantity $H(t)$ is a loop function displayed in appendix B. It contains the low-energy constant L_9. The indices attached to $H(t)$ denote the masses running in the loop.

Since L_9 is the only unknown occurring in $F_V^\pi(t)$ and in $f_+(t)$, we need experimental information on the *slope* of one of these two form factors to obtain a parameter-free low-energy representation of the other.

The analogous low-energy representation of the scalar form factor is

$$\begin{aligned} f_0(t) &= 1 + \frac{1}{8F^2}\left(5t - 2\Sigma_{K\pi} - 3\frac{\Delta_{K\pi}^2}{t}\right)\bar{J}_{K\pi}(t) \\ &+ \frac{1}{24F^2}\left(3t - 2\Sigma_{K\pi} - \frac{\Delta_{K\pi}^2}{t}\right)\bar{J}_{K\eta}(t) \\ &+ \frac{t}{\Delta_{K\pi}}\left(\frac{F_K}{F_\pi} - 1\right). \end{aligned} \tag{3.28}$$

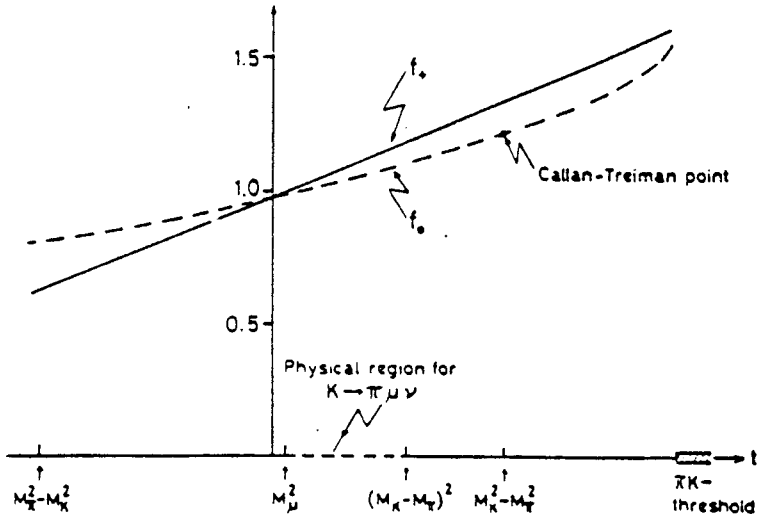

Figure 3.1: The vector and scalar form factors $f_+(t)$ and $f_0(t)$.

The function $\bar{J}(t)$ is listed in appendix B, and $\Sigma_{K\pi}$ and $\Delta_{K\pi}$ stand for

$$\begin{aligned} \Sigma_{K\pi} &= M_K^2 + M_\pi^2 \\ \Delta_{K\pi} &= M_K^2 - M_\pi^2 \ . \end{aligned} \tag{3.29}$$

The measured value [18] $F_K/F_\pi = 1.22 \pm 0.01$ may be used to obtain a parameter-free prediction of the scalar form factor $f_0(t)$.

B) Momentum dependence of the vector form factor

In the spacelike interval $\sqrt{-t} < 350$ MeV the low-energy representation (3.27) for the electromagnetic form factor $F_V^\pi(t)$ is very well approximated by the first two terms in the Taylor series expansion around $t = 0$,

$$F_V^\pi(t) = 1 + \frac{1}{6} < r^2 >_V^\pi t + \cdots \ . \tag{3.30}$$

Likewise, the linear approximation

$$f_+(t) = f_+(0) \left\{ 1 + \frac{1}{6} < r^2 >_V^{K\pi} t + \cdots \right\} \tag{3.31}$$

reproduces the low-energy representation (3.27) very well, see Fig. 3.1. This is in agreement with the observed Dalitz plot distribution, which is consistent with a form factor linear in t. The charge radii are

$$< r^2 >_V^\pi = \frac{12 L_9^r}{F^2} - \frac{1}{32\pi^2 F^2} \left\{ 2 \ln \frac{M_\pi^2}{\mu^2} + \ln \frac{M_K^2}{\mu^2} + 3 \right\}$$

$$< r^2 >_V^{K\pi} = < r^2 >_V^{\pi} - \frac{1}{64\pi^2 F^2}\left\{3h_1\left(\frac{M_\pi^2}{M_K^2}\right) + 3h_1\left(\frac{M_\eta^2}{M_K^2}\right) + \frac{5}{2}\ln\frac{M_K^2}{M_\pi^2} + \frac{3}{2}\ln\frac{M_\eta^2}{M_K^2} - 6\right\} \tag{3.32}$$

where

$$h_1(x) = \frac{1}{2}\frac{(x^3 - 3x^2 - 3x + 1)}{(x-1)^3}\ln x + \frac{1}{2}\left(\frac{x+1}{x-1}\right)^2 - \frac{1}{3}\ . \tag{3.33}$$

To evaluate these relations numerically, we use the measured charge radius of the pion:

$$< r^2 >_V^{\pi} = 0.439 \pm 0.008\text{fm}^2 \quad \text{Ref.[29]} \tag{3.34}$$

as input and obtain the prediction

$$\lambda_+ \ = \ \frac{1}{6}M_{\pi^+}^2 < r^2 >_V^{K\pi} = 0.031 \tag{3.35}$$

in agreement with the experimental results (3.22), (3.23) [5] . From this (and from the considerably more detailed discussion in Ref. [16]), one concludes, in agreement with other theoretical investigations [30], that the measured charge radii $< r^2 >_V^{\pi}$ and $< r^2 >_V^{K\pi}$ are consistent with the low-energy prediction.

C) Momentum dependence of $f_0(t)$. Dashen-Weinstein and Callan-Treiman relations

In the physical region of K_{l3} decay the low-energy representation (3.28) for the scalar form factor is approximated by the linear formula

$$f_0(t) = f_+(0)\left\{1 + \frac{1}{6} < r^2 >_S^{K\pi} t + \cdots\right\} \tag{3.36}$$

to within an accuracy of 1 %. (See Fig. 3.1). The curvature generated by higher order terms is also expected to be negligible in the physical region of the decay [16]. For the slope $< r^2 >_S^{K\pi}$ one obtains

$$\begin{aligned} < r^2 >_S^{K\pi} &= \frac{6}{M_K^2 - M_\pi^2}\left(\frac{F_K}{F_\pi} - 1\right) + \delta_2 + O(\hat{m}, m_s) \\ \delta_2 &= -\frac{1}{192\pi^2 F^2}\left\{15h_2\left(\frac{M_\pi^2}{M_K^2}\right) + \frac{19M_K^2 + 3M_\eta^2}{M_K^2 + M_\eta^2}h_2\left(\frac{M_\eta^2}{M_K^2}\right) - 18\right\} \end{aligned} \tag{3.37}$$

[5] We do not quote an error for the result (3.35), because one should estimate higher order chiral corrections for this purpose.

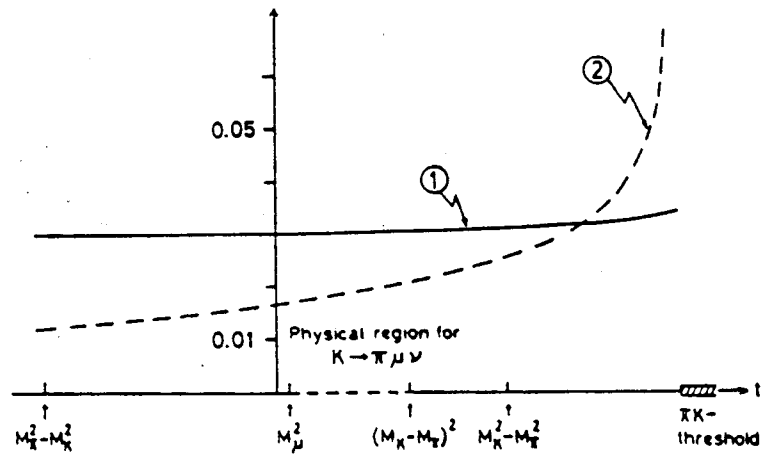

Figure 3.2: The normalized slopes of the vector and the scalar form factors. Curve 1: the normalized slope $M_{\pi^+}^2 df_+(t)/dt$. Curve 2: the normalized slope $M_{\pi^+}^2 df_0(t)/dt$. Near the πK threshold $t_0 = (M_K + M_\pi)^2$, the vector form factor behaves as $f_+(t) = f_+(t_0) + O[(t - t_0)]$, whereas $f_0(t) = f_0(t_0) + O[(\sqrt{t - t_0})]$. The slope of the scalar form factor is therefore singular at $t = (M_K + M_\pi)^2$.

where

$$\begin{aligned} h_2(x) &= \frac{3}{2}\left(\frac{1+x}{1-x}\right)^2 + \frac{3x(1+x)}{(1-x)^3}\ln x, \\ h_2(x) &= h_2\left(\frac{1}{x}\right)\ , \ h_2(1) = 1, \\ \hat{m} &= (m_u + m_d)/2\ . \end{aligned} \tag{3.38}$$

This (parameter-free) prediction is a modified version of the Dashen-Weinstein relation [31], which results if the nonanalytic contribution δ_2 is dropped. Dashen, Li, Pagels and Weinstein [32] were the first to point out that the low-energy singularities generated by the Goldstone bosons affect this relation. The modified relation is formulated as a prediction for the slope of $f_0(t)$ at the unphysical point $t_1 = M_K^2 + M_\pi^2$. Their expression for this slope however has two shortcomings: (i) it does not account for all corrections of order $\mathcal{M}$; (ii) The slope at t_1 differs substantially from the slope in the physical region of the decay [16, 33], see Fig. 3.2.

Algebraically, the correction δ_2 is of the same order in the low-energy expansion as the term involving $F_K/F_\pi - 1$. Numerically, the correction is however small: δ_2 reduces the prediction by 11 %. With $F_K/F_\pi = 1.22 \pm 0.01$ the low-energy theorem (3.37) implies

$$< r^2 >_S^{K\pi} \ = \ 0.20 \pm 0.05 \text{fm}^2$$

$$\lambda_0 \;=\; \frac{1}{6} M_{\pi^+}^2 \,<r^2>_S^{K\pi} = 0.017 \pm 0.004 \qquad (3.39)$$

where the error is an estimate of the uncertainties due to higher order contributions. The prediction (3.39) is in agreement with the high-statistics experiment [20] quoted in (3.23) but in flat disagreement with some of the more recent data listed in (3.24).

In the formulation of Dashen and Weinstein [31], the Callan-Treiman relation [34] states that the scalar form factor evaluated at $t = M_K^2 - M_\pi^2$ differs from F_K/F_π only by terms of order m_u, m_d: the quantity

$$\Delta_{\rm CT} = f_0(M_K^2 - M_\pi^2) - \frac{F_K}{F_\pi} \qquad (3.40)$$

is of order $\hat{m}$. Indeed, the low-energy representation (3.28) leads to

$$\Delta_{\rm CT} = -\frac{M_\pi^2}{2F^2}\left\{\bar{J}_{K\pi}(M_K^2 - M_\pi^2) + \frac{1}{3}\bar{J}_{K\eta}(M_K^2 - M_\pi^2)\right\} + O(\hat{m}m_s) \;. \qquad (3.41)$$

Numerically, $\Delta_{\rm CT} = -3.5 \cdot 10^{-3}$. The Callan-Treiman relation should therefore hold to a very high degree of accuracy. If the form factor is linear from $t = 0$ to $t = M_K^2 - M_\pi^2$ then the slope must be very close to

$$\lambda_0^{\rm CT} = \frac{{M_{\pi^+}}^2}{M_K^2 - M_\pi^2}\left(\frac{F_K}{F_\pi} - 1\right) = 0.019, \qquad (3.42)$$

in agreement with (3.39) and with the experimental result of Ref. [20], but in disagreement with, e.g., the value found in Ref. [22]. We see no way to reconcile the value $\lambda_0 = 0.050$ with chiral symmetry.

3.6 Improvements at DAFNE

DAFNE provides the opportunity to improve our knowledge of K_{l3} decays in a very substantial manner - in particular, it should be possible to clarify the issue of the slope λ_0 of the scalar form factor f_0. To illustrate, we compare in table 3.1 the hitherto obtained number of events (third column) with the expected ones at DAFNE (fourth column). The last column displays the remarkable increase in statistics obtainable at DAFNE.

Table 3.1: Rates of K_{l3} decays. The number of events in the third column corresponds to those data which are of relevance for the determination of the slope λ_0 of the scalar form factor.

		♯ events		
	branching ratio	Particle Data Group	DAFNE 1 year	improvement
$K^+ \rightarrow \pi^0 \mu^+ \nu_\mu$	$3.18 \cdot 10^{-2}$	10^5	$3 \cdot 10^8$	$3 \cdot 10^3$
$K_L \rightarrow \pi^\pm \mu^\mp \nu$	$27 \cdot 10^{-2}$	$4 \cdot 10^6$	$3 \cdot 10^8$	70

4 Radiative K_{l3} decays

The decay channels considered in this subsection are

$$\begin{aligned} K^+(p) &\to \pi^0(p')l^+(p_l)\nu_l(p_\nu)\gamma(q) \qquad [K^+_{l3\gamma}] \\ K^0(p) &\to \pi^-(p')l^+(p_l)\nu_l(p_\nu)\gamma(q) \qquad [K^0_{l3\gamma}] \end{aligned}$$

and the charge conjugate modes. We only consider real photons ($q^2 = 0$).

4.1 Matrix elements

The matrix element for $K^+_{l3\gamma}$ has the general structure

$$\begin{aligned} T &= \frac{G_F}{\sqrt{2}} e V_{us}^* \varepsilon^\mu(q)^* \Big\{ (V^+_{\mu\nu} - A^+_{\mu\nu})\overline{u}(p_\nu)\gamma^\nu(1-\gamma_5)v(p_l) \\ &\quad + \frac{F^+_\nu}{2p_l q}\overline{u}(p_\nu)\gamma^\nu(1-\gamma_5)(m_l - \not{p}_l - \not{q})\gamma_\mu v(p_l)\Big\} \equiv \varepsilon^{\mu *} A^+_\mu . \end{aligned} \tag{4.1}$$

The diagram of Fig. 4.1.a corresponding to the first part of Eq. (4.1) includes Bremsstrahlung off the K^+. The lepton Bremsstrahlung diagram of Fig. 4.1.b is represented by the second part of Eq. (4.1). The hadronic tensors $V^+_{\mu\nu}, A^+_{\mu\nu}$ are defined as

$$I^+_{\mu\nu} = i\int d^4x e^{iqx}\langle \pi^0(p') \mid T\{V^{em}_\mu(x) I^{4-i5}_\nu(0)\} \mid K^+(p)\rangle, \qquad I = V, A. \tag{4.2}$$

F^+_ν is the K^+_{l3} matrix element

$$F^+_\nu = \langle \pi^0(p') \mid V^{4-i5}_\nu(0) \mid K^+(p)\rangle. \tag{4.3}$$

The tensors $V^+_{\mu\nu}$ and $A^+_{\mu\nu}$ satisfy the Ward identities

$$\begin{aligned} q^\mu V^+_{\mu\nu} &= F^+_\nu \\ q^\mu A^+_{\mu\nu} &= 0 \end{aligned} \tag{4.4}$$

leading in turn to

$$q^\mu A^+_\mu = 0\ , \tag{4.5}$$

as is required by gauge invariance.

For $K^0_{l3\gamma}$, one obtains the corresponding amplitudes and hadronic tensors by making the replacements

$$\begin{aligned} K^+ &\to K^0, \qquad \pi^0 \to \pi^- \\ V^+_{\mu\nu} &\to V^0_{\mu\nu}, \qquad A^+_{\mu\nu} \to A^0_{\mu\nu} \\ F^+_\nu &\to F^0_\nu, \qquad A^+_\mu \to A^0_\mu . \end{aligned} \tag{4.6}$$

To make the infrared behaviour transparent, it is convenient to separate the tensors $V^+_{\mu\nu}, V^0_{\mu\nu}$ into two parts:

$$\begin{aligned} V^+_{\mu\nu} &= \hat{V}^+_{\mu\nu} + \frac{p_\mu}{pq} F^+_\nu \\ V^0_{\mu\nu} &= \hat{V}^0_{\mu\nu} + \frac{p'_\mu}{p'q} F^0_\nu . \end{aligned} \tag{4.7}$$

Due to Low's theorem, the amplitudes $\hat{V}^{+,0}_{\mu\nu}$ are finite for $q \to 0$. The axial amplitudes $A^{+,0}_{\mu\nu}$ are automatically infrared finite. The Ward identity (4.4) implies that the vector amplitudes $\hat{V}^{+,0}_{\mu\nu}$ are transverse:

$$q^\mu \hat{V}^{+,0}_{\mu\nu} = 0. \tag{4.8}$$

For on-shell photons, Lorentz and parity invariance together with gauge invariance allow the general decomposition (dropping the superscripts +,0 and terms that vanish upon contraction with the photon polarization vector)

$$\begin{aligned} \hat{V}_{\mu\nu} &= V_1 \left(g_{\mu\nu} - \frac{W_\mu q_\nu}{qW} \right) + V_2 \left(p'_\mu q_\nu - \frac{p'q}{qW} W_\mu q_\nu \right) \\ &\quad + V_3 \left(p'_\mu W_\nu - \frac{p'q}{qW} W_\mu W_\nu \right) + V_4 \left(p'_\mu p'_\nu - \frac{p'q}{qW} W_\mu p'_\nu \right) \\ A_{\mu\nu} &= i\varepsilon_{\mu\nu\rho\sigma}(A_1 p'^\rho q^\sigma + A_2 q^\rho W^\sigma) + i\varepsilon_{\mu\lambda\rho\sigma} p'^\lambda q^\rho W^\sigma (A_3 W_\nu + A_4 p'_\nu) \\ F_\nu &= C_1 p'_\nu + C_2 (p - p')_\nu \\ W &= p_l + p_\nu . \end{aligned} \tag{4.9}$$

With the decomposition (4.7) we can write the matrix element for $K^+_{l3\gamma}$ in (4.1) in a form analogous to Eq. (1.2) for $K_{l2\gamma}$:

$$\begin{aligned} T &= \frac{G_F}{\sqrt{2}} e V^*_{us} \varepsilon^\mu(q)^* \Big\{ (\hat{V}^+_{\mu\nu} - A^+_{\mu\nu}) \bar{u}(p_\nu) \gamma^\nu (1 - \gamma_5) v(p_l) \\ &\quad + F^+_\nu \bar{u}(p_\nu) \gamma^\nu (1 - \gamma_5) \left[\frac{p_\mu}{pq} - \frac{(\not{p}_l + \not{q} - m_l)\gamma_\mu}{2p_l q} \right] v(p_l) \Big\} . \end{aligned} \tag{4.10}$$

The four invariant vector amplitudes $V_1, \ldots, V_4$ and the four axial amplitudes $A_1, \ldots, A_4$ are functions of three scalar variables. A convenient choice for these variables is

$$E_\gamma = pq/M_K, \; E_\pi = pp'/M_K, \; W = \sqrt{W^2} \tag{4.11}$$

where W is the invariant mass of the lepton pair. The amplitudes C_1, C_2 can be expressed in terms of the K_{l3} form factors and depend only on the variable $(p-p')^2 = M_K^2 + M_\pi^2 - 2M_K E_\pi$. For the full kinematics of $K_{l3\gamma}$ two more variables are needed, e.g.

$$E_l = pp_l/M_K, \; x = p_l q/M_K^2. \tag{4.12}$$

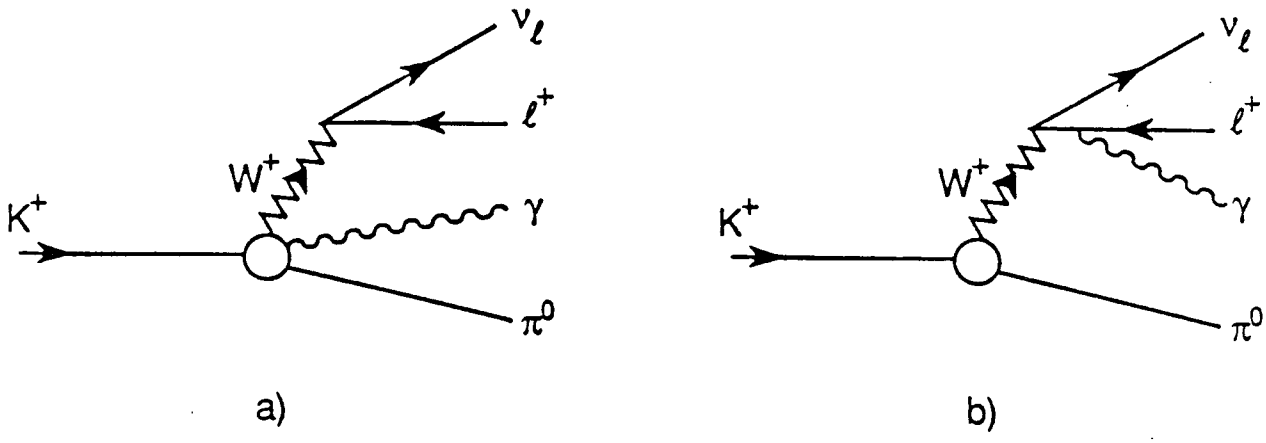

Figure 4.1: Diagrammatic representation of the $K^+_{l3\gamma}$ amplitude.

The variable x is related to the angle $\theta_{l\gamma}$ between the photon and the charged lepton in the K rest frame:

$$xM_K^2 = E_\gamma(E_l - \sqrt{E_l^2 - m_l^2}\cos\theta_{l\gamma}). \tag{4.13}$$

T invariance implies that the vector amplitudes $V_1, \ldots, V_4$, the axial amplitudes $A_1, \ldots, A_4$ and the K_{l3} form factors C_1, C_2 are (separately) relatively real in the physical region. We choose the standard phase convention in which all amplitudes are real.

For $\theta_{l\gamma} \to 0$ (collinear lepton and photon), there is a lepton mass singularity in (4.1) which is numerically relevant for $l = e$. The region of small $E_\gamma, \theta_{l\gamma}$ is dominated by the K_{l3} matrix elements. The new theoretical information of $K_{l3\gamma}$ decays resides in the tensor amplitudes $\hat{V}_{\mu\nu}$ and $A_{\mu\nu}$. The relative importance of these contributions can be enhanced by cutting away the region of low $E_\gamma, \theta_{l\gamma}$. It may turn out to be of advantage to reduce the statistics by applying more severe cuts than necessary from a purely experimental point of view.

4.2 Decay rates

The total decay rate is given by

$$\Gamma(K \to \pi l \nu \gamma) = \frac{1}{2M_K(2\pi)^8} \int d_{LIPS}(p; p', p_l, p_\nu, q) \sum_{spins} |\, T \,|^2 \tag{4.14}$$

in terms of the amplitude T in (4.1). The square of the matrix element, summed over photon and lepton polarizations, is a bilinear form in the invariant amplitudes

$V_1,\ldots,V_4$, $A_1,\ldots,A_4$, C_1, C_2. Pulling out common factors, we write (4.14) in the form

$$\Gamma(K \to \pi l \nu\gamma) = \frac{4\alpha G_F^2 \mid V_{us} \mid^2}{(2\pi)^7 M_K} \int d_{LIPS}(p;p',p_l,p_\nu,q)\; SM. \tag{4.15}$$

SM, the reduced matrix element squared, is given in App. E as a function of scalar products and invariant amplitudes. For the actual numerical calculations, we have found it useful to employ a tensor decomposition different from the one in Eqs. (4.7) and (4.9)

$$\begin{aligned} V_{\mu\nu} &= B_1 g_{\mu\nu} + B_2 W_\mu q_\nu + B_3 p'_\mu q_\nu + B_4 W_\mu p'_\nu \\ &\quad + B_5 W_\mu W_\nu + B_6 p'_\mu W_\nu + B_7 p'_\mu p'_\nu \; . \end{aligned} \tag{4.16}$$

One advantage is that (4.16) applies equally well to both charge modes while (4.7) does not. Moreover, the expression for SM in App. E is more compact when written in terms of the B_i. In the numerical evaluation of the amplitudes, gauge invariance can of course be used to express three of the B_i in terms of the remaining ones and of C_1, C_2.

To get some feeling for the magnitude of the various decay rates, let us first consider the tree level amplitudes to lowest order p^2 in CHPT. With the sign conventions of Ref.[35] exhibited in section 1, these amplitudes are [9, 36] :

$\underline{K^+_{l3\gamma}}$:

$$\begin{aligned} V^+_{\mu\nu} &= \frac{1}{\sqrt{2}}\left[g_{\mu\nu} + \frac{(p'+W)_\mu (2p'+W)_\nu}{pq}\right] \\ A^+_{\mu\nu} &= 0 \\ F^+_\nu &= \frac{1}{\sqrt{2}}(p+p')_\nu \end{aligned} \tag{4.17}$$

$\underline{K^0_{l3\gamma}}$:

$$\begin{aligned} V^0_{\mu\nu} &= -g_{\mu\nu} + \frac{p'_\mu (2p'+2q+W)_\nu}{p'q} \\ A^0_{\mu\nu} &= 0 \\ F^0_\nu &= (p+p')_\nu . \end{aligned} \tag{4.18}$$

In table 4.1 the corresponding branching ratios are presented for the four decay modes for $E_\gamma \geq 30 MeV$ and $\theta_{l\gamma} \geq 20°$. For $K^0_{l3\gamma}$, the rates are to be understood as $\Gamma(K_L \to \pi^\pm l^\mp \nu\gamma)$. The number of events correspond to the design values for DAFNE (cf. App. A).

Table 4.1: Branching ratios for tree level amplitudes for $E_\gamma \geq 30MeV$ and $\theta_{l\gamma} \geq 20°$ in the K rest frame.

decay	BR(tree)	#events/yr
$K^+_{e3\gamma}$	2.8×10^{-4}	2.5×10^6
$K^+_{\mu 3\gamma}$	1.9×10^{-5}	1.7×10^5
$K^0_{e3\gamma}$	3.6×10^{-3}	4.0×10^6
$K^0_{\mu 3\gamma}$	5.2×10^{-4}	5.7×10^5

Table 4.2: Experimental results for $K_{l3\gamma}$ decays

decay	exp.	$E_{\gamma,min}$	# events	BR	
$K^+_{e3\gamma}$	[37]	$10MeV$	192	$(2.7 \pm 0.2) \times 10^{-4}$	$0.6 < \cos\theta_{e\gamma} < 0.9$
$K^+_{e3\gamma}$	[38]	$10MeV$	13	$(3.7 \pm 1.3) \times 10^{-4}$	$-"-$
$K^+_{e3\gamma}$	[39]	$30MeV$	16	$(2.3 \pm 1.0) \times 10^{-4}$	$\cos\theta_{e\gamma} < 0.9$
$K^+_{\mu 3\gamma}$	[39]	$30MeV$	0	$< 6.1 \times 10^{-5}$	90% *c.l.*
$K^0_{e3\gamma}$	[40]	$15MeV$	10	$(1.3 \pm 0.8) \times 10^{-2}$	

4.3 Previous experiments

The data sample for $K_{l3\gamma}$ decays is very limited and it is obvious that DAFNE will be able to make significant improvements. The present experimental status is summarized in table 4.2.

A comparison between tables 4.1 and 4.2 shows the tremendous improvement in statistics to be expected at DAFNE. We shall come back to the question whether this improvement will be sufficient to test the standard model at the next-to-leading order, $O(p^4)$, in CHPT.

4.4 Theory

Prior to CHPT, the most detailed calculations of $K_{l3\gamma}$ amplitudes were performed by Fearing, Fischbach and Smith [41] using current algebra techniques.

In the framework of CHPT, the amplitudes are given by (4.17) and (4.18) to leading order in the chiral expansion.

A) CHPT to $O(p^4)$

There are in general three types of contributions [35]: anomaly, local contributions due to $\mathcal{L}_4$ and loop amplitudes.

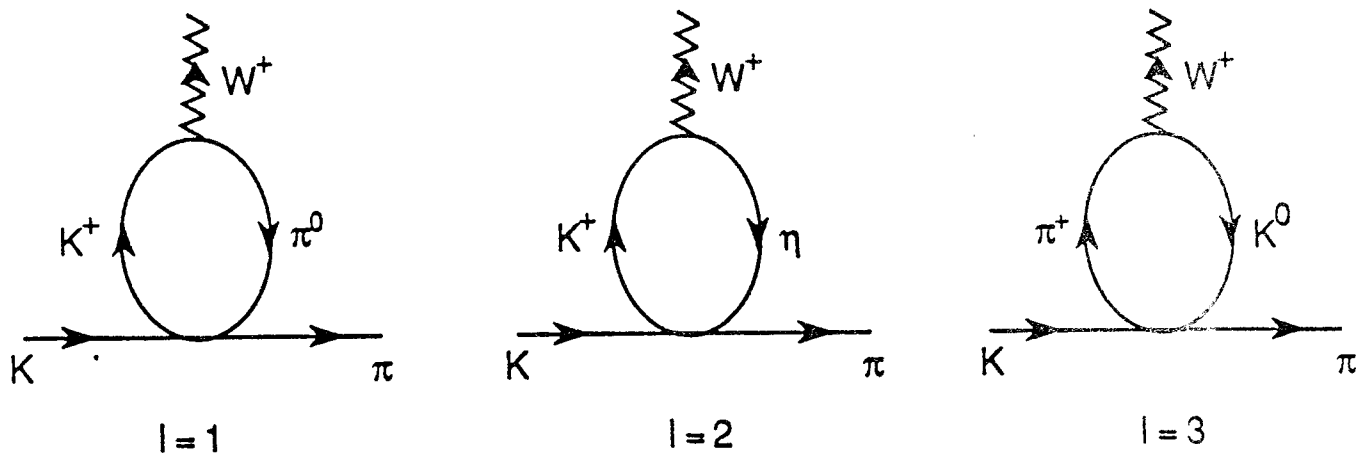

Figure 4.2: Loop diagrams (without tadpoles) for K_{l3} at $O(p^4)$. For $K_{l3\gamma}$, the photon must be appended on all charged lines and on all vertices.

The anomaly contributes to the axial amplitudes

$$\begin{aligned} A^+_{\mu\nu} &= \frac{i\sqrt{2}}{16\pi^2 F^2}\left\{\varepsilon_{\mu\nu\rho\sigma}q^\rho(4p'+W)^\sigma + \frac{4}{W^2-M_K^2}\varepsilon_{\mu\lambda\rho\sigma}W_\nu p'^\lambda q^\rho W^\sigma\right\} \quad (4.19)\\ A^0_{\mu\nu} &= -\frac{i}{8\pi^2F^2}\varepsilon_{\mu\nu\rho\sigma}q^\rho W^\sigma. \end{aligned}$$

The loop diagrams for $K_{l3\gamma}$ are shown in Fig. 4.2. We first write the K^+_{l3} matrix element in terms of three functions f_1^+, f_2^+, f_3^+ which will also appear in the invariant amplitudes V_i^+. Including the contributions from the low-energy constants L_5, L_9 in $\mathcal{L}_4$, the K_{l3} matrix element F_ν^+ is given by

$$\begin{aligned} F_\nu^+ &= f_1^+(t)p'_\nu + \left[\frac{1}{2}(M_K^2 - M_\pi^2 - t)f_2^+(t) + f_3^+(t)\right](p-p')_\nu \\ f_1^+(t) &= \sqrt{2} + \frac{4\overline{L_9}}{\sqrt{2}F^2}t + 2\sum_{I=1}^{3}(c_2^I - c_1^I)B_2^I(t) \\ f_2^+(t) &= -\frac{4\overline{L_9}}{\sqrt{2}F^2} + \frac{1}{t}\sum_{I=1}^{3}\left\{(c_1^I - c_2^I)\left[2B_2^I(t) - \frac{(t+\Delta_I)\Delta_I J_I(t)}{2t}\right] - c_2^I\Delta_I J_I(t)\right\} \\ f_3^+(t) &= \frac{F_K}{\sqrt{2}F_\pi} + \frac{1}{2t}\sum_{I=1}^{3}\left\{(c_1^I + c_2^I)(t+\Delta_I) - 2c_3^I\right\}\Delta_I J_I(t) \quad (4.20)\\ \overline{L_9} &= L_9^r(\mu) - \frac{1}{256\pi^2}\ln\frac{M_\pi M_K^2 M_\eta}{\mu^4} \\ \Delta_I &= M_I^2 - m_I^2\ ,\ t = (p-p')^2\ . \end{aligned}$$

Table 4.3: Coefficients for the $K^+_{l3\gamma}$ loop amplitudes corresponding to the diagrams $I = 1,2,3$ in Fig. 4.2. All coefficients c_i^I must be divided by $6\sqrt{2}F^2$.

I	M_I	m_I	c_1^I	c_2^I	c_3^I
1	M_K	M_π	1	-2	$-M_K^2 - 2M_\pi^2$
2	M_K	M_η	3	-6	$-M_K^2 - 2M_\pi^2$
3	M_π	M_K	0	-6	$-6M_\pi^2$

$\overline{L_9}$ is a scale independent coupling constant and we have traded the tadpole contribution together with L_5 for F_K/F_π in $f_3^+(t)$. The sum over I corresponds to the three loop diagrams of Fig. 4.2 with coefficients c_1^I, c_2^I, c_3^I displayed in table 4.3. We use the Gell-Mann–Okubo mass formula throughout to express M_η^2 in terms of M_K^2, M_π^2. The functions $J_I(t)$ and $B_2^I(t)$ can be found in App. B.

The standard K_{l3} form factors $f_+(t), f_-(t)$ as given in the previous subsection [16] are

$$\begin{aligned} f_+(t) &= \frac{1}{\sqrt{2}} f_1^+(t) \\ f_-(t) &= \frac{1}{\sqrt{2}} \left[(M_K^2 - M_\pi^2 - t) f_2^+(t) + 2 f_3^+(t) - f_1^+(t) \right]. \end{aligned} \tag{4.21}$$

It remains to calculate the infrared finite tensor amplitude $\hat{V}^+_{\mu\nu}$. The invariant amplitudes V_i^+ can be expressed in terms of the previously defined functions f_i^+ and of additional amplitudes I_1, I_2, I_3. Diagrammatically, the latter amplitudes arise from those diagrams in Fig. 4.2 where the photon is not appended on the incoming K^+ (non-Bremsstrahlung diagrams). The final expressions are

$$\begin{aligned} V_1^+ &= I_1 + p'W_q f_2^+(W_q^2) + f_3^+(W_q^2) \\ V_2^+ &= I_2 - \frac{1}{pq} \left[p'W_q f_2^+(W_q^2) + f_3^+(W_q^2) \right] \\ V_3^+ &= I_3 + \frac{1}{pq} \left[p'W f_2^+(W^2) + f_3^+(W^2) - p'W_q f_2^+(W_q^2) - f_3^+(W_q^2) \right] \\ V_4^+ &= \frac{f_1^+(W^2) - f_1^+(W_q^2)}{pq} \\ W_q &= W + q = p - p' . \end{aligned} \tag{4.22}$$

The amplitudes I_1, I_2, I_3 in Eq.(4.22) are given by

$$
\begin{aligned}
I_1 &= \frac{4qW}{\sqrt{2}F^2}(\overline{L_9}+\overline{L_{10}}) + \frac{8p'q}{\sqrt{2}F^2}\overline{L_9} \\
&\quad + \sum_{I=1}^{3}\left\{\left[(W_q^2+\Delta_I)(c_1^I+c_2^I) - 2(c_2^I p'W_q + c_3^I)\right]\left[\frac{(W_q^2-\Delta_I)\hat{J}_I}{2W_q^2} - 2G_I)\right]\right. \\
&\quad + \frac{(c_2^I-c_1^I)}{2}\left[\frac{p'W_q}{W_q^2}\left(\frac{(W_q^4-\Delta_I^2)\hat{J}_I}{W_q^2} + 4\hat{B}_2^I\right) + p'(W-q)L_m^I\right] \\
&\quad \left. + \frac{2(c_2^I-c_1^I)}{qW}\left[p'q(F_I-(W_q^2+\Delta_I)G_I) + p'W(\hat{B}_2^I - B_2^I)\right]\right\} \\
I_2 &= -\frac{8\overline{L_9}}{\sqrt{2}F^2} + \frac{2}{qW}\sum_{I=1}^{3}(c_2^I-c_1^I)\left[F_I-(W^2+\Delta_I)G_I\right] \\
I_3 &= -\frac{4\overline{L_9}}{\sqrt{2}F^2} + \sum_{I=1}^{3}\left\{2(c_2^I-c_1^I)\left[G_I + \frac{L_m^I}{4} + \frac{\hat{B}_2^I - B_2^I}{qW}\right] - c_1^I\frac{\Delta_I J_I}{W^2}\right\} \qquad (4.23) \\
\overline{L_{10}} &= L_{10}^r(\mu) + \frac{1}{256\pi^2}\ln\frac{M_\pi M_K^2 M_\eta}{\mu^4} \\
L_m^I &= \frac{\Sigma_I}{32\pi^2\Delta_I}\ln\frac{m_I^2}{M_I^2} \\
F_I &= \hat{B}_2^I - \frac{W^2}{4}L_m^I + \frac{1}{qW}\left(W^2B_2^I - W_q^2\hat{B}_2^I\right) \\
G_I &= \frac{M_I^2}{2}C(W_q^2,W^2,M_I^2,m_I^2) + \frac{1}{8qW}\left[(W_q^2+\Delta_I)\hat{J}_I - (W^2+\Delta_I)J_I\right] + \frac{1}{64\pi^2} \\
J_I &\equiv J_I(W^2),\ \hat{J}_I \equiv J_I(W_q^2) \\
B_2^I &\equiv B_2^I(W^2),\ \hat{B}_2^I \equiv B_2^I(W_q^2).
\end{aligned}
$$

The function $C(W_q^2, W^2, M_I^2, m_I^2)$ is given in App. B. All the invariant amplitudes $V_1^+, \ldots, V_4^+$ are real in the physical region. Of course, the same is true for the K_{l3} matrix element F_ν^+.

The $K_{l3\gamma}^0$ amplitude has a very similar structure. Both the K_{l3}^0 matrix element F_ν^0 and the infrared finite vector amplitude $\hat{V}_{\mu\nu}^0$ can be obtained from the corresponding quantities F_ν^+ and $\hat{V}_{\mu\nu}^+$ by the following steps:

- interchange p' and $-p$;
- replace $\frac{F_K}{F_\pi}$ by $\frac{F_\pi}{F_K}$ in f_3^+;
- insert the appropriate coefficients c_i^I for $K_{l3\gamma}^0$ listed in table 4.4;
- multiply F_ν^+ and $\hat{V}_{\mu\nu}^+$ by a factor $-\sqrt{2}$.

Table 4.4: Coefficients for the $K^0_{l3\gamma}$ loop amplitudes corresponding to the diagrams $I = 1,2,3$ in Fig. 4.2. All coefficients c_i^I must be divided by $6\sqrt{2}F^2$.

I	M_I	m_I	c_1^I	c_2^I	c_3^I
1	M_K	M_π	0	-3	$-3M_K^2$
2	M_K	M_η	6	-3	$M_K^2 + 2M_\pi^2$
3	M_π	M_K	4	-2	$-2M_K^2 + 2M_\pi^2$

Table 4.5: Branching ratios and expected number of events at DAFNE for $K^+_{l3\gamma}$.

$K^+_{e3\gamma}$	BR	#events/yr
full $O(p^4)$ amplitude	3.0×10^{-4}	2.7×10^6
tree level	2.8×10^{-4}	2.5×10^6
$O(p^4)$ without loops	3.2×10^{-4}	2.9×10^6

$K^+_{\mu3\gamma}$	BR	#events/yr
full $O(p^4)$ amplitude	2.0×10^{-5}	1.8×10^5
tree level	1.9×10^{-5}	1.7×10^5
$O(p^4)$ without loops	2.1×10^{-5}	1.9×10^5

B) Numerical results

In calculating the rates with the complete amplitudes of the previous subsection, we use the same cuts as for the tree level rates in Subsect. 4.2:

$$\begin{aligned} E_\gamma &\geq 30MeV \\ \theta_{l\gamma} &\geq 20°. \end{aligned} \tag{4.24}$$

The physical values of M_π and M_K are used in the amplitudes. M_η is calculated from the Gell-Mann–Okubo mass formula. The values of the other parameters can be found in section 1 and in appendix A.

The results for $K^+_{l3\gamma}$ and $K^0_{l3\gamma}$ are displayed in tables 4.5 and 4.6, respectively. For comparison, the tree level branching ratios of table 4.1 and the rates for the amplitudes without the loop contributions are also shown. The separation between loop and counterterm contributions is of course scale dependent. This scale dependence is absorbed in the scale invariant constants $\overline{L_9}, \overline{L_{10}}$ defined in Eqs.(4.20), (4.23). In other words, the entries in tables 4.5, 4.6 for the amplitudes without loops correspond to setting all coefficients c_i^I in tables 4.3, 4.4 equal to zero.

Table 4.6: Branching ratios and expected number of events at DAFNE for $K^0_{l3\gamma}$.

$K^0_{e3\gamma}$	BR	#events/yr
full $O(p^4)$ amplitude	3.8×10^{-3}	4.2×10^6
tree level	3.6×10^{-3}	4.0×10^6
$O(p^4)$ without loops	4.0×10^{-3}	4.4×10^6

$K^0_{\mu 3\gamma}$	BR	#events/yr
full $O(p^4)$ amplitude	5.6×10^{-4}	6.1×10^5
tree level	5.2×10^{-4}	5.7×10^5
$O(p^4)$ without loops	5.9×10^{-4}	6.5×10^5

4.5 Improvements at DAFNE

The numerical results given above demonstrate very clearly that the non-trivial CHPT effects of $O(p^4)$ can be detected at DAFNE in all four channels without any problem of statistics. Of course, the rates are bigger for the electronic modes. On the other hand, the relative size of the structure dependent terms is somewhat bigger in the muonic channels (around 8% for the chosen cuts). We observe that there is negative interference between the loop and counterterm amplitudes.

The sensitivity to the counterterm coupling constants L_9, L_{10} and to the chiral anomaly can be expressed as the difference in the number of events between the tree level and the $O(p^4)$ amplitudes (without loops). In the optimal case of $K^0_{e3\gamma}$, this amounts to more than 4×10^5 events/yr at DAFNE. Almost all of this difference is due to L_9. It will be very difficult to extract the coupling constant L_{10} from the total rates. A more detailed study is needed to determine whether L_{10} can be extracted from differential distributions.

The chiral anomaly is more important for $K^+_{l3\gamma}$, but even there it influences the total rates rather little. Once again, a dedicated study of differential rates is necessary to locate the chiral anomaly, if possible at all.

On the other hand, taking into account that L_9 is already known to good accuracy (see section 1), $K_{l3\gamma}$ decays will certainly allow for precise and unambiguous tests of the one-loop effects in CHPT [9].

5 K_{l4} decays

In this subsection we discuss the decays

$$K^+(p) \rightarrow \pi^+(p_1)\,\pi^-(p_2)\,l^+(p_l)\,\nu_l(p_\nu) \quad (5.1)$$
$$K^+(p) \rightarrow \pi^0(p_1)\,\pi^0(p_2)\,l^+(p_l)\,\nu_l(p_\nu) \quad (5.2)$$
$$K^0(p) \rightarrow \pi^0(p_1)\,\pi^-(p_2)\,l^+(p_l)\,\nu_l(p_\nu) \quad (5.3)$$

and their charge conjugate modes. The letter l stands for e or μ. We do not consider isospin violating contributions and correspondingly set $m_u = m_d$, $\alpha = 0$.

5.1 Kinematics

We start with the process (5.1). The full kinematics of this decay requires five variables. We will use the ones introduced by Cabibbo and Maksymowicz [42]. It is convenient to consider three reference frames, namely the K^+ rest system (Σ_K), the $\pi^+\pi^-$ center-of-mass system ($\Sigma_{2\pi}$) and the $l^+\nu_l$ center-of-mass system ($\Sigma_{l\nu}$). Then the variables are

1. s_π, the effective mass squared of the dipion system,
2. s_l, the effective mass squared of the dilepton system,
3. θ_π, the angle of the π^+ in $\Sigma_{2\pi}$ with respect to the dipion line of flight in Σ_K,
4. θ_l, the angle of the l^+ in $\Sigma_{l\nu}$ with respect to the dilepton line of flight in Σ_K, and
5. ϕ, the angle between the plane formed by the pions in Σ_K and the corresponding plane formed by the dileptons.

The angles θ_π, θ_l and ϕ are displayed in Fig. 5.1. In order to specify these variables more precisely, let $\vec{p}_1$ be the three-momentum of the π^+ in $\Sigma_{2\pi}$ and $\vec{p}_l$ the three-momentum of the l^+ in $\Sigma_{l\nu}$. Furthermore, let $\vec{v}$ be a unit vector along the direction of flight of the dipion in Σ_K, and $\vec{c}(\vec{d})$ a unit vector along the projection of $\vec{p}_1(\vec{p}_l)$ perpendicular to $\vec{v}(-\vec{v})$,

$$\vec{c} = (\vec{p}_1 - \vec{v}\vec{v}\cdot\vec{p}_1)/[\vec{p}_1^{\,2} - (\vec{p}_1\cdot\vec{v})^2]^{1/2}$$
$$\vec{d} = (\vec{p}_l - \vec{v}\vec{v}\cdot\vec{p}_l)/[\vec{p}_l^{\,2} - (\vec{p}_l\cdot\vec{v})^2]^{1/2} \ .$$

The vectors $\vec{v}$, $\vec{c}$ and $\vec{d}$ are indicated in Fig. 5.1. Then, one has

$$\begin{aligned} s_\pi &= (p_1+p_2)^2 \ , \ s_l = (p_l+p_\nu)^2 \\ \cos\theta_\pi &= \vec{v}\cdot\vec{p}_1/\mid\vec{p}_1\mid, \ \cos\theta_l = -\vec{v}\cdot\vec{p}_l/\mid\vec{p}_l\mid \\ \cos\phi &= \vec{c}\cdot\vec{d}, \ \sin\phi = (\vec{c}\times\vec{v})\cdot\vec{d}. \end{aligned} \quad (5.4)$$

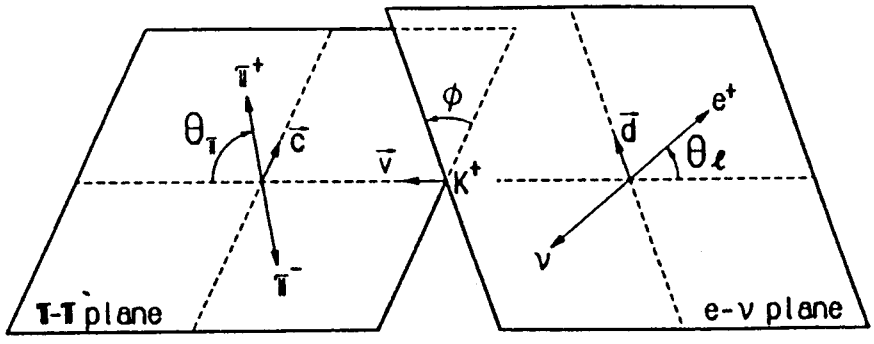

Figure 5.1: Kinematic variables for K_{l4} decays. The angle θ_π is defined in $\Sigma_{2\pi}$, θ_l in $\Sigma_{l\nu}$ and ϕ in Σ_K.

The range of the variables is

$$\begin{aligned} 4M_\pi^2 &\leq s_\pi \leq (M_K - m_l)^2 \\ m_l^2 &\leq s_l \leq (M_K - \sqrt{s_\pi})^2 \\ 0 &\leq \theta_\pi, \theta_l \leq \pi, 0 \leq \phi \leq 2\pi. \end{aligned} \tag{5.5}$$

It is useful to furthermore introduce the following combinations of four vectors

$$P = p_1 + p_2, \;\; Q = p_1 - p_2 \;, \;\; L = p_l + p_\nu \;, \;\; N = p_l - p_\nu \tag{5.6}$$

together with the corresponding Lorentz invariant scalar products

$$\begin{aligned} P^2 &= s_\pi, \;\; Q^2 = 4M_\pi^2 - s_\pi, \;\; L^2 = s_l, \;\; N^2 = 2m_l^2 - s_l, \\ PQ &= 0, \\ PL &= \frac{1}{2}(M_K^2 - s_\pi - s_l), \\ PN &= z_l PL + (1 - z_l) X \cos\theta_l, \\ QL &= \sigma_\pi X \cos\theta_\pi, \\ QN &= z_l QL + \sigma_\pi (1 - z_l) \left[PL \cos\theta_\pi \cos\theta_l \right. \\ &\quad \left. - (s_\pi s_l)^{1/2} \sin\theta_\pi \sin\theta_l \cos\phi \right] \\ LN &= m_l^2 \\ < LNPQ > &\equiv \epsilon_{\mu\nu\rho\sigma} L^\mu N^\nu P^\rho Q^\sigma \\ &= -(s_\pi s_l)^{1/2} \sigma_\pi (1 - z_l) X \sin\theta_\pi \sin\theta_l \sin\phi \end{aligned} \tag{5.7}$$

with

$$\begin{aligned} X &= ((PL)^2 - s_\pi s_l)^{1/2} = \frac{1}{2}\lambda^{1/2}(M_K^2, s_\pi, s_l) \\ z_l &= m_l^2 / s_l \\ \sigma_\pi &= (1 - 4M_\pi^2/s_\pi)^{1/2}. \end{aligned} \tag{5.8}$$

Below we will also use the variables

$$\begin{aligned} t &= (p_1 - p)^2 \\ u &= (p_2 - p)^2. \end{aligned} \tag{5.9}$$

These are related to s_π, s_l and θ_π by

$$\begin{aligned} t + u &= 2M_\pi^2 + M_K^2 + s_l - s_\pi \\ t - u &= -2\sigma_\pi X \cos\theta_\pi \ . \end{aligned} \tag{5.10}$$

5.2 Matrix elements

The matrix element for $K^+ \to \pi^+\pi^- l^+\nu_l$ is

$$T = \frac{G_F}{\sqrt{2}} V_{us}^* \bar{u}(p_\nu)\gamma_\mu(1-\gamma_5)\nu(p_l)(V^\mu - A^\mu) \tag{5.11}$$

where

$$\begin{aligned} I_\mu &= < \pi^+(p_1)\pi^-(p_2)\text{out} \mid I_\mu^{4-i5}(0) \mid K^+(p) >;\ I = V, A \\ V_\mu &= -\frac{H}{M_K^3}\epsilon_{\mu\nu\rho\sigma} L^\nu P^\rho Q^\sigma \\ A_\mu &= -i\frac{1}{M_K}[P_\mu F + Q_\mu G + L_\mu R] \end{aligned} \tag{5.12}$$

and $\epsilon_{0123} = 1$. The matrix elements for the other channels (5.2,5.3) may be obtained from (5.11,5.12) by isospin symmetry, see below.

The form factors F, G, R and H are real analytic functions of the three variables p_1p_2, p_1p and p_2p. Below, we will use instead the variables $\{s_\pi, s_l, \theta_\pi\}$ or $\{s_\pi, t, u\}$.

Remark: In order to agree with the notation used by Pais and Treiman [43] and by Rosselet et al. [44], we have changed our previous convention [45, 46] in the definition of the anomaly form factor H. See also the comments after Eq. (5.21).

5.3 Decay rates

The partial decay rate for (5.1) is given by

$$d\Gamma = \frac{1}{2M_K(2\pi)^8} \sum_{spins} \mid T \mid^2 d_{LIPS}(p; p_l, p_\nu, p_1, p_2). \tag{5.13}$$

The quantity $\sum_{spins} \mid T \mid^2$ is a Lorentz invariant quadratic form in F, G, R and H. All scalar products can be expressed in the 5 independent variables $s_\pi, s_l, \theta_\pi, \theta_l$ and ϕ, such that

$$\sum_{spins} \mid T \mid^2 = 2G_F^2 \mid V_{us} \mid^2 M_K^{-2} J_5(s_\pi, s_l, \theta_\pi, \theta_l, \phi) \ . \tag{5.14}$$

Carrying out the integrations over the remaining $4 \cdot 3 - 5 = 7$ variables in (5.13) gives [42]

$$d\Gamma_5 = G_F^2 \mid V_{us} \mid^2 N(s_\pi, s_l) J_5(s_\pi, s_l, \theta_\pi, \theta_l, \phi) ds_\pi ds_l d(\cos\theta_\pi) d(\cos\theta_l) d\phi \qquad (5.15)$$

where

$$N(s_\pi, s_l) = (1 - z_l)\sigma_\pi X/(2^{13}\pi^6 M_K^5) \ . \qquad (5.16)$$

The form factors F, G, R and H are independent of ϕ and θ_l. It is therefore possible to carry out two more integrations in (5.15) with the result

$$d\Gamma_3 = G_F^2 \mid V_{us} \mid^2 N(s_\pi, s_l) J_3(s_\pi, s_l, \theta_\pi) ds_\pi ds_l d(\cos\theta_\pi). \qquad (5.17)$$

The explicit form of J_5 is

$$\begin{aligned}
J_5 &= |F|^2 \left[(PL)^2 - (PN)^2 - s_\pi s_l + m_l^2 s_\pi\right] \\
&+ |G|^2 \left[(QL)^2 - (QN)^2 - Q^2 s_l + m_l^2 Q^2\right] \\
&+ |R|^2 \, m_l^2 \left[s_l - m_l^2\right] \\
&+ \frac{1}{M_K^4}|H|^2 \left[(m_l^2 - s_l)\left[Q^2 X^2 + s_\pi (QL)^2\right] - < LNPQ >^2\right] \\
&+ (F^* G + F G^*)\left[(PL)(QL) - (PN)(QN)\right] \\
&+ (F^* R + F R^*)\, m_l^2 \left[(PL) - (PN)\right] \\
&+ \frac{1}{M_K^2}(F^* H + F H^*)\left[(QN)(PL)^2 - (QL)(PL)(PN) - s_\pi s_l (QN) + m_l^2 s_\pi (QL)\right] \\
&+ (G^* R + G R^*)\, m_l^2 \left[(QL) - (QN)\right] \\
&+ \frac{1}{M_K^2}(G^* H + G H^*)\left[(PL)(QL)(QN) - (PN)(QL)^2 + s_l (PN) Q^2 - m_l^2 (PL) Q^2\right] \\
&+ \frac{i}{M_K^2} < LNPQ > \left[-(F^* G - F G^*) M_K^2 + (F^* H - F H^*)(PN)\right. \\
&+ \left.(G^* H - G H^*)(QN) + (R^* H - R H^*) m_l^2\right] \ . \qquad (5.18)
\end{aligned}$$

For data analysis it is useful to represent this result in a still different form which displays the θ_l and ϕ dependence more clearly [43]:

$$\begin{aligned}
J_5 &= 2(1 - z_l)\left[I_1 + I_2 \cos 2\theta_l + I_3 \sin^2\theta_l \cdot \cos 2\phi + I_4 \sin 2\theta_l \cdot \cos\phi + I_5 \sin\theta_l \cdot \cos\phi\right. \\
&+ \left. I_6 \cos\theta_l + I_7 \sin\theta_l \cdot \sin\phi + I_8 \sin 2\theta_l \cdot \sin\phi + I_9 \sin^2\theta_l \cdot \sin 2\phi\right] . \qquad (5.19)
\end{aligned}$$

One obtains

$$\begin{aligned}
I_1 &= \frac{1}{4}\left\{(1 + z_l)|F_1|^2 + \frac{1}{2}(3 + z_l)\left(|F_2|^2 + |F_3|^2\right)\sin^2\theta_\pi + 2 z_l |F_4|^2\right\} \\
I_2 &= -\frac{1}{4}(1 - z_l)\left\{|F_1|^2 - \frac{1}{2}\left(|F_2|^2 + |F_3|^2\right)\sin^2\theta_\pi\right\}
\end{aligned}$$

$$
\begin{aligned}
I_3 &= -\frac{1}{4}(1-z_l)\left\{|F_2|^2-|F_3|^2\right\}\sin^2\theta_\pi \\
I_4 &= \frac{1}{2}(1-z_l)\ \mathrm{Re}(F_1^* F_2)\sin\theta_\pi \\
I_5 &= -\{\ \mathrm{Re}(F_1^* F_3)+z_l\ \mathrm{Re}(F_4^* F_2)\}\sin\theta_\pi \\
I_6 &= -\left\{\ \mathrm{Re}(F_2^* F_3)\sin^2\theta_\pi - z_l\ \mathrm{Re}(F_1^* F_4)\right\} \\
I_7 &= -\{\ \mathrm{Im}(F_1^* F_2)+z_l\ \mathrm{Im}(F_4^* F_3)\}\sin\theta_\pi \\
I_8 &= \frac{1}{2}(1-z_l)\ \mathrm{Im}(F_1^* F_3)\sin\theta_\pi \\
I_9 &= -\frac{1}{2}(1-z_l)\ \mathrm{Im}(F_2^* F_3)\sin^2\theta_\pi\ , \qquad (5.20)
\end{aligned}
$$

where

$$
\begin{aligned}
F_1 &= X\cdot F+\sigma_\pi(PL)\cos\theta_\pi\cdot G \\
F_2 &= \sigma_\pi\,(s_\pi s_l)^{1/2}\,G \\
F_3 &= \sigma_\pi X\,(s_\pi s_l)^{1/2}\,\frac{H}{M_K^2} \\
F_4 &= -(PL)F-s_l R-\sigma_\pi X\cos\theta_\pi\cdot G\ . \qquad (5.21)
\end{aligned}
$$

The definition of $F_1,\ldots,F_4$ in (5.21) corresponds to the combinations used by Pais and Treiman [43] (the different sign in the terms $\sim PL$ is due to our use of the metric diag$(+---)$). The form factors $I_1,\ldots,I_9$ agree with the expressions given in [43]. We conclude that our convention for the relative phase in the definition of the form factors in Eq. (5.12) agrees with the one used by Pais and Treiman. The comparison of (5.18) with [44, table II] shows furthermore that it also agrees with this reference.

The quantity J_3 can now easily be obtained from (5.19) by integrating over ϕ and θ_l,

$$
J_3=\int d\phi\ d(\cos\theta_l)J_5=8\pi(1-z_l)\left[I_1-\frac{1}{3}I_2\right]. \qquad (5.22)
$$

5.4 Isospin decomposition

The K_{l4} decays (5.2) and (5.3) involve the same form factors as displayed in Eq. (5.12). We denote by A_{+-}, A_{00} and A_{0-} the current matrix elements of the processes (5.1)-(5.3). These are related by isospin symmetry [6],

$$
A_{+-}=\frac{A_{0-}}{\sqrt{2}}-A_{00}\ . \qquad (5.23)
$$

This relation also holds for the individual form factors, which may be decomposed into a symmetric and an antisymmetric part under $t\leftrightarrow u$ ($p_1\leftrightarrow p_2$). Because of

[6] We use the Condon-Shortley phase conventions.

Bose symmetry and of the $\Delta I = \frac{1}{2}$ rule of the relevant weak currents, one has

$$\begin{aligned}(F,G,R,H)_{00} &= -(F^+,G^-,R^+,H^-)_{+-} \\ (F,G,R,H)_{0-} &= \sqrt{2}(F^-,G^+,R^-,H^+)_{+-}\end{aligned} \tag{5.24}$$

where

$$F^{\pm}_{+-} = \frac{1}{2}[F(s_\pi,t,u) \pm F(s_\pi,u,t)] \tag{5.25}$$

and $F(s_\pi,t,u)$ is defined in Eq. (5.12).

The isospin relation for the decay rates is

$$\Gamma(K^+ \to \pi^+\pi^- l^+\nu_l) = \frac{1}{2}\Gamma(K_L \to \pi^0\pi^\pm l^\mp \nu) + 2\Gamma(K^+ \to \pi^0\pi^0 l^+\nu_l) \ . \tag{5.26}$$

Isospin violating contributions affect the matrix elements and phase space, as a result of which this relation is modified. In order to illustrate the (substantial) effects from asymmetries in phase space, we take constant form factors F, G and set $R = 0, H = 0$. Eq. (5.26) then reads (with physical masses for $K^+ \to \pi^+\pi^- l^+\nu_l, \pi^0\pi^0 l^+\nu_l$ and with $M_{\pi^0} = M_{\pi^\pm} = 137$ MeV in $K_L \to \pi^0\pi^\mp l^\pm \nu$)

$$\begin{aligned}(16.0F^2 + 3.1G^2)\Gamma_0 &= (20.1F^2 + 2.0G^2)\Gamma_0 \\ \Gamma_0 &= V_{us}^2 \cdot 10^2 \text{sec}^{-1}\end{aligned} \tag{5.27}$$

in the electron mode and

$$(1.79F^2 + 0.25G^2)\Gamma_0 = (2.64F^2 + 0.20G^2)\Gamma_0 \tag{5.28}$$

in the muon mode.

5.5 Partial wave expansion

The form factors may be written in a partial wave expansion in the variable θ_π. We consider a definite isospin $\pi\pi$ state. Suppressing isospin indices, one has [47, 48]

$$\begin{aligned}F &= \sum_{l=0}^{\infty} P_l(\cos\theta_\pi) f_l - \frac{\sigma_\pi P L}{X}\cos\theta_\pi G \\ G &= \sum_{l=1}^{\infty} P_l'(\cos\theta_\pi) g_l \\ R &= \sum_{l=0}^{\infty} P_l(\cos\theta_\pi) r_l + \frac{\sigma_\pi s_\pi}{X}\cos\theta_\pi G \\ H &= \sum_{l=0}^{\infty} P_l'(\cos\theta_\pi) h_l\end{aligned} \tag{5.29}$$

where

$$P_l'(z) = \frac{d}{dz}P_l(z) \ . \tag{5.30}$$

Table 5.1: Rates of K_{e4} decays.

		♯ events		
	branching ratio	Particle Data Group	DAFNE 1 yr	improve-ment
$K^+ \to \pi^+\pi^- e^+\nu_e$	$3.91 \cdot 10^{-5}$	$3 \cdot 10^4$	$3 \cdot 10^5$	10
$K^+ \to \pi^0\pi^0 e^+\nu_e$	$2.1 \cdot 10^{-5}$	< 50	$2 \cdot 10^5$	$> 4 \cdot 10^3$
$K_L \to \pi^0\pi^\pm e^\mp\nu$	$6.2 \cdot 10^{-5}$	16	$7 \cdot 10^4$	$4 \cdot 10^3$

The partial wave amplitudes f_l, g_l, r_l and h_l depend on s_π and s_l. Their phase coincides with the phase shifts δ_l^I in elastic $\pi\pi$ scattering (angular momentum l, isospin I). More precisely, the quantities

$$\begin{aligned} & e^{-i\delta^0_{2l}} X_{2l} \\ & e^{-i\delta^1_{2l+1}} X_{2l+1} \ ; \ l = 0, 1, \ldots \ ; \ X = f, g, r, h \end{aligned} \tag{5.31}$$

are real in the physical region of K_{l4} decay. The form factors F_1 and F_4 therefore have a simple expansion

$$\begin{aligned} F_1 &= X \sum_l P_l(\cos\theta_\pi) f_l \\ F_4 &= -\sum_l P_l(\cos\theta_\pi)(PL f_l + s_l r_l). \end{aligned} \tag{5.32}$$

On the other hand, the phase of the projected amplitudes

$$F_{2l} = \int P_l(\cos\theta_\pi) F_2 d(\cos\theta_\pi) \ ; \ l = 0, 1, 2, \ldots \tag{5.33}$$

is not given by δ_l^I, e.g., $e^{-i\delta_1^1} F_{20}$ is <u>not</u> real in the isospin one case. A similar remark applies to F_3.

5.6 Previous experiments

We display in table 5.1 the number of events collected so far. The data are obviously dominated by the work of Rosselet et al. [44], which measures the $\pi^+\pi^-$ final state with good statistics. The authors parametrize the form factors as

$$\begin{aligned} F &= f_s e^{i\delta_0^0} + f_p e^{i\delta_1^1} \cos\theta_\pi + \text{D-wave} \\ G &= g e^{i\delta_1^1} + \text{D-wave} \\ H &= h e^{i\delta_1^1} + \text{D-wave} \end{aligned} \tag{5.34}$$

with f_s, f_p, g and h assumed to be real [7] . Furthermore, they put $m_e = 0$, such that the form factors R and F_4 drop out in the decay distribution. Despite the good statistics, the experiment has not been able to separate out the full kinematic behaviour of the matrix elements. Therefore certain approximations/assumptions had to be made. For example, no dependence on s_l was seen within the limits of the data, so that the results were quoted assuming that such a dependence is absent. Similarly, f_p was found to be compatible with zero, and hence put equal to zero when the final result for g was derived. A dependence on s_π was seen, and found to be compatible with

$$\begin{aligned} f_s(q^2) &= f_s(0)[1 + \lambda_f q^2] \\ g(q^2) &= g(0)[1 + \lambda_g q^2] \\ h(q^2) &= h(0)[1 + \lambda_h q^2] \\ q^2 &= (s_\pi - 4M_\pi^2)/4M_\pi^2 \end{aligned} \tag{5.35}$$

with

$$\lambda_f = \lambda_g = \lambda_h = \lambda. \tag{5.36}$$

These approximations to the form factors do not agree completely with what is found in the theoretical predictions. Dependence on s_l and non-zero values for higher partial waves all occur in the theoretical results.

The experimental results for the threshold values and the slopes of the form factors are [44]

$$\begin{aligned} f_s(0) &= 5.59 \pm 0.14 \\ g(0) &= 4.77 \pm 0.27 \\ h(0) &= -2.68 \pm 0.68 \\ \lambda &= 0.08 \pm 0.02. \end{aligned} \tag{5.37}$$

We have used [1] $\mid V_{us} \mid = 0.22$ in transcribing these results. (We note that from Eqs. (5.34 - 5.37) and $f_p = 0$ we obtain $\Gamma_{K_{e4}} = (2.94 \pm 0.16) \cdot 10^3$ sec^{-1}. This value must be compared with $\Gamma_{K_{e4}} = (3.26 \pm 0.15) \cdot 10^3$ sec^{-1} obtained in the same experiment.) In addition to the threshold values (5.37) of the form factors, the phase shift difference $\delta = \delta_0^0 - \delta_1^1$ was determined [44] in five energy bins. The S-wave scattering length a_0^0 was then extracted by using a model of Basdevant, Froggatt and Petersen [49]. This model is based on solutions to Roy equations. The result for the scattering length is

$$a_0^0 = 0.28 \pm 0.05. \tag{5.38}$$

A study by [50], based on a more recent solution to Roy equations, gives

$$a_0^0 = 0.26 \pm 0.05. \tag{5.39}$$

[7] Note that, according to what is said in the previous subsection, the terms denoted by "D-wave" in Eq. (5.34) all contain (complex) contributions which are proportional to $P_l(\cos\theta_\pi), l \geq 0$.

Turning now to the other channels, we consider the measured branching ratios

$$BR(K^+ \to \pi^0\pi^0 e^+\nu_e) = \left(2.0^{+0.5}_{-0.4}\right)\cdot 10^{-5} \quad [25 \text{ events}] \quad [37] \tag{5.40}$$

and

$$BR(K_L \to \pi^0\pi^\mp e^\pm\nu) = \begin{cases} (6.2 \pm 2.0)\cdot 10^{-5} & [16 \text{ events}] & [51] \\ (5.8 \pm 0.2 \pm 0.4)\cdot 10^{-5} & [780 \pm 40 \text{ events}] & [52] \end{cases} . \tag{5.41}$$

The kinematic dependence of the form factors on the variables s_π, s_l and θ_π has not yet been resolved experimentally in these decays. In order to proceed, we assume that the A_{00} and A_{0-} form factors are independent of θ_π, e.g., $F_{00} = F_{00}(s_\pi, t+u)$ etc. As a result of this assumption, G_{00}, H_{00}, F_{0-} and R_{0-} all vanish by Bose statistics. The contribution from R_{00} is completely negligible in the electron mode, and the contribution from the anomaly form factor to the decay (5.41) is tiny. We neglect it altogether, as a result of which the above decays are fully determined by F_{00} and G_{0-}. We write

$$F_{00} = F_0(1+\lambda q^2)\,, \quad G_{0-} = G_0(1+\lambda q^2) \tag{5.42}$$

and obtain for the rate

$$2\Gamma_{K^+\to\pi^0\pi^0 e^+\nu_e} = |F_0 V_{us}|^2(2.01 + 1.7\lambda + O(\lambda^2))\cdot 10^3 \text{sec}^{-1} \tag{5.43}$$

$$\Gamma_{K_L\to\pi^0\pi^\mp e^\pm\nu} = |G_0 V_{us}|^2(0.406 + 0.47\lambda + O(\lambda^2))\cdot 10^3 \text{sec}^{-1} \tag{5.44}$$

where we have used physical phase space in (5.43) and $M_\pi^0 = M_\pi^\pm = 137$ MeV in (5.44). This finally gives with $\lambda = 0.08$ from (5.37)

$$\begin{aligned} |F_0| &= 5.58^{+0.7}_{-0.6} \quad [37] \\ |G_0| &= \begin{cases} 7.5 \pm 1.2 & [51] \\ 7.3 \pm 0.3 & [52] \end{cases} \end{aligned} \tag{5.45}$$

which compares rather well with the isospin predictions (5.24)

$$\begin{aligned} |F_0| &= |f_s(0)| = 5.59 \pm 0.14 \\ |G_0| &= \sqrt{2}|g(0)| = 6.75 \pm 0.38 \ . \end{aligned} \tag{5.46}$$

5.7 Theory

The theoretical predictions of K_{l4} form factors have a long history which started in the sixties with the current algebra evaluation of F, G, R and H. For an early review of the subject and for references to work prior to CHPT we refer the reader to [26] (see also [27]). Here we concentrate on the evaluation of the form factors in the framework of CHPT [45, 46]. We restrict our consideration to the isospin symmetry limit $m_u = m_d, \alpha = 0$.

A) The one-loop result

In Ref. [45, 46], the form factors F, G and H have been evaluated in CHPT at order p^4. The analytic expression for R has not yet been worked out to this accuracy [53]. This form factor only contributes significantly to $K_{\mu 4}$ decays.

The chiral representation of the form factors at order E^2 was originally given by Weinberg [54],

$$\begin{aligned} F &= G = \frac{M_K}{\sqrt{2}F_\pi} = 3.74 \\ H &= 0. \end{aligned} \tag{5.47}$$

We write the result for F at next-to-leading order in the form

$$\begin{aligned} F(s_\pi,t,u) &= \frac{M_K}{\sqrt{2}F_\pi}\left\{1 + F^+(s_\pi,t,u) + F^-(s_\pi,t,u) + O(E^4)\right\} \\ F^\pm(s_\pi,t,u) &= U_F^\pm(s_\pi,t,u) + P_F^\pm(s_\pi,t,u) + C_F^\pm \end{aligned} \tag{5.48}$$

and will use below an analogous expression for the form factor G. The superscript $+(-)$ denotes a term which is even (odd) under crossing $t \leftrightarrow u$. The contributions $U_F^\pm(s_\pi,t,u)$ denote the unitarity corrections generated by the one-loop graphs which appear at order E^4. They have the form

$$\begin{aligned} U_F^+(s_\pi,t,u) &= F_\pi^{-2}\left[\Delta_0(s_\pi) + a_F(t) + a_F(u)\right] \\ U_F^-(s_\pi,t,u) &= F_\pi^{-2}\left[b_F(t) - b_F(u)\right] \end{aligned} \tag{5.49}$$

with

$$\begin{aligned} \Delta_0(s_\pi) &= \frac{1}{2}(2s_\pi - M_\pi^2)J^r_{\pi\pi}(s_\pi) + \frac{3s_\pi}{4}J^r_{KK}(s_\pi) + \frac{M_\pi^2}{2}J^r_{\eta\eta}(s_\pi) \\ a_F(t) &= \frac{1}{32}\left[(14M_K^2 + 14M_\pi^2 - 19t)J^r_{K\pi}(t) + (2M_K^2 + 2M_\pi^2 - 3t)J^r_{\eta K}(t)\right] \\ &+ \frac{1}{16}\left[(3M_K^2 - 7M_\pi^2 + 5t)K_{K\pi}(t) + (M_K^2 - 5M_\pi^2 + 3t)K_{\eta K}(t)\right] \\ &- \frac{1}{8}\left[9(L_{K\pi}(t) + L_{\eta K}(t)) + (3M_K^2 - 3M_\pi^2 - 9t)(M^r_{K\pi}(t) + M^r_{\eta K}(t))\right] \\ b_F(t) &= a_F(t) - \frac{1}{2}(M_K^2 + M_\pi^2 - t)J^r_{K\pi}(t). \end{aligned} \tag{5.50}$$

The loop integrals $J^r_{\pi\pi}(s_\pi),\ldots$ which occur in these expressions are listed in the appendix B. The functions J^r_{PQ} and M^r_{PQ} depend on the scale μ at which the loops are renormalized. The scale drops out in the expression for the full amplitude (see below).

The imaginary part of $F_\pi^{-2}\Delta_0(s_\pi)$ contains the $I = 0$, S-wave $\pi\pi$ phase shift

$$\delta_0^0(s_\pi) = (32\pi F_\pi^2)^{-1}(2s_\pi - M_\pi^2)\sigma_\pi + O(E^4) \tag{5.51}$$

as well as contributions from $K\bar{K}$ and $\eta\eta$ intermediate states. The functions $a_F(t)$ and $b_F(t)$ are real in the physical region.

The contribution $P_F^{\pm}(s_\pi,t,u)$ is a polynomial in s_π,t,u obtained from the tree graphs at order E^4. We find

$$P_F^{\pm}(s_\pi,t,u)=\frac{1}{F_\pi^2}\sum_{i=1}^{9}p_{i,F}^{\pm}(s_\pi,t,u)L_i^r \tag{5.52}$$

where

$$\begin{aligned}
p_{1,F}^{+} &= 32(s_\pi-2M_\pi^2)\\
p_{2,F}^{+} &= 8(M_K^2+s_\pi-s_l)\\
p_{3,F}^{+} &= 2(M_K^2-8M_\pi^2+5s_\pi-s_l)\\
p_{4,F}^{+} &= 32M_\pi^2\\
p_{5,F}^{+} &= 4M_\pi^2\\
p_{9,F}^{+} &= 2s_l\\
p_{3,F}^{-} &= -2(t-u).
\end{aligned} \tag{5.53}$$

The remaining coefficients $p_{i,F}^{\pm}$ are zero. The symbols L_i^r denote the renormalized coupling constants discussed in section 1.

Finally we come to the contributions $C_F^{\pm}$ which contain logarithmic terms, independent of s_π,t and u:

$$\begin{aligned}
C_F^{+} &= (256\pi^2F_\pi^2)^{-1}\left[5M_\pi^2\ln\frac{M_\pi^2}{\mu^2}-2M_K^2\ln\frac{M_K^2}{\mu^2}-3M_\eta^2\ln\frac{M_\eta^2}{\mu^2}\right]\\
C_F^{-} &= 0\ .
\end{aligned} \tag{5.54}$$

The corresponding decomposition of the form factor G,

$$G^{\pm}=U_G^{\pm}+P_G^{\pm}+C_G^{\pm}, \tag{5.55}$$

has the following explicit form:

$$\begin{aligned}
U_G^{+}(s_\pi,t,u) &= F_\pi^{-2}\left[\Delta_1(s_\pi)+a_G(t)+a_G(u)\right]\\
U_G^{-}(s_\pi,t,u) &= F_\pi^{-2}\left[b_G(t)-b_G(u)\right]
\end{aligned} \tag{5.56}$$

with

$$\begin{aligned}
\Delta_1(s_\pi) &= 2s_\pi\left\{M_{\pi\pi}^r(s_\pi)+\frac{1}{2}M_{KK}^r(s_\pi)\right\}\\
a_G(t) &= \frac{1}{32}\left[(2M_K^2+2M_\pi^2+3t)J_{K\pi}^r(t)-(2M_K^2+2M_\pi^2-3t)J_{\eta K}^r(t)\right]\\
&+ \frac{1}{16}\left[(-3M_K^2+7M_\pi^2-5t)K_{K\pi}(t)+(-M_K^2+5M_\pi^2-3t)K_{\eta K}(t)\right]\\
&- \frac{3}{8}\left[L_{K\pi}(t)+L_{\eta K}(t)-(M_K^2-M_\pi^2+t)(M_{K\pi}^r(t)+M_{\eta K}^r(t))\right]\\
b_G(t) &= a_G(t)-\frac{1}{2}(M_K^2+M_\pi^2-t)J_{K\pi}^r(t).
\end{aligned} \tag{5.57}$$

The imaginary part of $F_\pi^{-2}\Delta_1(s_\pi)$ contains the $I=1$, P-wave phase shift

$$\delta_1^1(s_\pi) = (96\pi F_\pi^2)^{-1} s_\pi \sigma_\pi^{3/2} + O(E^4) \tag{5.58}$$

as well as contributions from $K\bar{K}$ intermediate states. The functions a_G, b_G are real in the physical region.

The polynomials

$$P_G^\pm = \frac{1}{F_\pi^2} \sum_{i=1}^{9} p_{i,G}^\pm(s_\pi, t, u) L_i^r \tag{5.59}$$

are

$$\begin{aligned}
p_{3,G}^+ &= -2(M_K^2 + s_\pi - s_l) \\
p_{5,G}^+ &= 4M_\pi^2 \\
p_{9,G}^+ &= 2s_l \\
p_{2,G}^- &= 8(t-u) \\
p_{3,G}^- &= \frac{1}{4} p_{2,G}^-.
\end{aligned} \tag{5.60}$$

The remaining $p_{i,G}^\pm$ vanish. The logarithms contained in $C_G^\pm$ are

$$C_G^\pm = -C_F^\pm. \tag{5.61}$$

The form factor H starts only at $O(E^4)$. The prediction is

$$H = -\frac{\sqrt{2} M_K^3}{8\pi^2 F_\pi^3} = -2.66 \tag{5.62}$$

in excellent agreement with the experimental value.

The results for F and G must satisfy two nontrivial constraints: i) Unitarity requires that F and G contain, in the physical region $4M_\pi^2 \leq s_\pi \leq (M_K - m_l)^2$, imaginary parts governed by S- and P-wave $\pi\pi$ scattering [these imaginary parts are contained in the functions $\Delta_0(s_\pi), \Delta_1(s_\pi)$]. ii) The scale dependence of the low-energy constants L_i^r must be compensated by the scale dependence of $U_{F,G}$ and $C_{F,G}$ for all values of $s_\pi, t, u, M_\pi^2, M_K^2$. [Since we work at order E^4, the meson masses appearing in the above expressions satisfy the Gell-Mann-Okubo mass formula.] We have checked that these constraints are satisfied.

B) Comparison with experiment

One striking feature of the chiral prediction for the form factors is that the only important dependence on the low-energy constants is through L_1, L_2 and L_3. We proceed by fixing L_4, L_5 and L_9 at the values found in other processes (see section 1, in particular table 1).

Table 5.2: Predictions of chiral symmetry following from the fit to the K_{e4} data [44] alone (column 3) and the combined determination from $\pi\pi$ [55] and K_{e4} data [44] (last column). The first column gives the prediction of the leading order term in the low-energy expansion of the $\pi\pi$ amplitude.

	leading order	experiment	K_{e4} alone	$K_{e4} + \pi\pi$
λ_g		0.08 ± 0.02	0.06 ± 0.02	0.06 ± 0.02
a_0^0	0.16	0.26 ± 0.05	0.20	0.20
b_0^0	0.18	0.25 ± 0.03	0.26	0.26
a_0^2	-0.045	-0.028 ± 0.012	-0.040	-0.041
b_0^2	-0.089	-0.082 ± 0.008	-0.069	-0.070
a_1^1	0.030	0.038 ± 0.002	0.037	0.036
b_1^1			0.045	0.043
a_2^0		$(17 \pm 3) \cdot 10^{-4}$	$21 \cdot 10^{-4}$	$20 \cdot 10^{-4}$
a_2^2		$(1.3 \pm 3) \cdot 10^{-4}$	$3.5 \cdot 10^{-4}$	$3.5 \cdot 10^{-4}$

A rather extensive analysis of the chiral prediction and the data on $K^+ \to \pi^+\pi^- e^+\nu$ and elastic $\pi\pi$ scattering has been given in Refs. [45, 46]. We refer the reader to these articles for details. Here we mention the following points.

1. Fixing L_1, L_2 and L_3 from $f_s(0)$, $g(0)$ and the slope λ_f of the form factor f_s gives

$$\begin{aligned} L_1^r(M_\rho) &= [0.5 \pm 0.3] \cdot 10^{-3} \\ L_2^r(M_\rho) &= [1.6 \pm 0.3] \cdot 10^{-3} \\ L_3 &= [-3.2 \pm 1.1] \cdot 10^{-3} \ . \end{aligned} \tag{5.63}$$

The error bar corresponds [46] to an increase of χ^2 by one. It does not include the error due to unknown higher order corrections in the chiral expansion of the form factor. Having determined L_1, L_2 and L_3, one may then work out the form factors from the representation (5.48-5.61). The result is shown in Fig. 5.2, where we plot for the electron mode the quantity

$$f_s(s_\pi) = \left\{ \frac{1}{(s_l^{\max} - s_l^{\min})} \int_{s_l^{\min}}^{s_l^{\max}} ds_l \left| \frac{1}{2} \int_{-1}^{1} d(\cos\theta_\pi) F(s_\pi, s_l, \cos\theta_\pi) \right|^2 \right\}^{1/2} \tag{5.64}$$

and similarly for $g(s_\pi)$. The lowest order results Eq. (5.47) (labelled "tree") plus the experimental central values and the central values corresponding to Eq. (5.63) are displayed. Note that the slope of the g form factor has not been included in the fit and is thus a prediction. It matches very well with the experimental data.

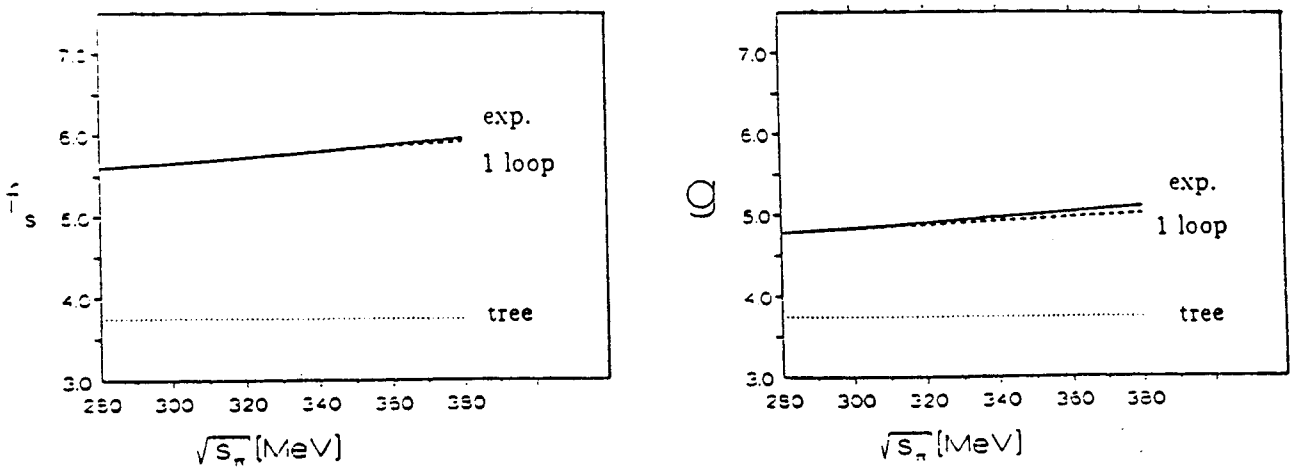

Figure 5.2: The form factors $f_s(s_\pi)$ and $g(s_\pi)$ (Eq. 5.64) according to the chiral representation (electron mode). The dotted lines show the lowest order result (5.47), and the dashed lines correspond to L_1, L_2 and L_3 from (5.63). The experimental result (5.37) is displayed by a solid line.

2. The decay $K^+ \to \pi^+\pi^- e^+\nu_e$ allows one to test the large N_C prediction

$$(L_2^r - 2L_1^r)/L_3 = 0 \qquad \text{(large } N_C\text{)}. \tag{5.65}$$

From the values in Eq. (5.63), we see that a small non-zero result for this combination is preferred, but that it is consistent with zero within the errors. The fit was also done [46] using the variables

$$\begin{aligned} X_1 &= L_2^r - 2L_1^r - L_3 \\ X_2 &= L_2^r \\ X_3 &= (L_2^r - 2L_1^r)/L_3 \end{aligned} \tag{5.66}$$

with the result

$$\begin{aligned} X_1 &= (3.8 \pm 0.9) \cdot 10^{-3} \\ X_2 &= (1.6 \pm 0.3) \cdot 10^{-3} \\ X_3 &= -0.19^{+0.16}_{-0.27} \ . \end{aligned} \tag{5.67}$$

(X_1 and X_3 are scale independent, X_2 is evaluated at the rho mass.) The result is that the large N_C prediction works remarkably well.

3. Having determined the low-energy constants, one is in a position to study the predictions. The coefficients L_1, L_2 and L_3 also govern elastic $\pi\pi$-scattering,

and the real test of the theory is that these coefficients are simultaneously compatible with the elastic $\pi\pi$ amplitude. The most straightforward way to check this is to predict the $\pi\pi$ threshold parameters. The chiral predictions were worked out in Ref. [56, 57]. If we use the determination (5.63), we obtain the prediction in table 5.2, third column. (For $\bar{l}_3, \bar{l}_4$ which occur in a_l^I, b_l^I we have used the central value $\bar{l}_3 = 2.9, \bar{l}_4 = 4.3$ from Ref. [56]). The predictions are within $1\frac{1}{2}$ standard deviations of the data in all cases. Note, in particular, the nice agreement for the $I = 0, 2$ D-wave scattering lengths a_2^0, a_2^2. Furthermore, it is comforting to see that the SU(2)×SU(2) prediction [56, 57]

$$a_0^0 = 0.20 \pm 0.01 \tag{5.68}$$

survives the K_{e4} test unharmed.

4. It is of interest to provide the best determination of the low-energy constants by including the maximum amount of data. This includes the K_{e4} form factors $f_s(0), g(0)$ and λ_f, as well as the direct determination of $\delta_0^0 - \delta_1^1$ in K_{e4} decay. We take the other information as the $\pi\pi$ threshold parameters $a_1^1, a_2^0, a_2^2, b_0^2$ as well as the universal curve [58]

$$\begin{aligned} X(a_0^0, a_0^2) &= 2a_0^0 - 5a_0^2 - 0.96(a_0^0 - 0.3) \\ &\quad -0.7(a_0^0 - 0.3)^2 \\ &= 0.69 \pm 0.04 \ . \end{aligned} \tag{5.69}$$

The results of the fit are shown in the last column of table 5.2. The corresponding values for L_1, L_2 and L_3 are

$$\begin{aligned} L_1^r(M_\rho) &= (0.7 \pm 0.5) \cdot 10^{-3} \\ L_2^r(M_\rho) &= (1.2 \pm 0.4) \cdot 10^{-3} \\ L_3 &= (-3.6 \pm 1.3) \cdot 10^{-3} \ . \end{aligned} \tag{5.70}$$

The error includes the theoretical error bar, see Ref. [46]. [The one-loop representation (5.48-5.62) of the form factors F, G and H, evaluated at the central values (5.70), gives $\Gamma_{K_{e4}} = 2.5 \cdot 10^3$ sec^{-1}. This is somewhat lower than the experimental [44] width $\Gamma_{K_{e4}} = 3.26 \cdot 10^3$ sec^{-1} and the value $\Gamma_{K_{e4}} = 2.94 \cdot 10^3$ sec^{-1} which follows from (5.37). The reason for considering nevertheless (5.70) as the present best estimate for L_1, L_2 and L_3 is discussed at some length in [46]: since the chiral corrections to the tree level result $F = G = 3.74$ are large, one should not expect that the one-loop corrections already do the complete job - rather, higher order terms have any right to also contribute accordingly. The above result for L_1, L_2 and L_3 includes an estimate for these additional terms. (The experimental width for K_{e4} is within the uncertainties $\Delta L_1, \Delta L_2$ and ΔL_3 quoted.)]

5.8 Improvements at DAFNE

The chiral analysis of K_{l4} decays has been used so far for three purposes:

1. The K_{e4} data from Ref. [44] make predictions for the slope of the G form factor and for the $\pi\pi$ scattering lengths. These are given in table 5.2.

2. The same K_{e4} data allow one to test the large N_C prediction, see Eqs. (5.65-5.67).

3. The full set of K_{e4} and $\pi\pi$ scattering data allows the best determination of the coefficients L_1, L_2 and L_3 in the chiral Lagrangian, see (5.70).

In the next generation of K_{l4} decay experiments, there is the opportunity to improve the phenomenology of K_{l4} (see table 5.1):

1. The present experimental uncertainty on G is still too large to provide a precise value for the large N_C parameter $(L_2^r - 2L_1^r)/L_3$. ($K^0 \to \pi^0\pi^- e^+\nu_e$ decays are mainly sensitive to G_{+-}^+ which in turn can be used to pin down L_3. $K^+ \to \pi^0\pi^0 e^+\nu_e$ is mainly sensitive to F_{+-}^+ which contains L_1, L_2 and L_3.)

2. The observation of all K_{l4} reactions with high statistics could provide a cleaner separation of the various isospin amplitudes.

3. A very useful innovation would be to analyze the experimental data directly using the framework of chiral perturbation theory. Rather than making assumptions about the absence of P-waves, D-waves etc., one could parametrize the data using the full chiral perturbation formulas, and directly decide the quality of the fit and the favoured values of the low-energy constants.

4. Finally, we come to a most important point. As we mentioned already, $K^+ \to \pi^+\pi^- e^+\nu_e$ has been used [50] to determine the isoscalar S-wave scattering length with the result $a_0^0 = 0.26 \pm 0.05$. This value must be compared with the SU(2)×SU(2) prediction [56, 57] $a_0^0 = 0.20 \pm 0.01$. Low-energy $\pi\pi$ scattering is one of the few places where chiral symmetry allows one to make a precise prediction within the framework of QCD. In their article, Rosselet et al. comment about the discrepancy between $a_0^0 = 0.26 \pm 0.05$ and the leading order result [59] $a_0^0 = 0.16$ in the following manner: "... it appears that this prediction can be revised without any fundamental change in current algebra or in the partial conservation of axial-vector current [60, 61]." Today, we know that this is not the case: It would be a major difficulty for QCD, should the central value $a_0^0 = 0.26$ be confirmed with a substantially smaller error.

   K_{l4} decays are – at present [62] – the only available source of clean information on $\pi\pi$ S-wave scattering near threshold. We therefore feel that it would be rather appropriate to clarify this issue.

Acknowledgements

We thank G. Pancheri for the perfect organization of the DAFNE Workshops and the INFN for the hospitality in Frascati. We have enjoyed numerous interesting discussions with the members of the working groups, and we are grateful to L. Maiani and N. Paver for reading the manuscript and for valuable suggestions at various stages of this work. We thank J. Beringer for checking traces in $K_{l2\gamma}$, M. Candusso for doing the contour plots and C. Riggenbach for providing us with numerical routines for K_{l4}. E.A. Ivanov has kindly made available to us unpublished work by D.Yu. Bardin and collaborators on radiative pion and kaon decays.

A Notation

The notation for phase space is the one without the factors of 2π. For the decay rate of a particle with four momentum p into n particles with momenta $p_1, \ldots, p_n$ this is

$$d_{LIPS}(p; p_1, \ldots, p_n) = \delta^4(p - \sum_{i=1}^{n} p_i) \prod_{i=1}^{n} \frac{d^3 p_i}{2p_i^0} \ . \tag{A.1}$$

We use a covariant normalization of one-particle states,

$$< \vec{p}\,' | \vec{p} >= (2\pi)^3 2p^0 \delta^3(\vec{p}\,' - \vec{p}) \ , \tag{A.2}$$

together with the spinor normalization

$$\bar{u}(p,r)u(p,s) = 2m\delta_{rs} \ . \tag{A.3}$$

The kinematical function $\lambda(x,y,z)$ is defined as

$$\lambda(x,y,z) = x^2 + y^2 + z^2 - 2(xy + yz + zx) \ . \tag{A.4}$$

We take the standard model in the current $\times$ current form, i.e., we neglect the momentum dependence of the W-propagator. The currents used in the text are :

$$\begin{aligned} V_\mu^{4-i5} &= \bar{q}\gamma_\mu \frac{1}{2}(\lambda_4 - i\lambda_5)q \ = \ \bar{s}\gamma_\mu u \\ A_\mu^{4-i5} &= \bar{q}\gamma_\mu\gamma_5 \frac{1}{2}(\lambda_4 - i\lambda_5)q \ = \ \bar{s}\gamma_\mu\gamma_5 u \\ V_\mu^{em} &= \bar{q}\gamma_\mu Q q \\ Q &= \mathrm{diag}(2/3, -1/3, -1/3) \ . \end{aligned} \tag{A.5}$$

The numerical values used in the programs are the physical masses for the particles as given by the Particle Data Group [1]. In addition we have used the values for the decay constants derived from the most recent measured charged pion and kaon semileptonic decay rates[1, 18] :

$$\begin{aligned} F_\pi &= 93.2 \ MeV \\ F_K &= 113.6 \ MeV. \end{aligned} \tag{A.6}$$

We do not need values for the quark masses. For the processes considered in this report we can always use the lowest order relations to rewrite them in terms of the pseudoscalar meson masses (see section 1). For the KM matrix element $|V_{us}|$ we used the central value, 0.220, of Ref. [1]. The numerical values for the $L_i^r(M_\rho)$ are those given in section 1.

The number of events quoted for DAFNE are based on a luminosity of $5 \cdot 10^{32}\ cm^{-2}s^{-1}$, which is equivalent [63] to an annual rate of $9 \cdot 10^9$ ($1.1 \cdot 10^9$) tagged $K^\pm$ (K_L) (1 year = 10^7 s assumed).

Whenever we quote a branching ratio for a semileptonic K^0 decay, it stands for the branching ratio of the corresponding K_L decay, e.g.,

$$BR(K^0 \to \pi^- l^+ \nu) \equiv BR(K_L \to \pi^\pm l^\mp \nu) \; . \tag{A.7}$$

We use the Condon-Shortley phase conventions throughout.

B Loop integrals

In this appendix we define the functions appearing in the loop integrals used in the text. First we define the functions needed for loops with two propagators, mainly in the form given in Ref. [35]. We consider a loop with two masses, M and m. All needed functions can be given in terms of the subtracted scalar integral $\bar{J}(t) = J(t) - J(0)$,

$$J(t) = -i \int \frac{d^4p}{(2\pi)^d} \frac{1}{((p+k)^2 - M^2)(p^2 - m^2)} \tag{B.1}$$

with $t = k^2$. The functions used in the text are then :

$$\begin{aligned}
\bar{J}(t) &= -\frac{1}{16\pi^2} \int_0^1 dx \, \log \frac{M^2 - tx(1-x) - \Delta x}{M^2 - \Delta x} \\
&= \frac{1}{32\pi^2} \left\{ 2 + \frac{\Delta}{t} \log \frac{m^2}{M^2} - \frac{\Sigma}{\Delta} \log \frac{m^2}{M^2} - \frac{\sqrt{\lambda}}{t} \log \frac{(t+\sqrt{\lambda})^2 - \Delta^2}{(t-\sqrt{\lambda})^2 - \Delta^2} \right\} , \\
J^r(t) &= \bar{J}(t) - 2k , \\
M^r(t) &= \frac{1}{12t} \{t - 2\Sigma\} \bar{J}(t) + \frac{\Delta^2}{3t^2} \bar{J}(t) + \frac{1}{288\pi^2} - \frac{k}{6} \\
&\quad - \frac{1}{96\pi^2 t} \left\{ \Sigma + 2 \frac{M^2 m^2}{\Delta} \log \frac{m^2}{M^2} \right\} , \\
L(t) &= \frac{\Delta^2}{4t} \bar{J}(t) , \\
K(t) &= \frac{\Delta}{2t} \bar{J}(t) , \\
H(t) &= \frac{2}{3} \frac{L_9^r}{F^2} t + \frac{1}{F^2} [t M^r(t) - L(t)], \\
\Delta &= M^2 - m^2 , \\
\Sigma &= M^2 + m^2 , \\
\lambda &= \lambda(t, M^2, m^2) = (t + \Delta)^2 - 4tM^2 .
\end{aligned} \tag{B.2}$$

In the text these are used with subscripts,

$$\bar{J}_{ij}(t) = \bar{J}(t) \quad \text{with} \quad M = M_i, m = M_j \tag{B.3}$$

and similarly for the other symbols. The subtraction point dependent part is contained in the constant k

$$k = \frac{1}{32\pi^2} \frac{M^2 \log\left(\frac{M^2}{\mu^2}\right) - m^2 \log\left(\frac{m^2}{\mu^2}\right)}{M^2 - m^2}, \tag{B.4}$$

where μ is the subtraction scale.

In addition, in subsection 4 these functions and symbols appear in a summation over loops I with

$$\begin{aligned} J_I(t) &= \bar{J}(t) \quad \text{with} \quad M = M_I, m = m_I \ ; \\ \Sigma_I &= M_I^2 + m_I^2 \end{aligned} \tag{B.5}$$

and again similarly for the others. There the combination B_2 appears as well :

$$\begin{aligned} B_2(t, M^2, m^2) &= B_2(t, m^2, M^2) \\ &= \frac{1}{288\pi^2}(3\Sigma - t) - \frac{\lambda(t, M^2, m^2)\bar{J}(t)}{12t} + \frac{t\Sigma - 8M^2m^2}{384\pi^2\Delta}\log\frac{M^2}{m^2} \ . \end{aligned} \tag{B.6}$$

The last formula to be defined is the three propagator loop integral function $C(t_1, t_2, M^2, m^2)$ where one of the three external momenta has zero mass and two of the propagators have the same mass M. Here $t_1 = (q_1 + q_2)^2$, $t_2 = q_2^2$ and $q_1^2 = 0$.

$$\begin{aligned} C(t_1, t_2, M^2, m^2) &= -i\int \frac{d^4p}{(2\pi)^d} \frac{1}{(p^2 - M^2)((p+q_1)^2 - M^2)((p+q_1+q_2)^2 - m^2)} \\ &= -\frac{1}{16\pi^2}\int_0^1 dx \int_0^{1-x} dy \frac{1}{M^2 - y(\Delta + t_1) + xy(t_1 - t_2) + y^2 t_1} \\ &= \frac{1}{(4\pi)^2(t_1 - t_2)}\left\{ Li_2\left(\frac{1}{y_+(t_2)}\right) + Li_2\left(\frac{1}{y_-(t_2)}\right) \right. \\ &\quad \left. - Li_2\left(\frac{1}{y_+(t_1)}\right) - Li_2\left(\frac{1}{y_-(t_2)}\right)\right\} \ , \\ y_\pm(t) &= \frac{1}{2t}\left\{ t + \Delta \pm \sqrt{\lambda(t, M^2, m^2)} \right\} \end{aligned} \tag{B.7}$$

where Li_2 is the dilogarithm

$$Li_2(x) = -\int_0^1 \frac{dy}{y}\log(1 - xy) \ . \tag{B.8}$$

C Decomposition of the hadronic tensors $I^{\mu\nu}$

Here we consider the tensors

$$I^{\mu\nu} = \int dx e^{iqx+iWy} < 0 \mid TV^{\mu}_{em}(x) I^{\nu}_{4-i5}(y) \mid K^{+}(p) > \ , \ I = V, A \qquad \text{(C.1)}$$

and detail its connection with the matrix element (1.2).

The general decomposition of $A^{\mu\nu}, V^{\mu\nu}$ in terms of Lorentz invariant amplitudes reads [7, 9] for $q^2 \neq 0$

$$\begin{aligned} \frac{1}{\sqrt{2}} A^{\mu\nu} &= -F_K \left\{ \frac{(2W^{\mu} + q^{\mu})W^{\nu}}{M_K^2 - W^2} + g^{\mu\nu} \right\} \\ &+ A_1(qWg^{\mu\nu} - W^{\mu}q^{\nu}) + A_2(q^2 g^{\mu\nu} - q^{\mu}q^{\nu}) \\ &+ \left\{ \frac{2F_K(F_V^K(q^2) - 1)}{(M_K^2 - W^2)q^2} + A_3 \right\} (qWq^{\mu} - q^2 W^{\mu})W^{\nu} \end{aligned} \qquad \text{(C.2)}$$

and

$$\frac{1}{\sqrt{2}} V^{\mu\nu} = iV_1 \epsilon^{\mu\nu\alpha\beta} q_{\alpha} p_{\beta} \qquad \text{(C.3)}$$

where the form factors $A_i(q^2, W^2)$ and $V_1(q^2, W^2)$ are analytic functions of q^2 and W^2. $F_V^K(q^2)$ denotes the electromagnetic form factor of the kaon ($F_V^K(0) = 1$). $A^{\mu\nu}$ satisfies the Ward identity

$$q_{\mu} A^{\mu\nu} = -\sqrt{2} F_K p^{\nu}. \qquad \text{(C.4)}$$

In the process (1.1) the photon is real. As a consequence of this, only the two form factors $A_1(0, W^2)$ and $V_1(0, W^2)$ contribute. We set

$$\begin{aligned} A(W^2) &= A_1(0, W^2) \\ V(W^2) &= V_1(0, W^2) \end{aligned} \qquad \text{(C.5)}$$

and obtain for the matrix element (1.2)

$$T = -iG_F/\sqrt{2} e V_{us}{}^{*} \epsilon_{\mu}^{*} \left\{ \sqrt{2} F_K l_1^{\mu} - (V^{\mu\nu} - A^{\mu\nu}) l_{\nu} \right\}_{|_{q^2=0}} \ , \qquad \text{(C.6)}$$

with

$$\begin{aligned} l^{\mu} &= \bar{u}(p_{\nu})\gamma^{\mu}(1 - \gamma_5)v(p_l) \\ l_1^{\mu} &= l^{\mu} + m_l \bar{u}(p_{\nu})(1 + \gamma_5) \frac{2p_l^{\mu} + \not{q}\gamma^{\mu}}{m_l^2 - (p_l + q)^2} v(p_l) \ . \end{aligned} \qquad \text{(C.7)}$$

Grouping terms into an IB and a SD piece gives (1.2,1.3). As a consequence of (C.4), T is invariant under the gauge transformation $\epsilon_{\mu} \rightarrow \epsilon_{\mu} + q_{\mu}$.

The amplitudes A_1, A_2 and V_1 are related to the corresponding quantities F_A, R and F_V used by the PDG [1] by

$$-\sqrt{2} M_K (A_1, A_2, V_1) = (F_A, R, F_V). \qquad \text{(C.8)}$$

The last term in (C.2) is omitted in [1]. It contributes to processes with a virtual photon, $K^{\pm} \to l^{\pm}\nu_l l'^{+} l'^{-}$.

Finally, the relation to the notation used in [2, 3] is

$$\begin{aligned} 2(A \pm V)^2 &= (a_k \pm v_k)^2 \quad [2] \\ \sqrt{2}(A, V) &= (F_A, F_V) \quad [3] \ . \end{aligned} \tag{C.9}$$

D Formulas for the traces in terms of x, y and z for the decays $K^+ \to l^+\nu l'^+ l'^-$

This is the FORTRAN program used to evaluate the differential decay rate in terms of the kinematic variables used in the text. The formfactors are A1,A2,A4 and V1 with their complex conjugates A1C, A2C, A4C and V1C, all made dimensionless by multiplying with the relevant power of M_K. T is the quantity $\left\{-\sum_{spins} \overline{T_\mu}^* \overline{T}^\mu\right\}$. The matrix element squared, before the integration over the lepton pair kinematic variables, is available on request from the authors.

```
C  ALL QUANTITIES ARE IN UNITS OF MK TO THE RELEVANT POWER
      W2   = 1.0 - X + Z
      P$W  = 1.0 - X/2.0
      P$PN = P$W - Y/2.0
      PL$PN= (W2 - RL)/2.0
      PL$W = RL + PL$PN
      PN$W = W2 - PL$W
      Q$W  = X/2.0 - Z
      Q$PL = Y/2.0 - PL$W
      Q$PN = P$PN - PN$W
      DENOM1 = 1.0/(2.0*Q$PL + Z)
      DENOM2 = 1.0/(X - Z)
      A11 = REAL ( A1 + A1C)
      A22 = REAL ( A2 + A2C)
      A44 = REAL ( A4 + A4C)
      VV  = REAL ( V1 + V1C)
      A12 = REAL (A1*A2C + A1C*A2)
      A14 = REAL (A1*A4C + A1C*A4)
      A1V = REAL (A1*V1C + A1C*V1)
      A24 = REAL (A2*A4C + A2C*A4)
      A2V = REAL (A2*V1C + A2C*V1)
      A4V = REAL (A4*V1C + A4C*V1)
      A1A1C = REAL (A1*A1C)
      A2A2C = REAL (A2*A2C)
      A4A4C = REAL (A4*A4C)
      V1V1C = REAL (V1*V1C)
      T = 0.0
      T = T + A1A1C * ( 16*Q$PL*Q$PN*W2 - 16*Q$PL*Q$W*PN$W - 16*Q$PN*
     +    Q$W*PL$W - 8*PL$PN*Z*W2 )
      T = T + A2A2C * (  - 16*Q$PL*Q$PN*Z - 8*PL$PN*Z**2 )
      T = T + A4A4C * ( 8*Q$W**2*PL$PN*Z*W2 - 16*Q$W**2*PL$W*PN$W*Z -
     +    8*PL$PN*Z**2*W2**2 + 16*PL$W*PN$W*Z**2*W2 )
      T = T + V1V1C * (  - 8*P$PN*Q$PL*X + 8*P$PN*Y*Z + 16*Q$PL*Q$PN
```

```
+      - 4*Q$PN*X*Y )
 T = T + FK**2*DENOM1**2 * (  - 32*Q$PL**2*PL$PN*Z**(-1)*RL - 32*
+     Q$PL*Q$PN*RL - 32*Q$PL*PL$PN*RL + 32*Q$PN*RL**2 + 8*PL$PN*Z*
+     RL + 32*PL$PN*RL**2 )
 T = T + FK**2*DENOM1*DENOM2 * ( 32*P$PN*Q$PL*RL + 32*Q$PL*PL$PN*X
+     *Z**(-1)*RL - 16*Q$PN*Y*RL - 32*PL$PN*Y*RL )
 T = T + FK**2*DENOM2**2 * (  - 8*PL$PN*X**2*Z**(-1)*RL + 32*PL$PN
+     *RL )
 T = T + FK*DENOM1*A11 * ( 16*Q$PN*Q$W*RL - 16*Q$PN*PL$W*RL + 16*
+     Q$W*PL$PN*RL + 8*PN$W*Z*RL )
 T = T + FK*DENOM1*A22 * (  - 16*Q$PL*Q$PN*RL + 24*Q$PN*Z*RL + 16*
+     PL$PN*Z*RL )
 T = T + FK*DENOM1*A44 * ( 16*Q$PL*Q$W*PN$W*RL - 8*Q$PN*Z*W2*RL +
+     8*Q$W*PN$W*Z*RL - 16*PL$W*PN$W*Z*RL )
 T = T + FK*DENOM1*VV * ( 16*P$PN*Z*RL - 8*Q$PN*X*RL )
 T = T + FK*DENOM2*A11 * (  - 16*P$PN*Q$W*RL + 16*P$W*Q$PN*RL )
 T = T + FK*DENOM2*A22 * (  - 16*P$PN*Z*RL + 8*Q$PN*X*RL )
 T = T + FK*DENOM2*A44 * ( 16*P$W*PN$W*Z*RL - 8*Q$W*PN$W*X*RL )
 T = T + A12 * (  - 8*Q$PL*PN$W*Z - 8*Q$PN*PL$W*Z - 8*Q$W*PL$PN*Z
+     )
 T = T + A14 * ( 8*Q$PL*PN$W*Z*W2 + 8*Q$PN*PL$W*Z*W2 - 16*Q$W*PL$W
+     *PN$W*Z )
 T = T + A1V * (  - 8*P$PN*Q$PL*Q$W - 8*P$PN*PL$W*Z - 4*Q$PL*PN$W*
+     X + 4*Q$PN*Q$W*Y + 4*Q$PN*PL$W*X + 4*PN$W*Y*Z )
 T = T + A24 * ( 8*Q$PL*Q$W*PN$W*Z + 8*Q$PN*Q$W*PL$W*Z - 8*Q$W**2*
+     PL$PN*Z + 8*PL$PN*Z**2*W2 - 16*PL$W*PN$W*Z**2 )
 T = T + A2V * (  - 16*P$PN*Q$PL*Z + 8*Q$PN*Y*Z )
 T = T + A4V * ( 8*P$PN*Q$PL*Z*W2 - 8*P$PN*Q$W*PL$W*Z - 8*P$W*Q$PL
+     *PN$W*Z + 8*P$W*Q$PN*PL$W*Z - 4*Q$PN*Y*Z*W2 + 4*Q$W*PN$W*Y*Z
+      )
 T = -T
```

E FORTRAN routine for the calculation of the reduced square of the $K_{l3\gamma}$ matrix element SM

```
      FUNCTION SM(EG,EP,W2,EL,X)
C THE FUNCTION SM CALCULATES THE REDUCED SQUARE OF THE MATRIX
C ELEMENT OF SUBSECT. 4 IN TERMS OF THE SCALAR VARIABLES EG(PHOTON
C ENERGY), EP(PION ENERGY), W2(INVARIANT MASS SQUARED OF LEPTON
C PAIR), EL(ENERGY OF CHARGED LEPTON) AND X=PL.Q/MK^2 AND IN
C TERMS OF THE VECTOR AMPLITUDES B1,..,B7, AXIAL AMPLITUDES
C A1, A2, A3  (A4=0 TO O(P^4)) AND C1, C2 DEFINED IN SUBSECT. 4.
C ALL DIMENSIONFUL QUANTITIES ARE NORMALIZED TO THE KAON MASS:
C MP=M(PION)/M(KAON), ML=M(LEPTON)/M(KAON), ETC.
      REAL ML,MP,ML2,MP2,ML4
      COMMON/MASSES/ML,MP
      ML2=ML**2
      MP2=MP**2
      ML4=ML**4
C SCALAR PRODUCTS: QPP=Q.P', PLPP=P(LEPTON).P', WPP=W.P',
C QW=Q.W, ALL SCALED TO M(KAON)=1; W=P(LEPTON)+P(NEUTRINO)
      QPP=EP+EG+(W2-MP2-1.)/2.
      PLPP=EL-X-(W2+ML2)/2.
      WPP=-EG+(1.-MP2-W2)/2.
      QW=-EP+(1.+MP2-W2)/2.
C FOR ILLUSTRATION, THE TREE LEVEL AMPLITUDES B1,...,B7,
C A1,A2,A3,C1,C2 FOR KO(L3GAMMA) ARE LISTED BELOW
      B1=-1.
      B2=0.
      B3=2./QPP
      B4=0.
      B5=0.
      B6=1./QPP
      B7=B3
      A1=0.
      A2=0.
      A3=0.
      C1=2.
      C2=1.
C IN THE FOLLOWING, SM IS CALCULATED IN TERMS OF SCALAR
C PRODUCTS, MASSES AND INVARIANT AMPLITUDES.
C THIS PART IS INDEPENDENT OF THE CHOICE OF SCALAR VARIABLES
C TO SPECIFY THE KINEMATICS (P(LEPTON).Q IS DENOTED X)
```

```
 R1=B1*(B1-B5*ML2)*(-ML2 + W2)
 R1=R1 + B1*B2*2*ML2*(X-QW)
 R11=B1*B3+B2*B4*W2+(B2*B7+B3*B4)*WPP+B3*B7*MP2
 R1=R1+R11*(4*X*PLPP-2*X*WPP-2*PLPP*QW-
+    QPP*ML2 + QPP*W2)
 R1=R1 + B1*(B4+B6)*2*ML2*(PLPP-WPP)
 R1=R1 + B1*A1*(-4*X*WPP + 4*PLPP*QW)
 R1=R1 + B1*A2*(4*X*W2-2*QW*ML2-2*QW*W2)
 R1=R1 + B2*(B2*W2+2*B3*WPP)*2*X*(X-QW)
 R1=R1 + B2*(B5*W2+B6*WPP)*2*ML2*(X-QW)
 R12=B2*A1+B3*A2+A3*ML2*(A2-C2/2./X)
 R1=R1+R12*(-2*X*QW*WPP+2*X*QPP*W2+2*PLPP
+    *QW**2-QW*QPP*ML2-QW*QPP*W2)
 R1=R1 + B3**2*2*MP2*X*(X-QW)
 R1=R1 + B3*(B5*WPP+B6*MP2)*2*ML2*(X-QW)
 R1=R1+(B4**2*W2+B7**2*MP2+2*B1*B7)*(-1./2.*ML2*MP2+1./2.*MP2*W2
+     + 2*PLPP**2-2*PLPP*WPP)
 R1=R1+(B4*(B5*W2+B6*WPP)+B7*(B5*WPP+B6*MP2))*2*ML2*(PLPP-WPP)
 R1=R1+B4*B7*WPP*(4*PLPP**2-4*PLPP*WPP-
+    ML2*MP2+MP2*W2)
 R1=R1+(B4*A1+B7*A2)*(-2*X*WPP**2+2*X*MP2*W2+2*PLPP
+    *QW*WPP-2*PLPP*QPP*W2-QW*ML2*MP2-QW*MP2*W2
+     + QPP*WPP*ML2 + QPP*WPP*W2)
 R1=R1+(B5*(B5*W2/2+B6*WPP)+B6**2*MP2/2)*ML2*(ML2-W2)
 R1=R1 + A1**2*(2*X**2*MP2-4*X*PLPP*QPP-2*X*
+    QW*MP2 + 2*X*QPP*WPP + 2*PLPP*QW*QPP)
 R1=R1 + A1*A2*(-4*X**2*WPP + 4*X*PLPP*QW + 2*X
+    *QW*WPP + 2*X*QPP*ML2-2*PLPP*QW**2-QW*QPP*
+    ML2-QW*QPP*W2)
 R1=R1 + (A1+C1/2./X)*A3*ML2*(2*X*QW*MP2-2*X*QPP*WPP
+    -2*PLPP*QW*QPP-2*QW**2*MP2 + 4*QW
+    *QPP*WPP + QPP**2*ML2-QPP**2*W2)
 R1=R1 + A2**2*(2*X**2*W2-2*X*QW*ML2-2*X*QW*
+    W2 + QW**2*ML2 + QW**2*W2)
 R1=R1+A3**2*ML2*(1./2.*QW**2*ML2*MP2-1./2.*QW**2
+    *MP2*W2-QW*QPP*WPP*ML2+QW*QPP*WPP*W2 + 1./
+    2.*QPP**2*ML2*W2-1./2.*QPP**2*W2**2)
 R2=C1**2*(-1./2.*ML4*MP2 + 1./2.*ML2*MP2*W2
+     + X**2*MP2-2*X*PLPP*QPP-X*QW*MP2 + 2*
+    X*QPP*WPP-X*ML2*MP2 + 2*PLPP**2*ML2 + 2*
+    PLPP*QPP*ML2-2*PLPP*WPP*ML2 + QW*ML2*MP2-2*
+    QPP*WPP*ML2)
 R2=R2 + C1*C2*(2*X**2*WPP-2*X*PLPP*QW + 4*X*
```

```
+     PLPP*ML2-X*QPP*ML2 + X*QPP*W2-4*X*WPP*
+     ML2 + 2*PLPP*ML4-2*WPP*ML4)
 R2=R2 + C2**2*(1./2.*ML**6-1./2.*ML4*W2 + 2*X**2*
+     ML2 + X**2*W2-3*X*QW*ML2 + 2*X*ML4-X*
+     ML2*W2-QW*ML4)
 RI=B1*C1*(-2*X*WPP + 2*PLPP*QW-2*PLPP*ML2
+      + QPP*ML2-QPP*W2 + 2*WPP*ML2)
 RI=RI + B1*C2*(-ML4 + ML2*W2-2*X*ML2-2*X*
+     W2 + 4*QW*ML2)
 RI=RI + B2*C1*(2*X**2*WPP-2*X*PLPP*QW-2*X*
+     PLPP*ML2-2*X*PLPP*W2-2*X*QW*WPP-X*QPP*
+     ML2 + X*QPP*W2 + X*WPP*ML2 + X*WPP*W2 + 2*
+     PLPP*QW**2 + PLPP*QW*ML2 + PLPP*QW*W2 + QW*QPP*
+     ML2-QW*QPP*W2 + 1./2.*QPP*ML4-1./2.*QPP*W2**2)
 RI=RI+B2*C2*ML2*(-2*X**2-X*ML2-X*W2
+     +2*QW**2+QW*ML2+QW*W2)
 RI=RI + B3*C1*(2*X**2*MP2-4*X*PLPP**2-4*X*
+     PLPP*QPP + 2*X*PLPP*WPP-2*X*QW*MP2 + 2*X*
+     QPP*WPP + 2*PLPP**2*QW + 2*PLPP*QW*QPP + PLPP*QPP*
+     ML2-PLPP*QPP*W2 + QPP**2*ML2-QPP**2*W2)
 RI=RI + B3*C2*(-4*X**2*PLPP + 2*X**2*WPP + 2*X*
+     PLPP*QW-2*X*PLPP*ML2-X*QPP*ML2-X*QPP*
+     W2 + 2*PLPP*QW*ML2 + 2*QW*QPP*ML2)
 RI=RI + B4*C1*(1./2.*ML4*MP2-1./2.*MP2*W2**2 + 2*
+     X*PLPP*WPP-2*X*WPP**2 + X*MP2*W2-2*PLPP**2
+     *QW-2*PLPP**2*ML2-2*PLPP**2*W2 + 2*PLPP*QW*WPP-
+     PLPP*QPP*ML2-PLPP*QPP*W2 + 2*PLPP*WPP*ML2 + 2*
+     PLPP*WPP*W2-QW*MP2*W2 + QPP*WPP*ML2 + QPP*WPP*W2)
 RI=RI + B4*C2*ML2*(-2*X*PLPP+X*WPP-
+     PLPP*QW-PLPP*ML2-PLPP*W2 + 2*QW*WPP
+     +1./2.*QPP*ML2-1./2.*QPP*W2 + WPP*ML2
+      + WPP*W2)
 RI=RI + B5*C1*ML2*(X*WPP-PLPP*QW-PLPP*
+     ML2-PLPP*W2-1./2.*QPP*ML2 + 1./2.*QPP*W2
+     +WPP*ML2 + WPP*W2)
 RI=RI + B5*C2*ML2*(-1./2.*ML4+1./2.*W2**2-X*
+     ML2+QW*W2)
 RI=RI + B6*C1*ML2*(X*MP2-2*PLPP**2-2*PLPP
+     *QPP+2*PLPP*WPP-QW*MP2 + 2*QPP*WPP)
 RI=RI + B6*C2*ML2*(-2*X*PLPP+X*WPP+
+     PLPP*QW-PLPP*ML2 + PLPP*W2-1./2.*QPP*
+     ML2 + 1./2.*QPP*W2)
 RI=RI + B7*C1*(2*X*PLPP*MP2-X*WPP*MP2-4*
```

```
+     PLPP**3-4*PLPP**2*QPP + 4*PLPP**2*WPP-PLPP*QW*
+     MP2 + 4*PLPP*QPP*WPP + PLPP*ML2*MP2-PLPP*MP2*
+     W2 + 1./2.*QPP*ML2*MP2-1./2.*QPP*MP2*W2)
 RI=RI + B7*C2*(-4*X*PLPP**2 + 4*X*PLPP*WPP-X
+     *MP2*W2-2*PLPP**2*ML2 + 2*PLPP*WPP*ML2 + QW*ML2
+     *MP2)
 RI=RI + A1*C1*(2*X**2*MP2-4*X*PLPP*QPP + 2*X*
+     PLPP*WPP-2*X*QW*MP2 + 4*X*QPP*WPP-X*ML2
+     *MP2-X*MP2*W2-2*PLPP**2*QW + PLPP*QPP*ML2 +
+     PLPP*QPP*W2 + 2*QW*ML2*MP2-2*QPP*WPP*ML2)
 RI=RI + A1*C2*(4*X**2*WPP-4*X*PLPP*QW-2*X*
+     QPP*ML2 + 2*QW*QPP*ML2)
 RI=RI + A2*C1*(-2*X**2*WPP + 2*X*PLPP*QW-2*X
+     *PLPP*W2 + X*QPP*ML2-X*QPP*W2 + X*WPP*ML2
+      + X*WPP*W2 + PLPP*QW*ML2 + PLPP*QW*W2-2*QW*WPP
+     *ML2-1./2.*QPP*ML4 + QPP*ML2*W2-1./2.*QPP*W2**2)
 RI=RI + A2*C2*(-4*X**2*W2 + 4*X*QW*ML2 + 2*X*
+     QW*W2-2*QW**2*ML2)
 SM=R1+RI/X+R2/X**2
 RETURN
 END
```

List of Tables

1 Phenomenological values and source for the renormalized coupling constants $L_i^r(M_\rho)$. The quantities Γ_i in the fourth column determine the scale dependence of the $L_i^r(\mu)$ according to Eq. (16). L_{11}^r and L_{12}^r are not directly accessible to experiment. 10

2 Occurrence of the low-energy coupling constants $L_1, \ldots, L_{10}$ and of the anomaly in the semileptonic decays discussed in chapter 2. . . . 11

1.1 The quantities X_I, N_I. $\mathrm{SD}^\pm$ and $\mathrm{INT}^\pm$ are evaluated with full phase space, IB with restricted kinematics (1.20). 20

1.2 Measured branching ratios $\Gamma(K \to l\nu_l\gamma)/\Gamma_{\text{total}}$. The $K_{e2\gamma}$ data are from [5, 2], the $K_{\mu 2\gamma}$ data from [3, 6]. The last column corresponds [3] to the cut (1.20). 24

1.3 Chiral prediction at order p^4 for the branching ratios $\Gamma(K \to l\nu_l\gamma)/\Gamma_{\text{total}}$. The cut used in the last column is given in Eq. (1.20). 26

2.1 Theoretical values for the branching ratios for the decay $K^+ \to \mu^+\nu e^+e^-$ for various cuts. 31

2.2 Theoretical values for the branching ratios for the decay $K^+ \to e^+\nu e^+e^-$ for various cuts. 32

3.1 Rates of K_{l3} decays. The number of events in the third column corresponds to those data which are of relevance for the determination of the slope λ_0 of the scalar form factor. 43

4.1 Branching ratios for tree level amplitudes for $E_\gamma \geq 30MeV$ and $\theta_{l\gamma} \geq 20°$ in the K rest frame. 48

4.2 Experimental results for $K_{l3\gamma}$ decays 48

4.3 Coefficients for the $K^+_{l3\gamma}$ loop amplitudes corresponding to the diagrams $I = 1,2,3$ in Fig. 4.2. All coefficients c_i^I must be divided by $6\sqrt{2}F^2$. 50

4.4 Coefficients for the $K^0_{l3\gamma}$ loop amplitudes corresponding to the diagrams $I = 1,2,3$ in Fig. 4.2. All coefficients c_i^I must be divided by $6\sqrt{2}F^2$. 52

4.5 Branching ratios and expected number of events at DAFNE for $K^+_{l3\gamma}$. 52
4.6 Branching ratios and expected number of events at DAFNE for $K^0_{l3\gamma}$. 53
5.1 Rates of K_{e4} decays. 60
5.2 Predictions of chiral symmetry following from the fit to the K_{e4} data [44] alone (column 3) and the combined determination from $\pi\pi$ [55] and K_{e4} data [44] (last column). The first column gives the prediction of the leading order term in the low-energy expansion of the $\pi\pi$ amplitude. 66

List of Figures

1.1 Contour plots for $f_{\rm IB}, \ldots, f_{\rm INT\pm}$ $[K_{\mu 2\gamma}]$. The numbering on the lines points towards increasing modulus. The normalization is arbitrary. . 21

1.2 Contour plots for $f_{\rm IB}, \ldots, f_{\rm INT\pm}$ $[K_{e2\gamma}]$. The numbering on the lines points towards increasing modulus. The normalization is arbitrary. . 22

1.3 The rate $dP(x)/dx$ in (1.39), evaluated with the form factors (1.38) and $N_{\rm tot} = 9 \cdot 10^9$. The solid line corresponds to $M_{K^*} = 890$ MeV, $M_{K_1} = 1.3$ GeV. The dashed line is evaluated with $M_{K^*} = 890$ MeV, $M_{K_1} = \infty$ and the dotted line corresponds to $M_{K^*} = M_{K_1} = \infty$. The total number of events is also indicated in each case. 27

3.1 The vector and scalar form factors $f_+(t)$ and $f_0(t)$. 39

3.2 The normalized slopes of the vector and the scalar form factors. Curve 1: the normalized slope $M_{\pi^+}^2 df_+(t)/dt$. Curve 2: the normalized slope $M_{\pi^+}^2 df_0(t)/dt$. Near the πK threshold $t_0 = (M_K + M_\pi)^2$, the vector form factor behaves as $f_+(t) = f_+(t_0) + O[(t - t_0)]$, whereas $f_0(t) = f_0(t_0) + O[(\sqrt{t - t_0})]$. The slope of the scalar form factor is therefore singular at $t = (M_K + M_\pi)^2$. 41

4.1 Diagrammatic representation of the $K^+_{l3\gamma}$ amplitude. 46

4.2 Loop diagrams (without tadpoles) for K_{l3} at $O(p^4)$. For $K_{l3\gamma}$, the photon must be appended on all charged lines and on all vertices. . . 49

5.1 Kinematic variables for K_{l4} decays. The angle θ_π is defined in $\Sigma_{2\pi}, \theta_l$ in $\Sigma_{l\nu}$ and ϕ in Σ_K. 55

5.2 The form factors $f_s(s_\pi)$ and $g(s_\pi)$ (Eq. 5.64) according to the chiral representation (electron mode). The dotted lines show the lowest order result (5.47), and the dashed lines correspond to L_1, L_2 and L_3 from (5.63). The experimental result (5.37) is displayed by a solid line. 67

Bibliography

[1] Particle Data Group, Phys. Lett. B239 (1990).

[2] J. Heintze et al., Nucl. Phys. B149 (1979) 365.

[3] Y. Akiba et al., Phys. Rev. D32 (1985) 2911.

[4] S.G. Brown and S.A. Bludman, Phys. Rev. B136 (1964) 1160;
D.A. Bryman et al., Phys. Rep. C88 (1982) 151.

[5] K.S. Heard et al., Phys. Lett. 55B (1975) 324.

[6] V.V. Barmin et al., Sov. J. Nucl. Phys. 47 (1988) 643.

[7] D. Yu. Bardin and E. A. Ivanov, Sov. J. Part. Nucl. 7 (1976) 286.

[8] J.F. Donoghue and B.R. Holstein, Phys. Rev. D40 (1989) 3700.

[9] J. Bijnens, G. Ecker and J. Gasser, Radiative semileptonic kaon decays, in preparation.

[10] J. Wess and B. Zumino, Phys. Lett. 37B (1971) 95;
E. Witten, Nucl. Phys. B223 (1983) 422;
N.K. Pak and P. Rossi, Nucl. Phys. B250 (1985) 279.

[11] G. Ecker, J. Gasser, A. Pich and E. de Rafael, Nucl. Phys. B321 (1989) 311;
G. Ecker, J. Gasser, H. Leutwyler, A. Pich and E. de Rafael, Phys. Lett. B223 (1989) 425;
J.F. Donoghue, C. Ramirez and G. Valencia, Phys. Rev. D39 (1989) 1947;
M. Praszalowicz and G. Valencia, Nucl. Phys. B341 (1990) 27.

[12] S. Krishna and H.S. Mani, Phys. Rev. D5 (1972) 678.

[13] A.M. Diamant-Berger et al., Phys. Lett. 62B (1976) 485.

[14] M.S. Atiya et al., Phys. Rev. Lett. 63 (1989) 2177.

[15] S. Egli et al., Phys. Lett. B175 (1986) 97;
S. Egli et al.,Phys. Lett. B222 (1989) 533.

[16] J. Gasser and H. Leutwyler, Nucl. Phys. B250 (1985) 517.

[17] N. Cabibbo and A. Maksymowicz, Phys. Lett. 9 (1964) 352.

[18] H. Leutwyler and M. Roos, Z. Phys. C25 (1984) 91;
J.F. Donoghue, B.R. Holstein and S.W. Klimt, Phys. Rev. D35 (1987) 934.

[19] Particle Data Group, Phys. Lett. B111 (1982).

[20] G. Donaldson et al., Phys. Rev. D9 (1974) 2960.

[21] V.K. Birulev et al., Nucl. Phys. B182 (1981) 1.

[22] Y. Cho et al., Phys. Rev. D22 (1980) 2688.

[23] D.G. Hill et al., Nucl. Phys. B153 (1979) 39.

[24] A.R. Clark et al., Phys. Rev. D15 (1977) 553.

[25] C.D. Buchanan et al., Phys. Rev. D11 (1975) 457.

[26] L.-M. Chounet, J.-M. Gaillard and M.K. Gaillard, Phys.Rep. C4 (1972) 199.

[27] E.P. Shabalin, Yad. Fiz. 49 (1989) 588 [Sov. J. Nucl. Phys. 49 (1989) 365]; ibid. 51 (1990) 464 [Sov. J. Nucl. Phys. 51 (1990) 296].

[28] J. Bijnens and F. Cornet, Nucl. Phys. B296 (1986) 557.

[29] S.R. Amendolia et al., Nucl. Phys. B277 (1986) 168 and references therein.

[30] M.F. Heyn and C.B. Lang, Z.Phys. 7C (1981) 169;
N. Zovko, Forts. Phys. 23 (1975) 185.

[31] R. Dashen and M. Weinstein, Phys. Rev. Lett. 22 (1969) 1337.

[32] R. Dashen, L.-F. Li, H. Pagels and M. Weinstein, Phys. Rev. D6 (1972) 834.

[33] B.G. Kenny, Phys. Rev. D15 (1977) 3481.

[34] C.G. Callan and S.B. Treiman, Phys. Rev. Lett. 16 (1966) 153.

[35] J. Gasser and H. Leutwyler, Nucl. Phys. B250 (1985) 465.

[36] B.R. Holstein, Phys. Rev. D41 (1989) 2829.

[37] V.N. Bolotov et al., Yad. Fiz. 44 (1986) 108 [Sov. J. Nucl. Phys. 44(1986) 68].

[38] F. Romano et al., Phys. Lett. 36B (1971) 525.

[39] D. Ljung and D. Cline, Phys. Rev. D8 (1973) 1307.

[40] K.J. Peach et al., Phys. Lett. 35B (1971) 351.

[41] E. Fischbach and J. Smith, Phys. Rev. 184 (1969) 1645;
H.W. Fearing, E. Fischbach and J. Smith, Phys. Rev. D2 (1970) 542.

[42] N. Cabibbo and A. Maksymovicz, Phys. Rev. B137 (1965) B438; erratum Phys. Rev. 168 (1968) 1926.

[43] A. Pais and S.B. Treiman, Phys. Rev. 168 (1968) 1858.

[44] L. Rosselet et al., Phys. Rev. D15 (1977) 574.

[45] J. Bijnens, Nucl. Phys. B337 (1990) 635.

[46] C. Riggenbach, J. Gasser, J.F. Donoghue and B.R. Holstein , Phys. Rev. D43 (1991) 127.

[47] F.A. Berends, A. Donnachie and G.C. Oades, Phys. Lett. 26B (1967) 109; Phys. Rev. 171 (1968) 1457.

[48] C. Riggenbach, University of Bern thesis (1992).

[49] J.L. Basdevant, C.D. Froggatt and J.L. Petersen, Nucl. Phys. B72 (1974) 413.

[50] C.D. Froggatt and J.L. Petersen, Nucl. Phys. B129 (1977) 89;
J.L. Petersen, CERN Yellow Report CERN 77-04 "The $\pi\pi$ Interaction".

[51] A.S. Carroll et al., Phys. Lett. 96B (1980) 407.

[52] A.R. Barker, Recent K^0 Decay Results from Fermilab E - 731, Fermilab preprint EFI 91-04, Proceedings of the SLAC Summer Institute on Particle Physics, July 1990, SLAC-378.

[53] G. Colangelo and J. Gasser, in preparation.

[54] S. Weinberg, Phys. Rev. Lett. 17 (1966) 336; 18 (1967) 1178E.

[55] M.M. Nagels et al., Nucl. Phys. B147 (1979) 189.

[56] J. Gasser and H. Leutwyler, Ann. Phys. 158 (1984) 142.

[57] J. Gasser and H. Leutwyler, Phys. Lett. B125 (1983) 321, 325.

[58] M.M. Nagels et al., Nucl. Phys. B147 (1979) 189;
D. Morgan and G. Shaw, Nucl. Phys. B10 (1968) 261;
J.L. Petersen, CERN Yellow Report CERN 77-04 "The $\pi\pi$ Interaction".
The coefficients in Eq. (5.69) are from this last reference.

[59] S. Weinberg, Phys. Rev. Lett. 17 (1966) 616.

[60] B. Bonnier and N. Johanneson, Nuovo Cimento 29A (1975) 565.

[61] J. Franklin, Phys. Rev. D11 (1975) 513.

[62] For a proposal to measure $\pi\pi$ and πK threshold parameters in dimeson atoms see L. Montanet and L. Nemenov, Letter of Intent to the SPSLC, CERN/SPSLC 91-47.

[63] P. Franzini, private communication.